School of Molecular and Cell Biology

University of the Witwatersrand

Johannesburg

Biosynthesis and Characterization of Metallic Nanoparticles Produced by *Paenibacillus castaneae*

A Dissertation submitted to the Faculty of Science of the University of Witwatersrand, Johannesburg, in full fulfilment of the requirements for the degree of Master of Science.

May 2017

Dishon Wayne Hiebner

396356

Supervisor: Dr Kulsum Kondiah

Co-supervisor: Dr Deran Reddy

Declaration of Independent Work

I, **DISHON WAYNE HIEBNER** (3963556), am a student registered for the degree of **Master of Science (MSc): Biotechnology** in the academic year 2017.

I hereby declare the following:

- I am aware that plagiarism (the use of someone else's work without their permission and/or without acknowledging the original source) is wrong.
- I confirm that the work submitted for assessment for the above degree is my own unaided work except where explicitly indicated otherwise and acknowledged.
- I have not submitted this work before for any other degree or examination at this or any other University.
- The information used in the Thesis/Dissertation/Research Report has been obtained by me while employed by, or working under the aegis of, any person or organization other than the University.
- I have followed the required conventions in referencing the thoughts and ideas of others.
- I understand that the University of the Witwatersrand may take disciplinary action against me if there is a belief that this is not my own unaided work or that I have failed to acknowledge the source of the ideas or words in my writing.

DW Hiebner _____ 01/06/17 _____

SIGNATURE OF CANDIDATE **DATE**

Abstract

Nanomaterials (NMs) have been shown to exhibit unique physical and chemical properties that are highly size and shape-dependent. The ability to control synthesis of nanoparticles (NPs) with particular shapes and sizes can lead to exciting new applications or enhancements of current systems in the fields of optics, electronics, catalytics, biomedicine and biotechnology. Due to increased chemical pollution as well as health concerns, biological synthesis of NMs has quickly emerged as potentially being an eco-friendly, scalable, and clean alternative to chemical and physical synthesis. In this study, the inference that the heavy metal-resistant bacteria, *Paenibacillus castaneae*, has the propensity to synthesize metal NPs was validated.

NP formation was achieved after the exposure of bacterial cell biomass or cell-free extracts (CFE) to excess metal ion precursors in solution. These include lead nitrate and calcium sulphate dehydrate, gold (III) chloride trihydrate and silver nitrate, respectively. All reactions were incubated at 37 °C for 72 h at 200 rpm and observed for a colour change. UV–visible (UV-Vis) spectral scans (200 nm – 900 nm) were measured on a Jasco V-630 UV-Vis spectrophotometer. For scanning electron microscopy (SEM), samples were fixed, dehydrated and loaded onto carbon-coated aluminium stubs. The stubs were then sputter-coated with either Au/Pd or Cr and analysed on the FEI Nova Nanolab 600 FEG-SEM/FIB. Size distribution analysis was done using transmission electron microscopy (TEM) using the FEI Tecnai T12 TEM and Image J software. Powder X-ray diffraction measurements were carried out on a Rigaku Miniflex-II X-ray diffractrometer.

Colour changes indicative of the synthesis of PbS, Au and Ag NPs were observed as a white precipitate (PbS), purple (Au) and yellow-brown (Ag) colour, respectively. This was confirmed by absorbance peaks at 325 nm and 550 nm (PbS), 595 nm (Au) and 440 nm (Ag) from UV-Vis analyses. Exposure of *P. castaneae* biomass and CFE to PbS ions in solution resulted in the production of nanospheres, irregularly-shaped NPs, nanorods, nanowires as well as large nanoflowers.

Exposure of *P. castaneae* biomass to Au^{3+} ions in solution produced Au nanospheres, nanotriangles, nanohexagons, nanopentagons and nanopolyhedrons. Ag/AgCl NP production occurred using both the *P. castaneae* biomass and CFE, and resulted in the synthesis of nanospheres only.

This is the first report of the biosynthesis of such a diverse set of anisotropic NPs by *P. castaneae*. It is also the first instance in which anisotropic PbS nanorods and nanowires, 3-D Au nanoprisms as well as "rough" Ag/AgCl nanospheres were bacterially produced. This study serves as an eco-friendly approach for the synthesis of NPs that is a simple yet amenable method for the large-scale commercial production of nanoparticles with technical relevance. This in turn expands the limited knowledge surrounding the biological synthesis of heavy metal NMs.

Keywords: *Paenibacillus castaneae*, heavy-metal resistance, biological synthesis, lead sulphide nanoparticles, gold nanoparticles, silver nanoparticles

Dedication

In memory of my mother

Dawn Vanessa Hiebner

1960 – 2008

Acknowledgments

Firstly, all thanks, praise, glory and honour to God, The Father. Without His grace and love, none of this would be possible.

I would like to thank Dr Kondiah for everything she has made possible for me. You have truly pushed me to become a great scientist and person and I owe the development of my scientific career. Thank you for all the patience and kindness and for always presenting me with an opportunity to learn more and always challenge myself. Thanks also goes to Dr Reddy who was always willing to lend a helping hand, always showed his willingness to go the extra mile for me and for all the hours spend on microscopes getting amazing images.

Without the love, support, care and everything in between from Keylene Naidoo, Darrelle, Delana-Rae, Deanndré, Dawn and Derrick Hiebner, I would not be where I am today. Thank you for standing by me, always pushing me to be better, for being my voice of reason and mostly for always being there whenever I needed you. Thank you to for providing me with all the necessary tools to become the person that I am today. Without your love and care this journey would have been a lonely one. Thank you for being my pillars of strength and always pushing me forward. Thank you for being the only family I'll ever need.

A very big thank you to all my colleagues in The Lab as well as The Reading Room for all their continuous motivation, advice, help, friendship and especially humour.
I would like to thank Prof Ziegler and Dr Gerber form the Wits MMU for always helping with all my microscopy needs.
Thank you to Prof Pillar and Dr Marimuthu for all the assistance with the PXRD equipment and analysis.
My sincere gratitude and appreciation goes out to the NRF-DST and the WITS PMA for the financial support throughout my MSc research.
I wish to thank the School of Molecular and Cell Biology and the University of the Witwatersrand for the opportunity to have conducted this research.

TABLE OF CONTENTS

List of Figures

List of Tables

List of Abbreviations

0-D	Zero dimensional
1-D	One dimensional
2-D	Two dimensional
3-D	Three dimensional
a.u.	Arbitrary units
$AgNO_3$	Silver nitrate
Au	Gold
AuPd	Gold palladium
$CaSO_4 \cdot H_2O$	Calcium sulphate dihydrate
CBNs	Carbon-based nanomaterials
$CdSO_4$	Cadmium sulphate
CFCs	Chlorofluorohydrocarbons
CO	Carbon monoxide
CTAB	Cetyltrimethylammonium bromide
DIC	Differential interference contrast microscopy
DMSO	Dimethyl sulfoxide
DTF	Dimethylformamide
DTT	Dichlorodiphenyltrichloroethane
EDS	Energy-dispersive X-ray spectroscopy
EPS	Extracellular polymeric substance
FDI	Foreign direct investment
Fe_3O_4	Iron oxide
FM	Fluorescence microscopy
FTIR	Fourier transform infrared spectroscopy
$HAuCl_4 \cdot 3H_2O$	Gold (III) chloride trihydrate
HCl	Hydrogen chloride

IR	Infrared
JCPDS	Joint Committee on Powder Diffraction Standards
KCl	Potassium chloride
LB	Luria-Bertani
LED	Light-emitting diodes
LSPR	Local surface plasmon resonance
MBN	Metal-based nanomaterial
MDG	Millennium Development Goals
MIC	Minimum inhibitory concentration
MT	Metallothioneins
NaCl	Sodium chloride
NDP	National Development Plan
NIR	Near-infrared
NMs	Nanomaterials
NP	Nanoparticle
NSN	National Strategy on Nanotechnology
$Pb(NO_3)_2$	Lead nitrate
PbS	Lead sulphide
PC	Phytochelatins
PCB	Polychlorinated biphenyls
PEG	Polyethylene glycol
PXRD	Powder X-ray diffraction
sdH_2O	Sterile deionized water
SEM	Scanning electron microscopy
SERS	Surface enhanced Raman scattering
SQUIDs	Superconducting quantum interference device
TCDD	Tetrachlorodibenzo-p-dioxin-like compounds
TEM	Transmission electron microscopy
UN	United Nations
UV-Vis	Ultraviolet-visual spectroscopy

CHAPTER 1: INTRODUCTION

1.1 Background

Nanotechnology is defined as the design, synthesis and characterization of materials, devices and systems at the nanoscale (<100 nm). It is also considered the control of phenomena associated with atomic and molecular interactions (Albanese, Tang and Chan, 2012). In the past few decades, nanotechnology has attracted much research interest due to its ability to not only bridge the gap between elemental atoms and bulk materials but also to be the interface between many schools of science. These include chemistry, physics, material science, engineering, medicine and biology (Schröfel *et al*., 2014). Knowledge generation in this new scientific field is on the increase worldwide. This has resulted in major scientific advances and a substantial shift in the manner in which devices, systems and materials are created and understood.

Effectively, all systems and materials have the potential to obtain the unique properties offered by development at the nanoscale (Stark *et al*., 2015). This renders them suitable for innumerable novel applications (Harikrishnan *et al.*, 2014). Expected breakthroughs in the future include an order magnitude increase in: green energy production, computer efficiency, human organ and tissue restoration and the creation of designer materials from the direct assembly of atoms or molecules (Roco and Bainbridge, 2005). There are currently widespread commercial and industrial applications for nanomaterials (NMs). These include energy production, packaging, bioengineering, agriculture, food and beverages, medicine, cosmetics, surface coating and polymers, pharmaceuticals, nutraceuticals, paints and inks, optoelectronics and computing (Ingale and Chaudhari, 2013)

The limitless potential of nanotechnology and its impact is not only centred around industrial outputs but also in solving societal problems in developing countries. This includes availability of potable water, cheaper energy and primary health-care; problems that have been recognized throughout the developing world (Kharissova *et al*., 2013). As with any new scientific development, the potential risks of

nanotechnology must also be considered. The possible adverse effects on human health and safety, environmental concerns as well as the potential displacement of current industries to accommodate nanotechnology, in both the private and public sectors, must be considered in the entire NM development process (Vance *et al*., 2015). The focus of much research has therefore tended towards the "greener" nanotechnologies. These include environmentally friendly chemical processes that incorporate the twelve principles of green chemistry (detailed explanation in Chapter 2, Page 29). These principles are implemented to achieve technologies and products that are considerably less energetically expensive, more environmentally sound, safe and also cost effective (Anastas and Warner, 1998). The commercial applications of nanotechnology are however still in the early stage of technical development, especially in the synthesis and development of novel NMs.

Nanocrystalline materials and nanoparticles (NPs) are defined as any object that behaves as a whole unit with respect to its transport and properties, and is characterized by a structural length or grain size of up to 100 nm (Harikrishnan *et al.*, 2014). NPs have distinctly different properties as compared to bulk materials. This includes vast alterations in optical, mechanical, electrical, thermal, dielectric, electronic, physical, chemical and biological characteristics (Bhadwal *et al.*, 2014). The sum total of atoms or molecules on the NP surface is comparable to those within the NP. Therefore, the properties of NPs are highly dependent on their structure and composition as well as size, shape, morphological sub-structure, phase and surface chemistry (Albanese, Tang and Chan, 2012). The methods of NP fabrication are highly significant in the inherent nature and characteristics of the produced NPs. For this reason, the fundamentals of NP synthesis have recently received much attention (Iravani *et al*., 2014).

The production of NPs is based on two fundamental approaches: the "top-down" approach and the "bottom-up" approach (Wang and Xia, 2004). "Top-down" fabrication is based on the removal of particular areas of the bulk material via chemical, mechanical or electrical processes and is highly dependent on the intrinsic nature of the initial bulk material substrate (Singh, Manikandan and

Kumaraguru, 2011). The "bottom-up" approach is characterized by the fabrication of NMs from atoms and molecules (basic building blocks), using chemical, electrical or thermal energy (Narayanan and Sakthivel, 2010).

Conventionally, the synthesis of NMs is achieved via either physical, chemical or biological methods, as summarized in Figure 1.1. Physical methods employ the use of high energy radiations, thermal energy, mechanical pressure and electrical energy to allow for the abrasion, melting, evaporation, or condensation of bulk materials to produce NPs. Even though the use of these "top-down" strategies can produce monodisperse NPs that are free from solvent contamination, the substantial waste production as well as high energy demand makes physical methods less economical (Dhand *et al*., 2015).

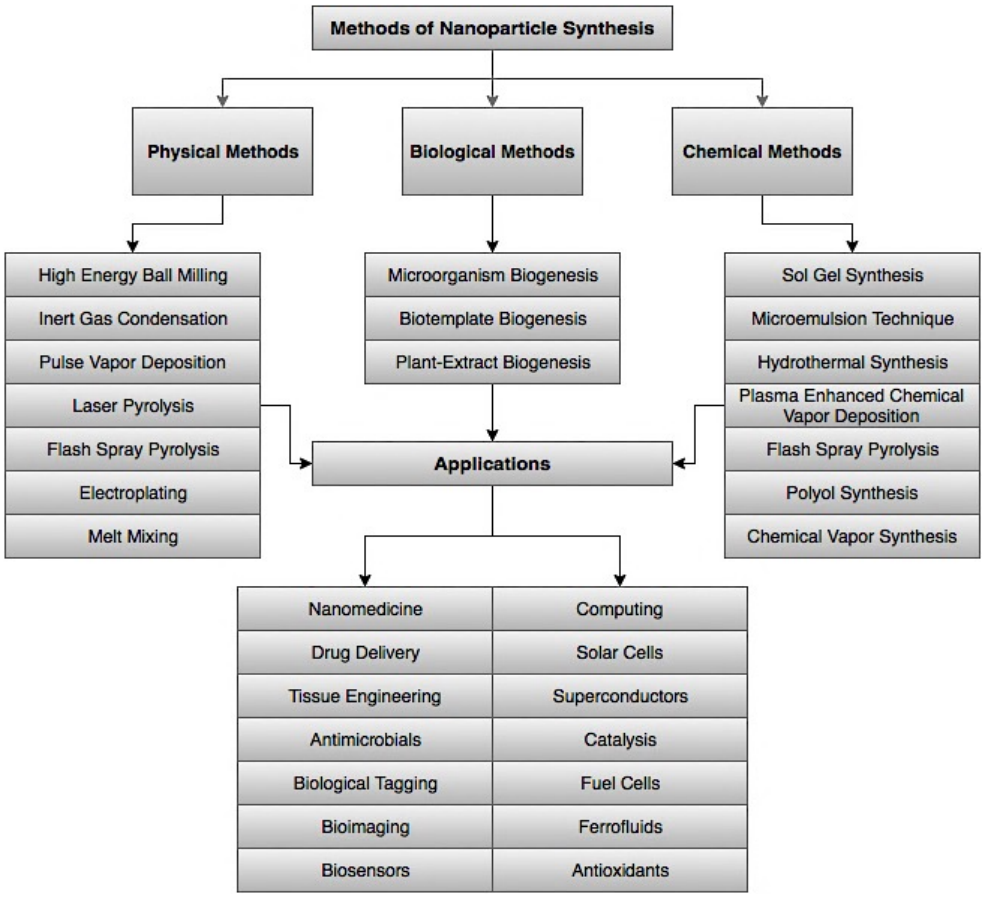

Figure 1.1 Overview of the methods and strategies for the synthesis of nanoparticles and their applications (adapted from Dhand *et al*., 2015).

Chemical methods are based on the reduction of ions or the decomposition of precursors in an energetically taxing reaction to form atoms. This is then followed by the aggregation of atoms to form NPs (Singh, Manikandan and Kumaraguru, 2011). These "bottom-up" methods commonly rely on the addition of reducing agents, as well as stabilizers and capping agents to ensure there is no agglutination and aggregation of NPs (Pileni, 1998). External energy sources are also used to ensure efficiency; these include ultraviolet light, thermal energy, microwaves, electric energy as well as γ-radiation (Tavakoli, Sohrabi and Kargari, 2007). Even though NPs fabricated using these methods often have a narrow size and shape distribution, which are highly desirable traits, the synthesis thereof often includes the use of toxic chemicals, high amounts of energy and highly deleterious organic solvents (Iravani *et al*., 2014).

Chemical processes are frequently environmentally unfriendly and even contribute to secondary environmental problems. The most prominent examples of such include the persistence of dichlorodiphenyltrichloroethane (DDT), polychlorinated biphenyls (PCBs) and tetrachlorodibenzo-p-dioxin (TCDD)-like compounds in water bodies, chlorofluorohydrocarbons (CFCs) and greenhouse gases in the atmosphere, or plastic in the ocean (Travis and Hester, 1991). For this reason, much research is now being centred around green chemistry and its application in nanoscience (Stark *et al*., 2015). Green chemistry is defined as the design, development and implementation of chemical processes to reduce or eliminate the usage and production of materials which are hazardous to human health and the environment (Mondal *et al*., 2014). The twelve principles of green chemistry allow for a simplistic approach into the development of safer, cleaner and cheaper NPs (Raveendran, Fu and Wallen, 2003)

The biological synthesis (biosynthesis) of NPs provides methods that have the advantage of being environmentally benign, cost effective, having low toxicity and providing an efficient one-step protocol for the fabrication of NPs (Thakkar, Mhatre and Parikh, 2010). These methods can be broadly grouped into three main categories: microorganism, biotemplate and plant extract biosynthesis (Kharissova

et al., 2013). Biological systems have long been known to produce elaborate inorganic structures and materials which often occur in the nanoscale. As a result, many prokaryotic and eukaryotic organisms have been used for the production of NPs (Schröfel *et al*., 2014). Bacteria, algae, fungi, viruses, plants and actinomycetes as well as their proteins and metabolites have been employed in the reduction of inorganic metal ion precursors to form metal or metal oxide NPs (Duan, Wang and Li, 2015).

Biosynthesis offers three major areas in which the principles of green chemistry can be applied and can therefore lead to profound improvements. These include: (i) the choice of solvent (ii) the reducing agent and (iii) the capping or stabilizing agent (Nadagouda and Varma, 2006). Conventional chemical solvents can be replaced by water while biomolecules are involved in the reduction, capping and stabilization of nanoparticles (Makarov *et al*., 2014). Biological molecules like proteins or peptides are multifunctional and complex in nature enabling them to function as both reducing and capping agents simultaneously, for a myriad of NP types (Kharissova *et al*., 2013). The use of many biological entities has been explored for the synthesis of diverse NMs. Of these, bacterial systems are preferred for the biosynthesis of metallic NPs (Park, Lee and Lee, 2016). Bacteria offer extracellular production of NPs, short generation times, the ability to survive harsh environments together with ease of culturing, downstream processing and genetic manipulation (Thakkar, Mhatre and Parikh 2010). These serve as the main advantages of bacterial synthesis methods.

The biosynthesis of NPs by bacteria can be viewed in two respects; as either an inherited or an acquired trait. The biosynthesis of NPs has been shown to be a unique biochemical feature of all members of a bacterial genus but does not necessarily include all closely-related members of that bacterial family. A case in point was reported where all known *Morganella* spp. could synthesize Ag NPs yet closely related genera of Enterobacteriaceae family could not (Parikh *et al*., 2011). This evidence suggests the biosynthesis of NPs is a phenotypic characteristic and therefore independent of environmental conditions. In contrast, the ability of

bacteria to survive in extreme environments such as those isolated from acid mine drainage (Mourato *et al*., 2011), soil from mining sites (Elcey, Kuruvilla, and Thomas, 2014), mine tailings (Nangia *et al*., 2009) or even hot springs (Juibari *et al*., 2015), has also been linked to the propensity of these organisms to synthesize NPs and therefore shows that the environmental conditions can, in certain cases, be very important in determining the genotypic trait. Thus, NP biosynthesis by bacteria can also be due to an acquired genetic predisposition and not a phenotypic characteristic.

A strong correlation between toxic metal ion resistance and the ability of these bacteria to produce metallic NPs has recently been identified (Ramanathan *et al*., 2013). Most of the transition metal ions (Pb^{2+}, Ag^{2+}, Hg^{2+}, Au^{3+}, Cu^{2+} etc.) are considered toxic to bacteria (Harrison, Ceri, and Turner, 2007). However, the ability of some bacteria to reduce toxic metals into their corresponding non-toxic forms, using a variety of different pathways, has been extensively reported (Flynn *et al*., 2014; Lloyd, 2003; Nangia *et al*., 2009; Narayanan and Sakthivel, 2010; Park *et al*., 2010).

Transition and noble metals are most commonly used in industry for their catalytic and semiconductor properties (Suib, 2013). Additional properties such as the Surface Enhanced Raman Scattering (SERS) of gold (Au) NPs (Israelsen, Hanson and Vargis, 2015), the antimicrobial activity of silver (Ag) NPs (Suresh *et al*., 2010) and the photovoltaic properties of lead sulphide (PbS) NPs (Jang *et al*., 2010), are all considerably increased when these materials are found in the nanoscale. The detoxification of transition and noble metals by heavy-metal ion resistant bacteria has inspired the development of facile protocols for the bacterial biosynthesis of NPs (Schröfel *et al*., 2014). It is therefore imperative that bacteria which are known to be metal ion resistant be challenged with different metal ions so as to assess its ability to produce NPs. This must be done in order to provide the basis for a simple green approach to NP biosynthesis.

1.2 Problem Statement

The development and growing demand for high definition displays, faster computing, and more effective antimicrobials has increased the requirement for materials with enhanced or novel properties (El-Nour *et al*., 2010; Hussain and Khan, 2013; Ingale and Chaudhari, 2013). Au NPs, Ag NPs and nanophosphors like PbS NPs are examples of such and boast unparalleled optical, electric and thermal properties (Kharissova *et al*., 2013). However, the production of these metal NPs at industrial scale relies on the chemical routes of synthesis, often resulting in the production of toxic effluents (Mohanpuria, Rana, and Yadav, 2008). Subsequently, the effluents may either be disposed of inefficiently or leak into the surrounding soil and water (Fletcher, 2002; Riba *et al*., 2002) resulting in several knock-on effects on human health, the economy and environment (Grimalt, Ferrer and Macpherson, 1999). Organic solvents that are often used in chemical synthesis of NPs as well as other industrial applications, such as dimethyl sulfoxide (DMSO), dimethylformamide (DMF) and cetyltrimethylammonium bromide (CTAB), are another major route of environmental contamination (Mulholland and Dyer, 1998).

The considerable increase in chemical pollution and occurrence of environmental contamination as well as the importance placed on clean and energy efficient technology has led to a drive towards using green technologies (Sheldon, 2016). Therefore, for large-scale industrial production of NMs, it is necessary to identify suitable facile processes which are cost effective, safe and environmentally benign. Bacterial biosynthesis is thus the most suitable candidate. *Paenibacillus castaneae* is a rod-shaped, gram variable and motile bacteria that was first isolated from the phylosphere of the sweet chestnut tree in Spain (Valverde *et al*., 2008). It has also been isolated from a heavy metal contaminated environment water line in Illinois, USA (White, Tancos and Lytle, 2011). An isolate of this bacterial species was cultured from acid mine decant sourced from mine tailings in the West Rand of Gauteng (26°06'26.8"S 27°43'20.2"E) and found to be highly resistant to heavy metals like Pb (Gauteng Department of Agriculture and Rural Development, 2016).

It was therefore inferred that *P. castaneae* has the propensity to synthesize metal NPs such as PbS, Au and Ag NPs after exposure to excess metal ion precursors in solution. The confirmation of NP biosynthesis would then be followed by the physicochemical and morphological characterization of NPs. This study sought to validate this suggestion.

1.3 Aim and Objectives

1.3.1 Aim

To synthesize and characterize metallic nanoparticles that are biologically produced by a heavy metal-resistant isolate of *P. castaneae*.

1.3.2 Objectives

To fulfil the aim of the study, the specific objectives were identified as follows:

- To synthesize PbS, Au and Ag nanoparticles through the exposure of *P. castaneae* to metal ion precursors in solution.

- To confirm the biosynthesis of metallic nanoparticles using Ultraviolet-visual (UV-Vis) spectroscopy, differential interference contrast (DIC) microscopy and fluorescence microscopy (FM).

- To characterize the morphology of metallic nanoparticles using scanning electron microscopy (SEM), transmission electron microscopy (TEM) and powder X-ray diffraction (PXRD).

1.4 Chapter Outline

This dissertation follows the structure outlined below.

Chapter 1 gives a brief introduction to the research area and outlines the problem statement. The main aims and specific objectives of this research, which are required in order to satisfy and successfully address the problem statement, are also discussed. This chapter also presents the outline of the dissertation.

Chapter 2 presents an in-depth review of the literature associated with NP synthesis, in particular, the synthesis of metallic NPs, mechanisms of NP formation and growth, and the microbial synthesis of NPs encompassing green chemistry.
Chapter 3 provides the details of all materials and methods utilized in order to accurately and reproducibly conduct the experimental procedure required to address the main aim and specific objectives.

Chapter 4 demonstrates and discusses the obtained results from the experimental research conducted. This chapter displays and discusses the results received for visual, physicochemical and morphological characterization of metallic NPs.

Chapter 5 puts forward the general conclusion, based on the highlighted objectives, and future recommendations from the present study.

CHAPTER 2: LITERATURE REVIEW

2.1 Nanotechnology in South Africa

Nanotechnology is no longer considered as just an emerging field of science; it is currently regarded as the fourth wave of the industrial revolution (Dai, 2006). Many of the major economic world powers, including Germany, the UK and the USA, are currently producing and supplying NMs and related products to consumers (Figure 2.1) (Youtie, Shapira, and Porter, 2008). The global market for nanotechnology is estimated to grow to as much as $3 trillion by 2020 (Khan, 2012). As the leader in science and technology on the African continent, South Africa has invested over R200 million into different aspects of nanotechnology. These include, but are not limited to, research and development in the health, water and sanitation as well as energy sectors (Mufamadi, 2015). However, the development of nanotechnology in South Africa is hindered by many obstacles. These include the public's negative perception of the technology, vague national regulations and standards as well as health and safety concerns (Musee *et al*., 2010).

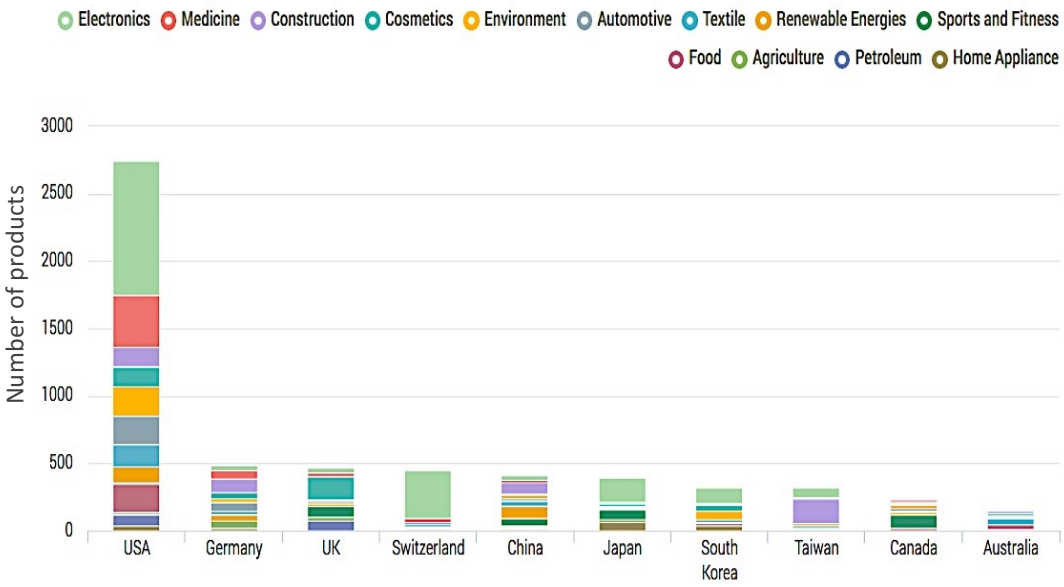

Figure 2.1. Share of countries which are active in the production of nanomaterials. Image retrieved from http://product.statnano.com/

Currently, South Africa has very few companies listed to produce nano-products and only a handful of initiatives and networks involved in nanotechnology research and development. For nanotechnology to improve the socio-economic status of South Africa, it is necessary to focus on the manufacturing of nano-products at a low cost, using inexpensive local materials, with a decreased risk to human health and the environment (Mufamadi, 2016). This should follow the establishment of successful and sustainable commercialization strategies from multi-stakeholder partnerships between the public and private sectors. For the country to meet some of its greatest demands, such as ending poverty and hunger, access to potable water and affordable sustainable energy, it must increase its long-term investment into infrastructure for research and development. The creation of employment opportunities, as well as the closing of gaps in skill shortages in emerging technologies are also paramount (Mufamadi, 2015).

The initiatives currently put into place have resulted in the establishment of characterization centres, the creation of research and innovation networks, the building of human capacity as well as the implementation of flagship projects. This is in parallel with the National Strategy on Nanotechnology (NSN) which was published by the South African Department of Science and Technology in 2005. South Africa is now in a position to start using local resources to develop nanotechnology into a sustainable sector of industry. In order to proceed forward, it is necessary to identify the specific gaps that need to be filled by NM research and development that are based not only on national but also international needs (Gardner, 2015). These gaps include the eco-friendly, efficient and cost-effective synthesis of novel NMs with unique characteristics. Furthermore, the understanding of the mechanisms involved in their formation and growth must also be identified.

2.2 Metal-based Nanomaterials

Nanomaterials can be broadly grouped into carbon-based NMs (CBNs) and metal-based NMs (MBNs) (Glezer, 2011). CBNs are industrially important materials due to the unique combination of physicochemical properties they offer. These include the use of carbon nanotubes and fullerenes for application in high-strength materials

as well as energy production and electronics (Baughman *et al*., 2002). MBNs have captivated scientists for over a century and are now frequently utilized in biomedical science, materials science and engineering. MBNs are produced in a myriad of shapes and sizes and possess many novel physical, chemical, magnetic, thermal, biological, optical and electrical properties (Pantidos and Horsfall, 2014). Of all MBNs, the noble and transition metal NMs have attracted the most scientific interest due to their direct application in virtually all sectors of industry. These include the agriculture, electronics, medicine, construction, cosmetics, food and textile industries (Mody *et al*., 2010).

2.2.1 Noble Metal Nanoparticles

Nobel metals are any number of metallic chemical elements that have excellent resistance to oxidation and corrosion in moist air. These include rhenium, ruthenium, rhodium, palladium, silver, osmium, iridium, platinum, and gold (Siegel *et al*., 2016). Noble metal NPs have been extensively researched by the scientific community owing to their unique optical, electromagnetic, catalytic and bactericidal properties (Siegel *et al*., 2016). These characteristics are not often shared by bulk materials and are thus strongly influenced by their shape and size (Sreeprasad and Pradeep, 2013). Au- and Ag-based NMs are particularly interesting due to their vast application in catalysis, chemical sensors, drug delivery and antimicrobial agents (Mourato *et al*., 2011).

Gold Nanoparticles

The existence of colloidal Au or Au NPs has been known for centuries and have a rich history in science. Combinations of Au salts and molten glass were used by artisans in the Middle Ages to produce gold colloids with a rich ruby colour. These were exploited for their aesthetic properties; in the colouration of glass, ceramics and pottery, as well as for their medicinal and cultural practices (Hutchings, Brust and Schmidbaur, 2008). Michael Faraday was the first to recognize that the colour of colloidal Au was due directly to the minuscule size of the gold particles (Faraday, 1857). He was the first to note the light scattering properties of colloidal gold, now referred to as the Faraday-Tyndall effect (Hirsch, Narurkar, and Carruthers, 2006).

Synthesis of Gold Nanoparticles

The two fundamental components in the synthesis of Au NPs are the choice of reducing agent and the stabilizing ligand. In terms of the wet chemistry methods, Au NPs have been produced within aqueous medium through the reduction of Au metal salts with an appropriate reducing agent in the presence of a suitable stabilizing agent (Zhao, Li and Astruc, 2013). To avoid agglomeration, which occurs through Van der Waals forces, the stabilization of Au NPs is achieved through either electrostatic or steric mechanisms. The most common method for Au NP *in situ* synthesis is the reduction of an Au^{3+} salt by sodium citrate under aqueous conditions (Schulz *et al*., 2014). The optimization of this method, pioneered by Turkevich, Stevenson and Hillier (1951), can lead to the synthesis of Au NPs with various distinct morphologies and sizes (Ding *et al*., 2015).

Of all metal NPs that have been biologically synthesized, Au NPs have received the most attention. Protein-capped Au NPs have been successfully synthesized using the fungal culture filtrate of *Fusarium* sp. MMT1 (Guria, Majumdar and Bhattacharyya, 2016). Ateeq *et al*. (2015) reported the biosynthesis of patuletin-coated Au NPs using a natural flavonoid extracted from flowers of *Tagetes patula* plant as the reductant and capping agent. Crocin (crocetin di-gentiobiose ester), a water-soluble sugar surfactant, was used in the biosynthesis of sugar-capped Au nano-disks (Khan, Al-Thabaiti and Bashir 2016).

Properties and Applications of Gold Nanoparticles

Au NPs are multifaceted materials used for a wide range of applications with well characterized optoelectronic, chemical and physical properties. Additionally, their surface chemistry can be easily modified (Brown *et al*., 2010). As well as size- and shape-dependent properties, Au NPs also have a large surface-area-to-volume ratio, low toxicity, excellent biocompatibility and can be easily paired with many surface ligands (Yeh, Creran and Rotello 2012). Significant physical characteristics include Local Surface Plasmon Resonance (LSPR), enhanced electronic efficiency, SERS activity and the ability to quench fluorescence. Au NPs also display a range of colours as a function of the size of their core (Jain *et al*., 2006). The properties of

Au NPs are highly influenced not only by size and shape but by temperature, solvent and solvent pH, core charge, surface ligands and can even be highly responsive to the proximity of the NPs to each other (Das *et al*., 2011).

The applications of Au NPs are extensive. These include electronics, photodynamic therapy, pharmaceuticals and drug delivery, sensors, probes, diagnostics and catalysis (Hutchings, Brust and Schmidbaur, 2008). An increase in the aggregation of small (d > 5 nm) Au NPs prompts interparticle surface plasmon coupling, resulting in a visible colour change from red to blue in nM concentrations (Srivastava, Frankam and Rotello, 2005). This effect provides a practical platform in which a change in aggregation (or redispersion of an aggregate) can be used for the absorption-based colorimetric sensing of any target analyte. This includes the use of Au NPs for the detection of metal and heavy-metal ions (Lin *et al*., 2002), anionic species (Martinez-Manez and Sancenón, 2003), proteins (Schofield *et al*., 2006) and small organic molecules (Aslan, Lakowicz, and Geddes, 2004). Au NPs can also be used in diagnostics for the detection of specific biomarkers. A typical example is the use of Au NP-based lateral flow immunoassays for home pregnancy tests (Idegami *et al*., 2008). The method can also be used to detect pathogens (Shukla *et al*., 2014), toxins (Shyu *et al*., 2002) and even water pollutants (Kuang *et al*., 2013).

A strong optical absorption and nonradiative energy dissipation of the particles allows for the application of Au NPs in photothermal therapy. Near-infrared (NIR) radiation, when applied to Au NPs, results in the excitation of free electrons in the plasmon band. This creates a pulsing of superheated electrons (Link and El-sayed, 2000). The immense heat generated by this process can therefore be used in cancer therapy to damage and destroy cancer cells and tissues in a more targeted and efficient manner than traditional photothermic therapies. For the *in vivo* therapy of deep tissues tumours, NIR light is required for its penetration but minimal absorption by haemoglobin and water molecules. Hirsch *et al.* (2003) first demonstrated the irreversible photothermal damage of breast carcinoma cells incubated with PEGylated gold nanoshells after their exposure to NIR light.

Silver and Silver Chloride Nanoparticles

The synthesis of citrate-stabilized colloidal Ag was first reported by Lea (1889) and has since been manufactured commercially for use in medicinal applications. The antiseptic properties of Ag however, have been known for over 2000 years. It is estimated that over 320 tons/year of Ag NPs are produced and used worldwide (Nowack, Krug and Height, 2011). Scientific advancement has led to the synthesis of various inorganic nanoparticles such as metals, metal oxides, metal sulphides and metal chlorides (Gopinath *et al*., 2013). Among metal chlorides and more specifically metal chloride NPs, silver chloride is perhaps the most widely recognized and extensively used (Husein, Rodil and Vera, 2005). The unique properties of both Ag and AgCl NPs have led to their incorporation into a variety of applications. These include cosmetic products, composite fibres, antimicrobial applications, electronic components and cryogenic superconducting materials (Wei *et al*., 2015).

Synthesis of Silver and Silver Chloride Nanoparticles

The most common method for the synthesis of Ag NPs is through the reduction of Ag ions by organic and/or inorganic reducing agents. Generally, sodium citrate, ascorbate sodium borohydride and N-dimethylformamide are used for the reduction of Ag ions to the zerovalent metallic Ag atoms (Wiley *et al*., 2005). Agglomeration into oligomeric clusters and the subsequent stabilization of Ag NPs is achieved using various surfactants, with functional groups such as amines, acids and thiols attached. This results in Ag NPs that are protected from aggregation and sedimentation as well as the loss of surface properties (Oliveira *et al*., 2005). Many technologies have been explored for the fabrication of silver halide NPs such as AgCl. The most common being the electrospinning and microemulsion methods (Putz *et al*., 2015). More facile methods, include direct co-precipitation using $AgNO_3$ and potassium-, hydrogen- or sodium chloride in mixed solvents of water and different alcohols. Depending on the solvent type and reaction conditions, either spherical, plate or rod-like NPs in the size range 10 nm – 300 nm can be prepared (Tiwari and Rao, 2008).

The biosynthesis of Ag and AgCl NPs has tended towards the use of one-step reactions with a decrease in strong reducing agents. Lorestani *et al*. (2015) reported the one-step green synthesis of silver nanoparticle-carbon nanotube reduced-graphene oxide composites using mild reduction in a hydrothermal reaction. Ag and AgCl NPs are also commonly produced through phytosynthesis. An aqueous extract from needles of *Pinus densiflora* (red pine) was used as the reducing agent through a photo-reduction process. This produced NPs that were capable of use as plasmonic photocatalysts (Kumar *et al*., 2016).

Properties and Applications of Silver and Silver Chloride Nanoparticles

Ag and AgCl NPs have many unique properties, including large surface area, many shape varieties, surface charges and coatings, state of agglomerations, dissolution rate as well as highly efficient electrical conductivity (Wei *et al*., 2015). It is well documented that the shape of these NPs dramatically affects these properties. Common shapes utilized in the biomedical field include spherical NPs, nanowires, nanorods, nanoplates, and nanocubes (Rycenga *et al*., 2011). Research has shown that the biological effects of Ag NPs are dependent on the magnitude of the surface charges of their surface coating, which directly impacts how they interact with biological systems (Reidy *et al*., 2013). Dissolution of Ag and AgCl NPs because of surface oxidation leads to the production and release of ionic silver. The rate of dissolution is determined by the chemical and surface properties of the NPs as well as their size. It is also further affected by the nature of the surrounding medium (Mishra *et al*., 2014).

Ag NPs are some of the most widely used materials in nanotechnology today. Owing to their unique optical, electronic, and antibacterial properties, Ag NPs have been widely used in biosensing (Kumar-Krishnan *et al*., 2016), photonics (Hu and Chan, 2004), electronics (Alshehri *et al*., 2012) and antimicrobial (Fernández *et al*., 2008) applications. The antiviral properties of Ag NPs have been well documented. Ag NPs have been shown to inhibit bacteriophage φX174, murine norovirus, adenovirus serotype 2 (Park *et al*., 2014), A/Human/Hubei/3/2005 (H3N2) influenza virus (Xiang *et al*., 2013), herpes simplex virus, human parainfluenza

virus (Gaikwad *et al*., 2013) in addition to the human immunodeficiency virus (Lara *et al*., 2011).

These antimicrobial properties allow Ag and AgCl NPs to be incorporated into multiple medical devices. These include wound dressings, tissue scaffolds, medical catheters, contraceptive devices, bone prostheses and coatings (Amendola, Polizzi and Meneghetti, 2007; Ge *et al*., 2014). Antimicrobial properties also allow for use in a wide range of consumer products, such as textiles, cosmetics, toothpaste, lotions, detergents, home appliances and food storage containers (Kessler, 2011; Thomas *et* al., 2007). The electronic applications of Ag and AgCl NPs span the preparation of active waveguides in optoelectronics, nanoelectronics, inks for printed circuit boards, battery-based intercalation materials, data storage, nonlinear optics and integral capacitors (Jeong *et al*., 2015; Kim *et al*., 2007; Lei *et al*., 2014). The large surface area as well as anisotropic nature of these NPs promotes an increased surface reactivity. This allows for the use of Ag NPs and Ag-inclusive nanocomposites for the catalysis of many reactions. These include CO oxidation (Khan *et al*., 2015), photodegradation of gaseous acetaldehyde (Hu *et al*., 2009), the reduction of p-nitrophenol to p-aminophenol (Zhang *et al*., 2012) and photo-oxidation in photographic material (Husein, Rodil, and Vera, 2005).

2.2.2 Semiconductor Nanoparticles

The focus of much nanotechnological research has been geared towards semiconductor nanoparticles; mainly due to their size- and shape-dependent physical and optical properties (Karim *et al*., 2014). The appeal of semiconductor NPs lies not only in their reduced cost of synthesis but more importantly, the conditionality of their optoelectronic properties as a function of size, morphology and surface chemistry. This leads to novel and improved applications in multiple areas such as optoelectronics, material science, chemical and electrical engineering, and biomedicine (Kim *et al*., 2003).

Lead Sulphide Nanoparticles

PbS is an important IV-VI group semiconductor. It has attracted much scientific attention because of its uniquely small direct-band gap (0.41 eV) and large excitonic Bohr radius of 18 nm (Karami, Ghasemi and Matini, 2013). Any NP with a size smaller than that of its Bohr's radius is considered a quantum dot. PbS NPs thus have size-dependent optical properties and have been shown to be tuneable light absorbers and emitters in optoelectronic devices such as light-emitting diodes (LEDs) and quantum-dot lasers (Wattoo *et al*., 2012). They have been shown to exist in a variety of highly structured but also amorphous morphologies, which both play a major role in the scope of their application. These morphologies include nanocrystals, nanorods, dendrites, nanotubes, star-shaped, nanocubes, and flower-like nanocrystals (Dong *et al*., 2006; Karim *et al*., 2014)

Synthesis of Lead Sulphide Nanoparticles

Currently, the synthesis of PbS materials of high quality and purity utilises lead oxide and bis(trimethylsilyl) sulphide as precursors in an energetically taxing process. This reaction is highly air-sensitive and extremely toxic (Liu *et al*., 2009). Other solvothermal methods have also been developed and optimized to occur at room temperature, with the use of octadecene and oleic acid as the reaction medium and 2,2-dithiobis(benzothiazole) as the reducing agent (Karim *et al*., 2014). Due to the strong influence of size and shape on the optical properties of PbS NPs, much attention has been placed on controlling these parameters to optimally fine tune NPs for specific application. One such process is the surfactant-assisted homogeneous hydrolysis reaction route for the preparation of PbS nanorods using lead acetate as the precursor, thioacetamide as the reducing agent and sodium dodecyl sulphate as surfactant (Li *et al*., 2007).

Limited published data is available on the green synthesis of PbS NPs. The intracellular biosynthesis of stable PbS NPs by a marine yeast, *Rhodosporidium diobovatum* has been reported (Seshadri, Saranya and Kowshik, 2011). When challenged with Pb ions, *Torulopsis* sp., were also shown to synthesize intracellular PbS NPs that exhibit unique semiconductor properties (Kowshik *et al*., 2002).

Extracellular production of spherical PbS NPs using the phototrophic bacterium, *Rhodobacter sphaeroides* was reported by Bai and Zhang (2009). The bacterium was immobilized within 3 mm polyvinyl alcohol beads and exposed to Pb salts in solution to produce nanospheres with an average size of 10.5 ± 0.15 nm.

Properties and Applications of Lead Sulphide Nanoparticles

Semiconductor NPs possess physical properties that are intermediate between those of the elemental metals and the bulk solid. Due to the correlation between synthesis methods and the resulting properties of the NPs, the synthesis of these NPs is the subject of intense research (Jang *et al*., 2010). The potential applications of PbS NPs are vast. These include ion-selective sensors, photoconductors, solar cells, optoelectronic and photo voltaic devices, infrared (IR) detectors and biosensors (Feng *et al*., 2004). In semiconductor NPs, especially PbS NPs, when the diameter of the NP is smaller than the dimension of the exciton Bohr's radius, unique physical and chemical properties emerge due to the quantum confinement effect (Kim *et al*., 2003). A decrease in NP size results in a blue shift of the UV-Vis-NIR spectral peaks, which has implications in the design and fabrication of novel electronic devices as well as more efficient solar cells (Cao *et al*., 2006). PbS NPs have shown to be promising in their application in electrochemical DNA hybridization analysis assays. They have been used as a marker to label known oligonucleotide sequences and employed as DNA probes to detect single-stranded DNA based on a specific hybridization assay (Zhu *et al*., 2004).

2.3 Nanoparticle Formation and Growth

Even though NMs have been utilized and synthesized for many years, the exact mechanisms for formation and growth of these particles remains theoretical (Thanh, Maclean, and Mahiddine, 2014). This process has been described through the LaMer burst nucleation (LaMer, 1952), to explain the formation of singular atomic clusters, followed by the process of Ostwald ripening (Ostwald, 1900), used to describe the change in NP size.

2.3.1 Mechanisms of Formation and Growth

Nucleation is the process by which zerovalent atoms, which are free in solution, combine to produce a thermodynamically stable cluster. A supercritical nucleus capable of further growth is formed when the cluster exceeds its critical size. This is determined by the competition between the aggregate curvature and the free energy favouring growth of the new phase (Tojo, Barroso and de Dios, 2006). The first proposed theoretical mechanism for nucleation and growth was the LaMer mechanism in 1952. It defines the conceptual separation of reduction, nucleation and growth into separate stages (LaMer, 1952). This mechanism is divided into three processes: (i) a rapid increase in the concentration of free atoms in solution, (ii) the atoms forming clusters undergo "burst nucleation" which leads to the dramatic decrease in free atoms, (iii) the growth of stable particles under the control of the diffusion of free atoms through the solution via Ostwald ripening or coalescence. These stages are shown in Figure 2.2, where the concentration of free atoms is plotted as a function of reaction time (Thanh, Maclean and Mahiddine, 2014).

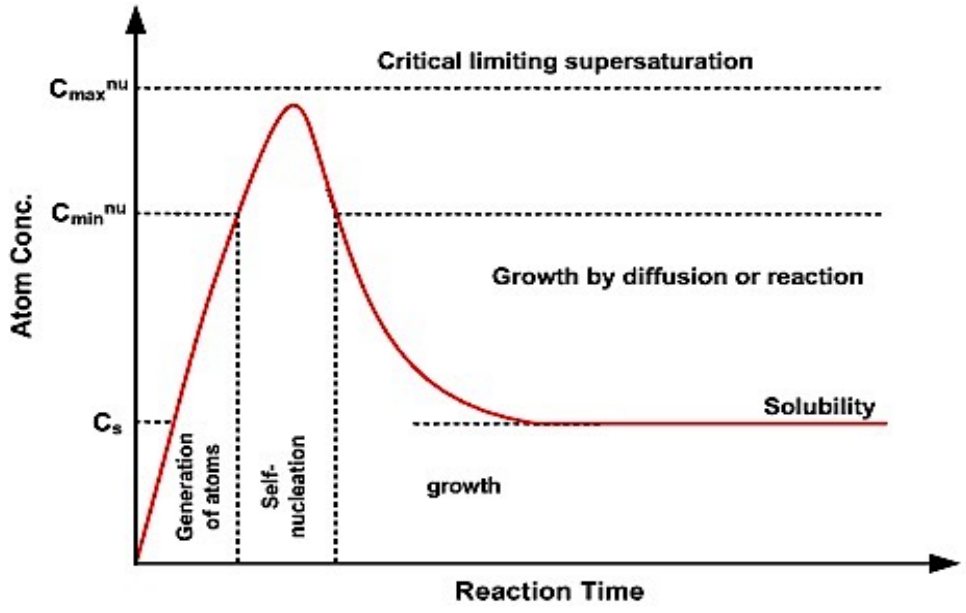

Figure 2.2. Schematic illustration of the nucleation and growth process of nanocrystals in solution. Precursors are initially dissolved in solvents to form free atoms. The generation of nuclei follows and the growth of nanocrystals occurs via the aggregation of nuclei through either Ostwald ripening, coalescence or oriented attachment (LaMer and Dinegar 1950).

Ostwald ripening is a spontaneous growth mechanism driven by a change in the solubility of NPs (Figure 2.3a). Changes in solubility are highly dependent on the NPs core size (Baldan, 2002). The high solubility and surface energy of smaller NPs within the solution allow them to redissolve. Thereafter, the growth of larger particles, through redissolved atoms, leads to an even larger single domain NP (Baldan, 2002). Coalescence and orientated attachment are growth mechanism phenomena that occur through the collision of particles. Coalescence occurs through the collision of NPs resulting in lattice planes that are randomly orientated between domains (Nair and Pradeep, 2002). Orientated attachment however, occurs through the collision of crystallographically aligned NPs in suspension (Figure 2.3b). Alternatively, coalescence occurs first, followed by the rotation of misaligned NPs in contact towards low-energy interface configurations. This leads to the perfect alignment of lattice planes (Lee *et al*., 2005).

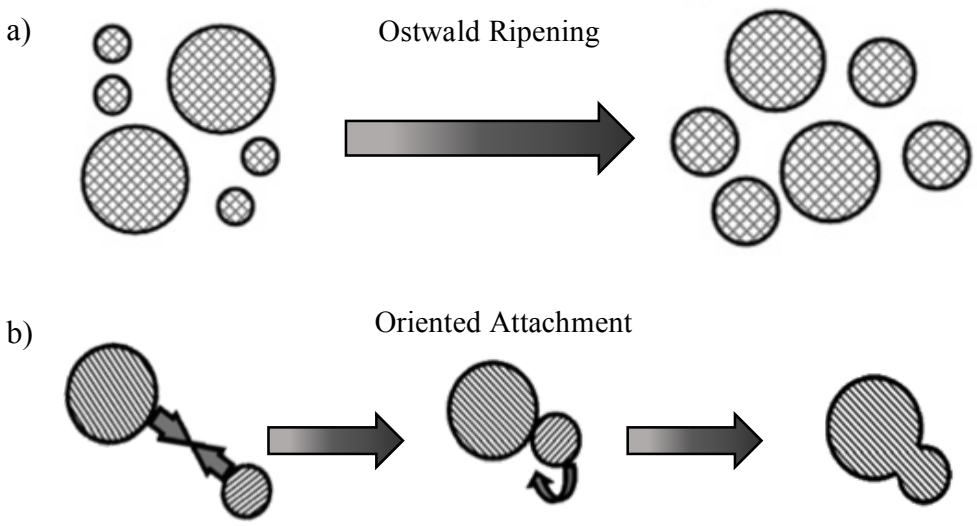

Figure 2.3. Schematic illustration of controlled nanoparticle growth. (a) Ostwald ripening mechanism in which smaller nanoparticles redissolve into solution to allow formation of a larger nanoparticle. (b) Oriented attachment mechanism whereby the collision and spontaneous self-organization of adjacent particles results in a common crystallographic orientation, followed by the joining of these particles at a planar interface. Image adapted from Zhang *et al*. (2010).

NMs can be categorized as isotropic (identical in all directions) or anisotropic (having different values when measured in different directions) in nature (Sajanlal *et al*., 2011). In contrast to isotropic NPs, anisotropic NPs give rise to novel features and unique physicochemical properties, primarily due to the number of step edges and kink sites on the NP surface, as well as higher surface area-to-volume ratio. For example, polyhedral Au NPs that exhibit high-index facets display excellent optical and catalytic properties (Rao, 2010). Au nanorods with varying ratios of length and width display different plasmon bands. Differences in plasmon bands within a single particle shape have direct implications in sensing, catalytic and SERS applications (Lu *et al*., 2009). Similar effects have been observed for branched Au NPs with multiple tips such as nanoflowers and nanostars.

Many anisotropic NPs have been synthesized to date. These include, nanobelts, nanosheets, nanorods, nanowires, nanotubes, nanohexagons, nanotriangles and nano-urchins (Lu *et al*., 2009; Wu, Yang and Wu, 2016). Anisotropic NPs not only provide an interesting system for studying the growth mechanism of NPs but are also useful for the investigation into the fundamentals of shape- and size-dependent characteristics of NMs (Lee *et al*., 2014). The morphology and form of NMs has a substantial effect on the properties of the material and thus the intended application.

Generally, NP growth occurs in either a thermodynamically controlled or kinetically controlled manner (Sajanlal *et al*., 2011). Thermodynamic growth often results in uniform growth of all crystal facets and subsequent formation of spherical structures (Figure 2.4). In the case of kinetically controlled growth, preferential and directional growth occurs that in turn results in the anisotropic growth, or growth in different crystal facets (Lee *et al*., 2014). In the chemical synthesis of anisotropic Au NPs, thermodynamically controlled nucleation and growth occurs initially to form spherical NPs. The subsequent preferential binding of surfactant molecules to specific crystal facets or planes occurs in a kinetically controlled manner (Lu *et al*., 2009). CTAB is shown to bind to the {100} crystal plane of Au NPs, with growth being continued in one dimension until all reagents and precursors have been exhausted. This then leads to the formation of Au hexagonal prisms or nanorods.

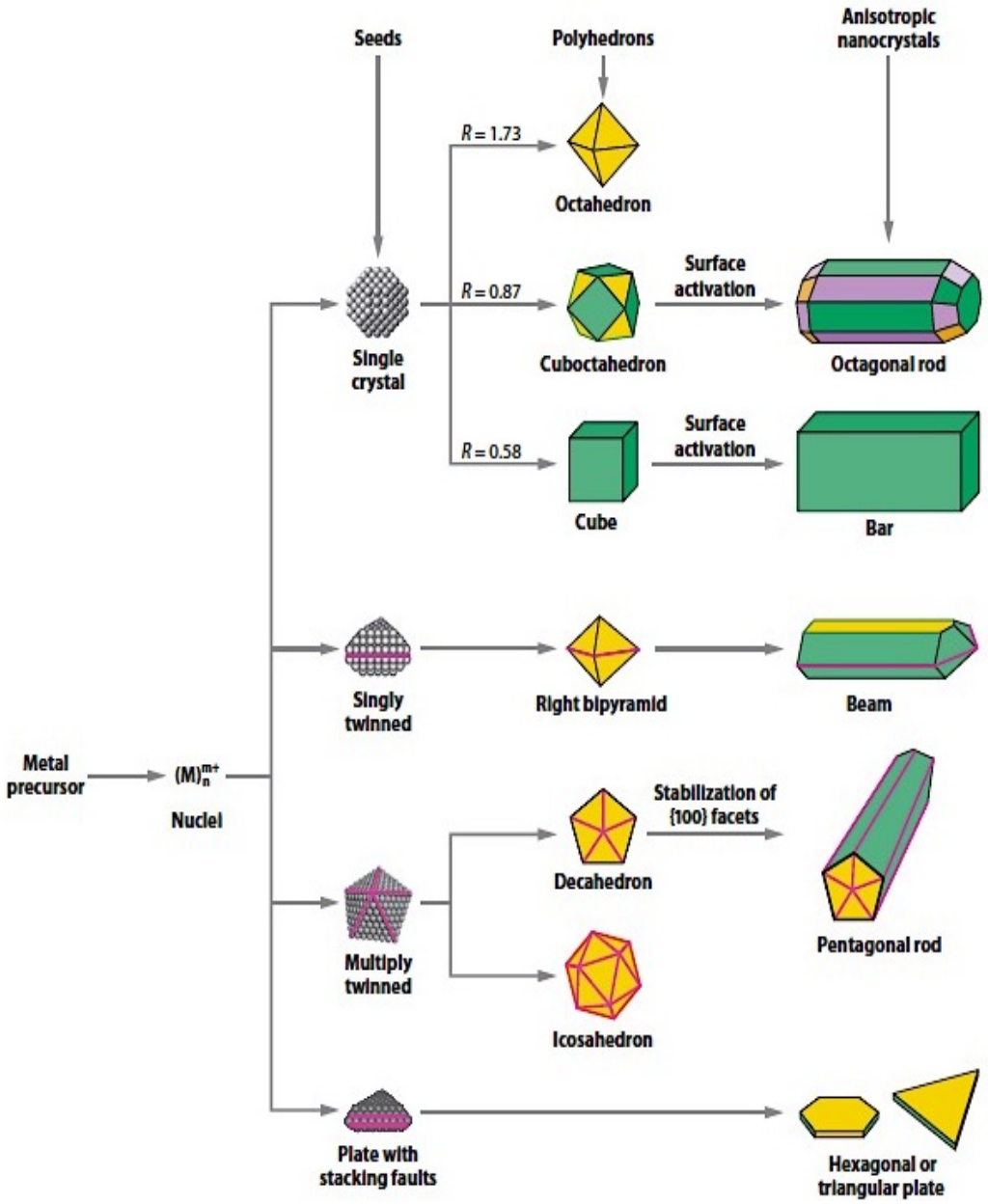

Figure 2.4. Schematic illustration showing the various stages of the reaction that leads to the formation of nanoparticles with different shapes. After nucleation and growth, stacking faults in the seeds results in plate-like structures. Green, orange, and purple represent the {100}, {111}, and {110} facets, respectively. The parameter R is defined as the ratio between the growth rates along the {100} and {111} directions. Twin planes are delineated in the drawing with magenta lines (Lu *et al*., 2009).

2.4 Structure of Nanoparticles

Nanomaterials, as with most materials, can be classified into several different categories, including distinct manufacturing, properties and applications. The properties that NPs are most frequently characterized into are their dimensionality, morphology, composition, purity, and level of aggregation or agglomeration (Tiwari, Tiwari, and Kim, 2012). NPs are also grouped into metals, insulators and semiconductors. This grouping however, leads to the exclusion of CBNs and other organic NPs. NPs can therefore also be classified into organic and inorganic or further divided into engineered (Au NPs), incidental (combustion reactions) and natural (proteins and viruses) NMs (Glezer, 2011). NMs can exist as zero (0-D), one (1-D), two (2-D) or three (3-D) dimensional structures depending on the number of dimensions that fall into the 1-100 nm size range (Figure 2.5).

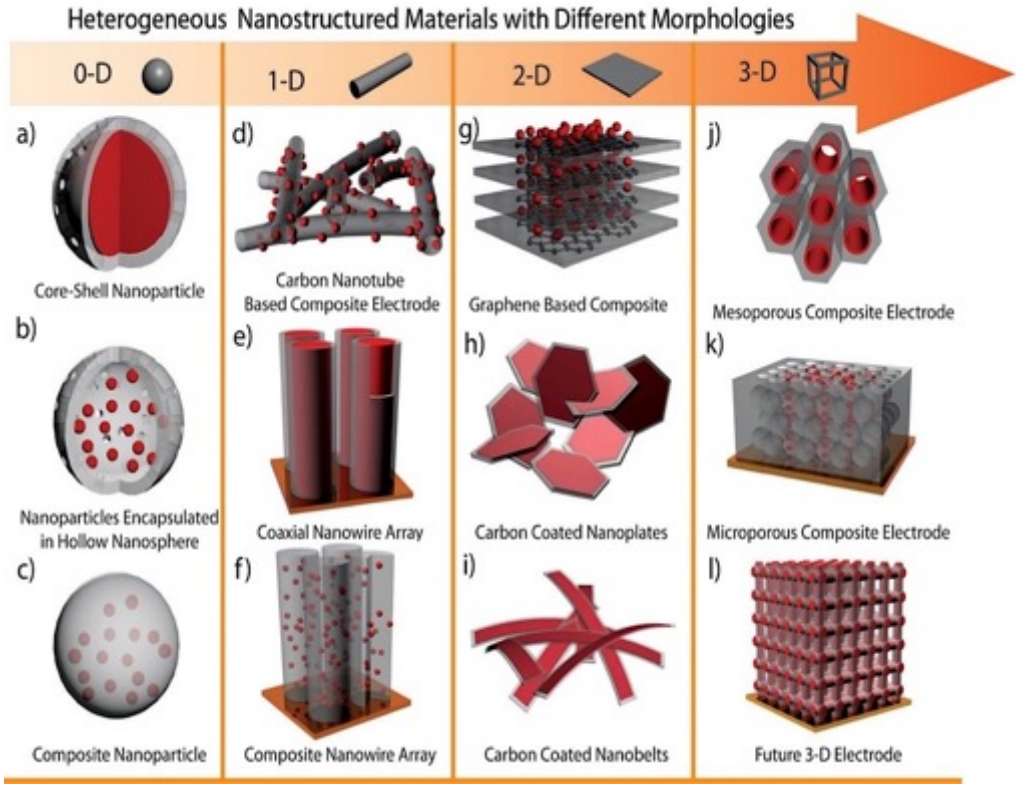

Figure 2.5. The classification of heterogeneous nanomaterials based on their structural complexity. Zero-dimensional (0-D), one-dimensional (1-D), two-dimensional (2-D), three-dimensional (3-D) as well as the even more complex hierarchical 3-D nanostructured networks and nanocomposites. (2016, April 27). Image retrieved from http://www.scs.illinois.edu/murphy/Ran/research/edu1.html.

Zero-dimensional NMs include nanoclusters, quantum dots and NPs in suspension. One-dimensional NMs are within the 1-100 nm size range in only one direction; these include nanorods, nanowires and nanotubes. Two-dimensional NMs comprise nanoplates, nanofilms or sheets with nanometre thickness. The structural elements in 0-D, 1-D and 2-D can either be suspended in a solvent or dispersed into a macroscopic matrix or substrate (Sajanlal *et al*., 2011). Three-dimensional NMs include all the structural elements of 0-D, 1-D and 2-D, which are in close contact with each other, to form nanopowders or multi-layered nanocomposite polycrystalline materials (Tiwari, Tiwari and Kim, 2012). These NMs can additionally either be homologous or hybrid heterologous structured materials. By controlling the experimental parameters such as precursor concentration, reducing agents, stabilizer and reaction conditions, it is therefore possible to control the shape of NPs

2.4.1 Effect of Nanostructure Shape, Size and Surface Chemistry on Metal-based Nanomaterials

Each of the properties of NPs depends on the type of motion that its electron can perform, which is determined by their spatial confinement. Therefore, the optical properties of colloidal metal NPs in the UV-Vis-NIR range is dictated by the LSPR (Lu *et al*., 2009). LSPR occurs in metal NPs through the collective oscillation of free surface electron changes which is driven by a specific wavelength of light (Figure 2.6) (Jain *et al*., 2006). When the incoming electromagnetic wave matches the frequency of the electron cloud, LSPR occurs and light of that specific wavelength is absorbed (Myroshnychenko *et al*., 2008). The frequency as well as the intensity of the resonance is determined by three factors: (a) the innate dielectric property of the metal NP, (b) the dielectric constant of the medium in which the metal is dispersed, (c) the pattern of surface polarization (Sajanlal *et al*., 2011). Correspondingly, any differences in shape or size of the NP can alter the surface polarization which in turn leads to a variation in the plasmon resonance (Lu *et al*., 2009). The interest in NPs with these characteristics is driven by their potential for unique application.

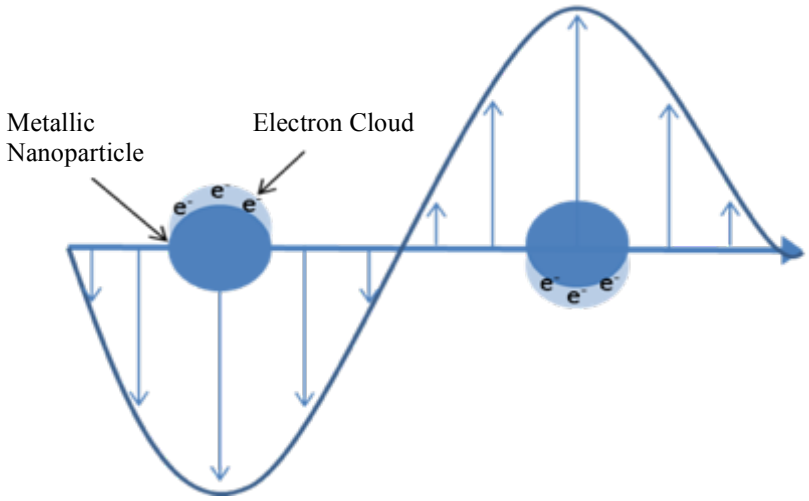

Figure 2.6. Schematic illustration of the LSPR of a metallic NP. The surface electron cloud oscillates in response to an appropriate wavelength of light. When wavelength of light matches the frequency of the electron cloud, LSPR occurs. Image retrieved from http://nanohybrids.net/pages/plasmonics.

Noble metal nanorods are well-placed to demonstrate the shape- and size-dependent LSPR of metallic NPs. As demonstrated by Nelayah *et al*. (2007), the UV-Vis-NIR spectrum of Au nanorods does not only show one resonance peak but rather two. Nanorods are more easily polarizable on the longitudinal axis, therefore the LSPR occurs at a higher wavelength and consequently a lower energy (Figure 2.7). For other anisotropic Au NPs such as nanoplates or nanoprisms, the LSPRs are generally divided into distinctive dipole and quadrupole plasmon modes (Nelayah *et al*. 2007). The LSPR can also generate a localized electric field within a few nanometres of the NPs surface. This is regarded as a near field effect that can enhance the Raman scattering cross sections on markers conjugated to the surface of the NPs (Israelsen, Hanson and Vargis, 2015). In terms of anisotropic NPs, the enhancement concerns the charge density localization formed at the vertex or outer tip of a NP. After the excitement of the free electron on the vertex of NPs by an electromagnetic field, a strong highly localized electromagnetic field develops leading to a large field enhancement. This phenomenon is responsible for the high SERS activity of anisotropic NPs (Lee *et al*., 2014).

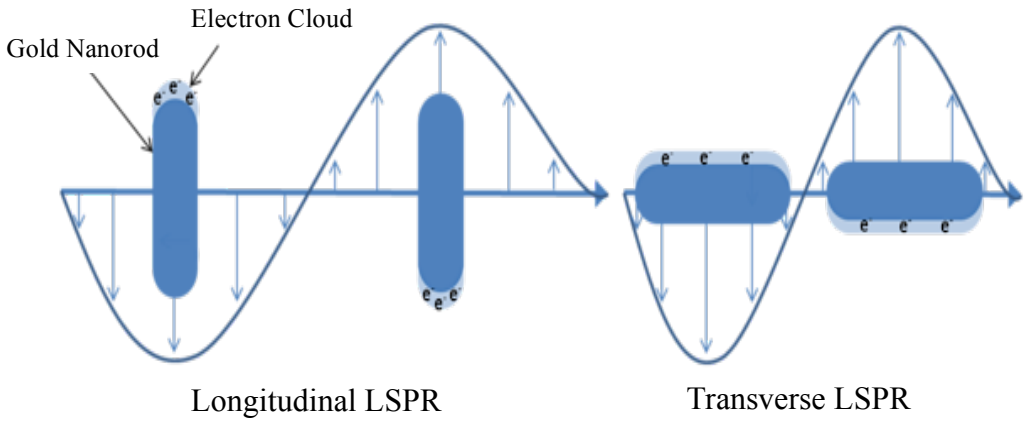

Figure 2.7. Schematic illustration of the two LSPRs of Au nanorods. The surface electron cloud oscillates along the transverse as well as longitudinal axis in response to an appropriate wavelength of light. Image retrieved from http://nanohybrids.net/ pages/plasmonics.

The large surface area to volume ratio of NPs also impacts its chemical reactivity. As reported by Jang and co-workers (1997), the rate of photochemical reactions of organic molecules absorbed on to the surface of Ag NPs is as a result of differing surface geometry. For certain reactions, Au NPs which were considered to be chemically inert have been found to be a highly efficient catalyst at sizes below 5 nm. Noble metal NPs involved in catalysis allow for lower reaction temperatures which is important for the development of energy-efficient green processes (Hvolbaek *et al*., 2007). NPs allow for an increased site for reactivity by increasing number of edges, corners, facets and faces. Such reactions thus have an increase in selectivity which leads to highly controlled catalytic activity. Such is the case for palladium NPs which showed increased catalytic activity for the hydrogenation of butyne-1,4-diol and of styrene oxide (Telkar *et al*., 2004). Even though various factors responsible for the growth of nanoparticles are known, the exact mechanism for growth lacks evidence. Anisotropic NPs do not only provide an interesting system for studying the growth mechanism of NPs but are also useful for the investigation into the fundamentals of shape- and size-dependent characteristics of NMs.

2.4.2 Methods of Nanoparticle Synthesis

Currently, a myriad of chemical, physical, biological and hybrid methods are available for the synthesis of dimensionally controlled NPs with high quality, as shown in Table 2.1. Traditionally, NPs are produced by chemical and physical methods following either the "top-down" or "bottom up" synthesis approaches respectively (Dhand *et al*., 2015).

The physical, or "top-down" methods for NP synthesis involves the application of mechanical pressure, high energy radiations, thermal radiation or electrical energy to result in the evaporation, melting, condensation or abrasion of materials to produce NPs. These methods have the advantage of being solvent-free and produce monodisperse NPs, but often involve a high amount of waste production and are usually very energetically taxing and thus not usually very economically viable (Daraio and Jin, 2012). The fundamentals of chemical NP synthesis are based on the "bottom-up" approach. NPs are therefore fabricated from their inherent building block: atoms and molecules. Chemical methods rely on the reduction or decomposition of materials and subsequent formation of NPs (Lu *et al*., 2009).

The conventional physiochemical methods of NP synthesis often require the use of high-energy inputs, expensive precursors and the addition of organic solvents. Furthermore, they are limited by the environmental pollution caused by heavy metals and toxic effluents. NM synthesis via biological methods is therefore at the forefront of green synthesis. These methods have advantages in nontoxicity, reproducibility, well-defined morphologies and easy scaling-up (Singh *et al*., 2016). More specifically, several microorganisms such as bacteria, fungi and plants and their biomolecules, have been explored to produce NPs. Biological methods are thus broadly divided into synthesis using biomolecules as templates, using plants and plant extracts as well as using microorganisms for NM synthesis.

Table 2.1. Summary of nanoparticle synthesis methods.

Synthesis type	Nanoparticle type	Principle	Methods	Advantages	Disadvantages	References
Physical	Carbon-based NMs, metal-based NMs, nanocomposites	Application of mechanical pressure, high energy radiations, thermal radiation or electrical energy to start materials	High-energy ball milling, laser pyrolysis, laser ablation, physical vapour deposition and melt mixing	Absence of chemical reagents, lack of contaminants, uniform distribution in thin films	Spatial limitations, high energy input, costly equipment, reduced quality	(Daraio and Jin, 2012; Duan, Wang and Li, 2015; Umer *et al*., 2012)
Chemical	Carbon-based NMs, metal-based NMs, nanocomposites	Chemically-driven reduction or decomposition, nucleation and stabilization	Sol–gel method, hydrothermal, chemical vapour, microemulsion technique	High controllability and reproducibility, well-understood, can be eco-friendly	Toxic chemical effluent and waste, high energy input, costly	(Dahl, Maddux, and Hutchison, 2007; Iravani *et al*., 2014; Lu *et al*., 2009)
Biological	Metal-based NMs, nanocomposites	Bacteria, fungi and plants (biomass or extracts), as well as their biomolecules	Exposure of bio-reductants to start materials	Nontoxicity, biocompatible, environmentally benign, reproducible, easy scaling-up	Mechanism not fully understood, polydispersity, prolonged reaction time	(Hulkoti and Taranath, 2014; Singh *et al*., 2016).

2.5 Principles of Green Chemistry in Nanotechnology

Nanotechnology is still currently in its "discovery phase" in which novel materials are being synthesized and characterized. Within this phase, research is predominantly focused on identifying new properties and applications for materials. Consequently, the evaluation of any unintended or hazardous properties are often overlooked (Dahl, Maddux and Hutchison, 2007). Due to the current and anticipated growth in the production, application and distribution of NMs in industry, the entire design process must also consider processes that minimize hazard and waste production. Green chemistry is the design of chemical-related products and processes that aim to reduce or eliminate the generation of hazardous substances and excess waste in order to provide more sustainable technology (Anastas, and Eghbali, 2010). The 12 principles of green chemistry have already been successfully employed in industries involved in the development of highly functionalized products (Sheldon, 2016). These include computer chips, biodegradable plastics, paint, general catalysis reactions involving metathesis as well as pharmacological agents such as Januvia^{TM} (diabetes type II) and Simvastatin (lowering cholesterol) (Dunn, 2012).

The application of green chemistry to NM synthesis will prove advantageous in the production-level and commercial scale design and development of NMs (Hutchison, 2008). Green nanotechnology strives to discover synthesis methods that eradicate the need for harmful reagents, enhances the overall efficiency, while providing a sufficient volume of final product in an economically viable manner (Sheldon, 2016). It therefore also provides a proactive design scheme that assures NMs are inherently safer by assessing the biological and ecological hazards in tandem with design. This seeks to maximize societal benefits while minimizing impact on the ecosystem (Duan, Wang and Li, 2015). The biosynthesis of NMs encompasses the essence of green chemistry and thus plays a prominent role in guiding nanobiotechnology (Nath and Banerjee, 2013). Many of the principles of green chemistry can be readily applied to the biosynthesis of NMs, as summarized in Figure 2.8. In nearly every case, several of the principles can be applied simultaneously to drive the best design or solution (Rani, 2014).

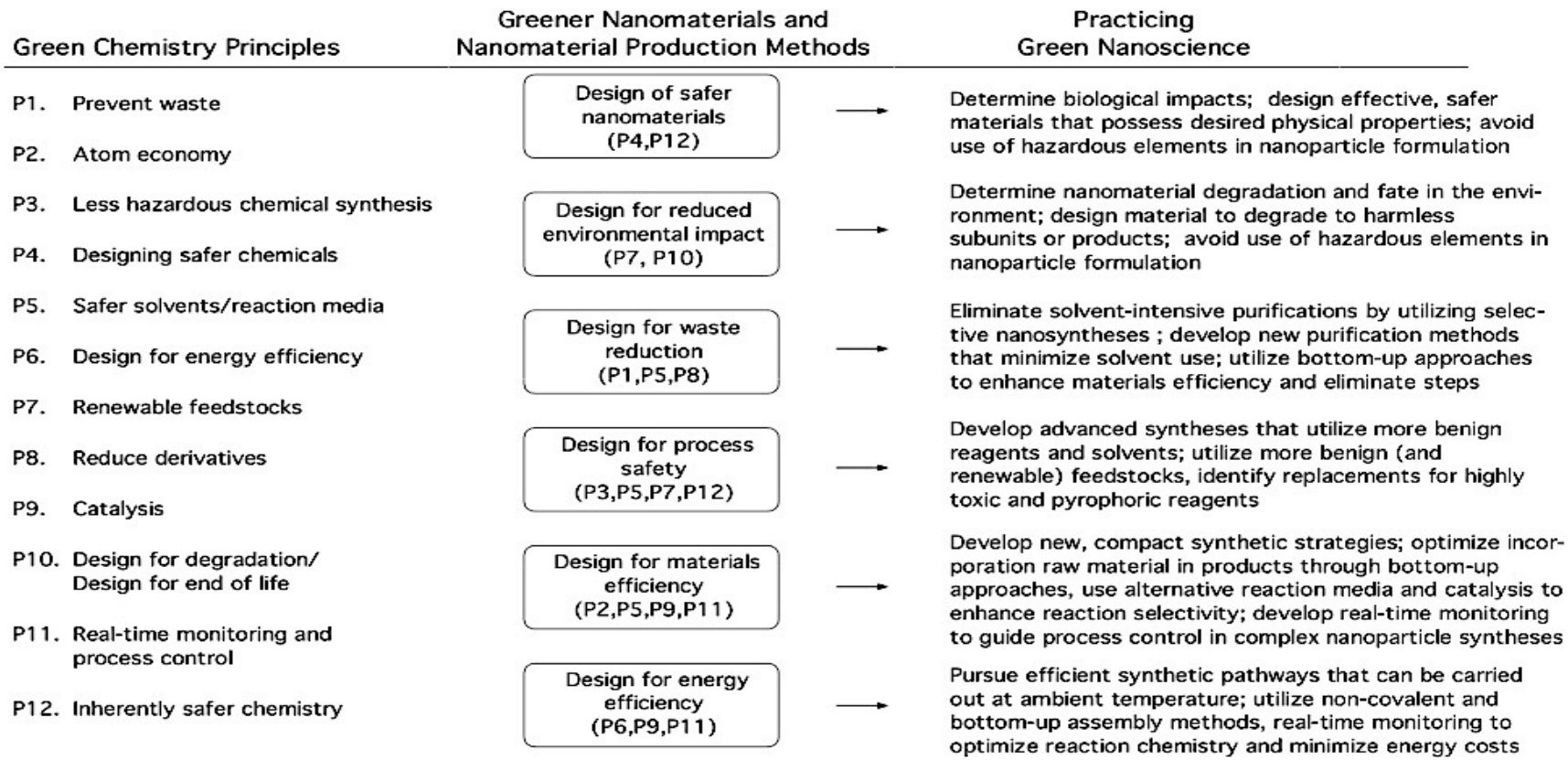

Figure 2.8. Translating the 12 green chemistry principles for application in the practice of green nanoscience. The principles are listed, in abbreviated form, along with the general approaches to designing greener nanomaterials and nanomaterial production methods and specific examples of how these approaches are being implemented in green nanoscience. Within the figure, PX, where X = 1-12, indicates the applicable green chemistry principle. *Note.* Retrieved from "Toward greener nanosynthesis" by J. A. Dahl, B. L. Maddux, and J. E Hutchison, 2007, *Chemical reviews, 107*(6), 2228-2269.

2.6 Microbial Synthesis of Metallic Nanoparticles

Microbial bio-reactors for NP synthesis include actinomycetes, algae, yeast and bacteria. Microorganisms have shown the ability to remove precursor ions from the environment and reduce metals to their elemental form (Ahemad and Kibret, 2013). This is achieved through the use of biomolecules such as enzymes, anionic functional groups, vitamins and reducing sugars. These can also serve as biogenic capping agents that reduce aggregation and therefore stabilize NPs (Kharissova *et al*., 2013). Synthesis using bacteria or bacterial by-products is not only gaining much scientific interest, but also commercial interest. This is because the large-scale synthesis of NPs using bacteria avoids the use of hazardous, toxic, and expensive chemical materials for the synthesis and stabilization processes. This method encompasses green nanotechnology and has many advantages over other microorganisms (Iravani *et al*., 2014). Most significant is providing a novel manufacturing technology that is environmentally benign and is commercially sound in terms of yield, reproducibility and scalable biosynthesis with low costs and at low energy input (Moon *et al*., 2010). Bacterial synthesis of NMs is therefore becoming the preferred method over other microbes.

2.6.1 Biosynthesis of Nanoparticles using Bacteria

Bacterial systems of biosynthesis are separated into extracellular or intracellular mechanisms, depending on the localization of NP synthesis. Intracellular synthesis involves either a specific or general transport mechanisms for ion movement into the cell (Konishi *et al*., 2004). The subsequent reduction and nucleation is followed by growth and capping of NPs to either be excreted back into the environment or compartmentalized within the cell (Nangia *et al*., 2009). Extracellular synthesis can either involve the binding of ions to the cell surface to form NPs or can be accomplished through biomolecules that are expelled into the environment and separated from the bacterial cell biomass (Juibari *et al*., 2015; Shivaji, Madhu and Singh, 2011). An increased ease of purification and suitability for downstream industrial processes are the main advantages of extracellular synthesis (Dhand *et al*., 2015). The most efficient method of bacterial biosynthesis is dependent on the optimization of each specific method for each metal and bacteria, respectively.

Various genera of bacteria have been reported for the synthesis of metallic nanoparticles including *Bacillus*, *Pseudomonas*, *Klebsiella*, *Escherichia*, *Enterobacter*, *Aeromonas*, *Corynebacterium*, *Lactobacillus*, *Pseudomonas*, *Weissella*, *Rhodobacter*, *Rhodococcus*, *Brevibacterium*, *Streptomyces*, *Desulfovibrio*, *Shewanella*, *Rhodopseudomonas*, *Pyrobaculum*, and others (Hulkoti and Taranath, 2014; Li *et al*., 2011; Narayanan and Sakthivel, 2010; Park *et al*., 2010; Park, Lee and Lee, 2016; Thakkar, Mhatre and Parikh, 2010). Inorganic metal NMs synthesized in different bacteria are summarized in Table 2.2. It should be noted that this is not an exhaustive list as other synthesized metal NMs including Fe, Au, Hg, Pb, Pd, Ag, Se, TeO, TiO, Co, Li, Ni, Pd, Pt, Rh, Ru etc. have been reported.

Table 2.2. List of the bacteria employed for the synthesis of metal nanoparticles.

Bacteria	Metal	Size (nm)	Reference
Pseudomonas stutzeri	Ag	~200	(Klaus *et al*., 1999)
Morganella sp.	Ag	20 - 30	(Parikh *et al*., 2008)
Rhodopseudomonas palustris	$CdSO_4$	6 - 11	(Bai *et al*., 2009)
Escherichia coli	CdS	2 - 5	(Sweeney *et al*., 2004)
Actinobacter spp.	Fe_3O_4	10 - 40	(Bharde *et al*., 2005)
Shewanella algae	Au	10 - 20	(Konishi *et al*., 2004)
Rhodopseudomonas capsulata	Au	10 - 20	(He *et al*., 2007)
Escherichia coli DH5α	Au	25 - 33	(Du *et al*., 2007)
Thermomonospora sp.	Au	8	(Ahmad *et al*., 2003)
Rhodococcus sp.	Au	5 - 15	(Ahmad *et al*., 2003)
Klebsiella pneumoniae	Ag	5 - 32	(Shahverdi *et al*., 2007)
Pseudomonas aeruginosa	Au	15 - 3	(Husseiny *et al*., 2007)
Shewanella oneidensis	Ur(IV)	-	(Marshall *et al*., 2006)
Recombinant E. coli	Gd, Pr, Co	-	(Park *et al*., 2010)

Although fabrication of NPs using microbial systems is highly researched, there is a knowledge deficiency in the underlying mechanisms of synthesis. This has led to challenges in developing highly controlled synthesis reactions. Much research is now

going into the identification of specific mechanisms to take full advantage of microbial synthesis of NPs (Duan, Wang and Li, 2015). In a recent study, Johnston *et al*. (2013) illustrated the synthesis of Au NPs by the bacterium *Delftia acidovorans*. NP synthesis was attributed to a small non-ribosomal peptide, delfibactin. Production of delfibactin was correlated to the resistance mechanism of *D. acidovorans* to toxic Au^{3+} ions. This was the first report of a probable mechanism responsible for the formation of metal NPs and how it can vary in different bacteria. Investigations into bacterial synthesis suggest the mechanisms to rely mostly on enzymatic reduction of metal ions and protein capping of NPs (Zhang *et al*., 2011). He *et al*. (2007) suggested a different mechanism for NP synthesis, through the reduction of Au^{3+} ions via an NADH-dependent reductase. The results demonstrated that spherical Au NPs in the range of 10 nm – 20 nm were observed at pH 7 whereas anisotropic nanoplates were observed at pH 4. The nitrate reductase enzyme was also found to be responsible for the synthesis of spherical Ag NPs in *Bacillus licheniformis* (Vaidyanathan *et al*. 2010).

Although the use of wild-type bacteria has been successful in NP synthesis, the use of genetically engineered bacteria has gained much interest. This is due to the development of methods allowing the production of a more diverse range metal NPs. These NPs have a wide array of properties for various applications and are synthesized using only a single bacterial isolate (Park *et al*., 2010). A well-established method of NP synthesis involves the overexpression of certain plant peptides. These include phytochelatins (PC) or metallothioneins (MT), which are used by plants in the detoxification of heavy metals from soil (Cobbett and Goldsborough, 2002). Genetically engineered *E. coli* expressing PC and/or MT has been reported for the synthesis of Cd, Cu, Hg, Pb, and Zn NPs via the complex formation of the metal ions through reduction and metal-binding affinity (Park, Lee and Lee, 2016).

Bacterial synthesis offers several advantages, but the inherent polydispersity of NPs remains a challenge. Much scientific effort has been put forward to develop strategies to fabricate NMs in a large variety of morphologies and sizes while maintaining monodispersity (Dhand *et al*., 2015). This is becoming increasingly evident in the process by which biological synthesis research is conducted (Gurunathan *et al*., 2009).

Recent studies have attempted to increase monodispersity by optimising the critical experimental parameters within stable synthesis systems. The control of the shape and size of NPs has been shown by either varying the environmental growth conditions or altering the functional molecules involved (Singh *et al*., 2016). Gurunathan *et al.* (2009) reported the synthesis of increasingly biocompatible and monodisperse 20 nm Ag NPs. This was achieved by the optimization of the reaction conditions, including pH, temperature, redox conditions, aeration, incubation period, salt concentration, mixing ratio, and level of irradiation.

2.7 Addressing the Call for Green Nanotechnology with Bacterial Biosynthesis

Nanotechnology has the potential to change the way in which the developing world's most critical problems are addressed. In 2005, the United Nations (UN) Millennium Project's Taskforce on Science, Technology and Innovation concluded that, with the use of nanotechnology, the objectives put forward in the Millennium Development Goals (MDGs) can be achieved (Gardner, 2015). These include the reduction of child mortality, improvement of maternal mortality as well as the combat of various diseases, including HIV/AIDS, cancer and malaria (Salamanca-Buentello *et al*., 2005). In parallel with the UN MDGs, The South African National Development Plan (NDP) 2030 aims to eliminate poverty and reduce inequality by 2030 (National Planning Commission, 2012). The main issues it aims to address are; water, electricity and sanitation, quality education and skills development, health-care, employment, a clean environment and adequate nutrition. As a major driving force of much current scientific research, nanotechnology can either directly or indirectly provide solutions in each of these facets (Drexler, 2013). South Africa's NSN was developed to globally position the country as a hub for research and development in the field (Department of Science and Technology, Government Gazette, 2007). The focus areas are health-care, water, energy, chemical and bioprocessing, mining and minerals, and advanced materials and manufacturing. Improved health-care, more specifically primary health-care, is one of the six pillars emphasized. The principal applications of nanotechnology in medicine are in the areas of drug discovery, development and delivery, tissue engineering, diagnostics and testing as well as medical devices and surgical treatments (Daraio and Jin, 2012).

Biologically synthesized NMs are currently being used to develop nanodevices and systems which function to prevent, treat and monitor specific diseases (Sharma *at al*., 2015). Another common problem in developing countries is chemical pollutants in water sources as well as the presence of bacteria and viruses that lead to water-borne diseases. Nano-based water treatment devices have already been developed and are currently being implemented worldwide. These have the potential to remove pollutants and contaminants from water sources (Savage and Diallo, 2005). Various other products such as nanosorbents, nanocatalysts and nanostructured membranes have also been developed and evaluated for this process (Qu, Alvarez and Li, 2013). The NDP also directs attention to the risks of carbon emissions and global warming and thus the need for alternative energy sources such as wind and solar power. The "solar steam device" has been developed and is intended for use in areas of developing countries without electricity. It uses nanoparticles to generate steam with solar energy. On a large scale, the devices have the ability to use sunlight to generate steam for use in running power plants. (Moon *et al*., 2015). Another important aspect of this NDP is to increase foreign direct investment (FDI), which has a direct impact on the economy of the country. An increase in FDI can catalyse industrialization and structural transformation, therefore creating new jobs (Sutton *et al*., 2016). Manufacture and processing of NMs in the country, with the use of locally available raw materials and resources, would create a new sector to attract foreign investment.

The benefits of using green chemistry in the application of NMs have been well vindicated (Anastas and Warner 1998; Duan, Wang and Li, 2015; Dunn, 2012). Moreover, the application of sustainably synthesized biologically-based NM has a highly significant scope of potential in multiple applications and offers even more benefits (Pantidos and Horsfall, 2014). The advantages of bacterial synthesis can thus be applied in the manufacturing and production of NMs in South Africa. Bacterial synthesis has long been used in industrial biotechnological processes and also to provide commercially important products. These include fermented foods such as cheese, wine and yogurt (Heller, 2001). In the mining industry, bacteria are used as bioleaching agents in the extraction of precious metals from ore (Rohwerder *et al*., 2003). Chemical manufacturing of ethanol, acetone and organic acids using bacteria

are a standard practice in the chemical processing industry (Qureshi *et al*., 2000). They are also implicated in the production of multiple pharmaceuticals and nutraceuticals additives such as vitamins, amino acids and sugars such as mannitol, sorbitol, and tagatose (Hugenholtz *et al.,* 2002; Lee *et al*., 2009). The recent popularity of healthy living has further developed the nutraceutical industry, and in turn allowed for the optimization of bacterial synthesis involved in producing many of its raw materials.

The current study seeks to provide a platform by which novel bacterially synthesized NMs can be produced. Due to the extreme environment from which *P. castaneae* (the bacteria of choice in this study) was isolated and cultured, as well as their inherent ability to resist the toxic effects of heavy-metal ions, it is proposed that this bacterium would have the ability to synthesize a range of noble and transition metal NPs. In this, the use of a single bacterial species, such as *P. castaneae*, to produce multiple morphologies, sizes and types of NMs will allow for green nanobiotechnology to take a step forward in realising its potential as a sustainable sector of industry. For NP synthesis methods to become commercially viable, the entire design and process should result in NMs that are non-toxic, biogenic, use significantly less energy and are environmentally safe. Therefore, with the use of frameworks and practical experience from other bacterial synthesis industries, it is anticipated that bacterial synthesis of NMs can lead to South Africa becoming the hub for the commercialization of these products in Africa.

CHAPTER 3: MATERIALS AND METHODS

3.1 Materials

All reagents used in the study were purchased from Sigma-Aldrich (St. Louis, MO, USA). The metal salts, lead nitrate ($Pb(NO_3)_2$), calcium sulphate dihydrate ($CaSO_4 \cdot 2H_2O$), gold (III) chloride trihydrate ($HAuCl_4 \cdot 3H_2O$) and silver nitrate ($AgNO_3$), were purchased as >99 % pure and filter-sterilized using 0.20 μm membrane filter (GVS Filter Technology, ME, USA) prior to use. Sterile de-ionised water (sdH_2O) was used for all experimental work.

3.2 Bacterial Culturing

The strain of *P. castaneae* used in this study was previously isolated from acid mine decant sourced from mine tailings in the West Rand of Gauteng (26°06'26.8"S 27°43'20.2"E) and identified to species level using the Biolog Microbial ID System. *P. castaneae* was cultured from glycerol stocks by streaking out on Luria-Bertani (LB) agar plates (pH 7) that were then incubated overnight at 37 °C. Isolated colonies were used to prepare an overnight pre-inoculum that was further inoculated 1:100 (v/v) into LB broth (pH 7) for the accumulation of biomass. The culture was incubated under continuous shaking on a platform rotary shaker (Labcon, CA, USA) (200rpm) at 37 °C for 24 hours. After incubation, cells were harvested at 5000 x *g* using a Heraeus Microfuge XR1 (Thermo Scientific, MA, USA) for 15 minutes at 25 °C. Both the cell pellet and supernatant were retained for NP synthesis.

3.3 Intracellular Nanoparticle Synthesis

P. castaneae cell biomass was prepared by washing twice in sdH_2O to remove any residual media constituents that could interfere with the intracellular synthesis of NPs. This was done through centrifugation at 3000 x *g* for 5 minutes each. To synthesize PbS NPs, 50 mL of 1 mM $Pb(NO_3)_2$ and 1 mM $CaSO_4 \cdot 2H_2O$ were mixed in equal volumes to which 1 g wet weight of biomass was added. One gram wet weight of biomass was added to 100 mL of 1 mM $HAuCl_4 \cdot 3H_2O$ or $AgNO_3$ for the synthesis of Au and Ag NPs, respectively. As a control, 1 g wet weight of biomass was resuspended in 100 mL of

sdH_2O. The solutions were incubated under continuous shaking on a platform rotary shaker (200 rpm) at 37 °C for 72 hours. During this time, they were observed visually for colour changes indicative of NP synthesis. The expected colour changes were; a white precipitate, pink-purple and yellow-brown for PbS NPs, Au NPs and Ag NPs, respectively.

3.4 Extracellular Nanoparticle Synthesis

Proteins that are secreted out of the bacterial cell into the growth medium are reported to be responsible for the extracellular reduction of metal ions (Iravani *et al*., 2014). These proteins would be present in the retained supernatant which was further processed for NP synthesis. The supernatant was centrifuged twice at 15 000 x *g* for 15 minutes and the pellet, consisting of any remaining cellular debris, was discarded resulting in the formation of a cell-free extract (CFE). For PbS NP synthesis the CFE was added to 1 mM $Pb(NO_3)_2$ and 1 mM $CaSO_4 \cdot 2H_2O$ in a 2:1:1 (v/v/v) ratio. For Au and Ag NP synthesis, the CFE was added to 1 mM $HAuCl_4 \cdot 3H_2O$ and 1 mM $AgNO_3$ in a 1:1 (v/v) ratio respectively. Two sets of controls were included for each synthesis and treated under the same conditions, (i) CFE was added to sdH_2O in a in a 1:1 v/v ratio and (ii) each metal precursor ion solution was added to uninoculated LB broth in a 1:1 v/v ratio. The solutions were incubated under continuous shaking on a platform rotary shaker (200 rpm) at 37 °C for 72 hours. During this time, they were observed visually for colour changes indicative of NP synthesis as previously described.

3.5 Preparation of Samples for Nanoparticle Analysis

Cells were separated from metal solutions by centrifugation at 5000 x *g* for 15 minutes at 25 °C. Both the supernatant and cell pellets were retained for analysis. NPs were separated from media constituents and unreacted metal ions by centrifugation at 20 000 x *g* for 15 minutes. The resulting NP pellets were washed twice with sdH_2O. Thereafter both the cell pellet and NP solutions were sonicated at room temperature for 5 minutes (Scientech Ultrasonic Cleaner, Labotech, SA) to ensure colloidal dispersion by reducing aggregation and agglomeration before each analytical procedure. NPs synthesized both intra- and extracellularly were analysed.

3.6 Characterization of Nanoparticles

3.6.1 Ultraviolet-visible (UV-Vis) Spectroscopy

Preliminary characterization of NP synthesis was carried out by performing a wavelength scan using UV-Vis spectroscopy. The reduction of metal ions and the subsequent synthesis of NPs was initially monitored by the visual observation of a colour change in the solution. The absorbance maxima in the UV-Vis spectra of NPs are attributed to the characteristic LSPRs of each metal NP, but are also dependent on size, morphology and level of aggregation (Myroshnychenko *et al*., 2008). Expected absorbance maxima ranges were between 310-330 nm for PbS NPs (Wang and Yang, 2000), 550-600 nm for Au NPs (Chandran *et al*., 2006) and 420-450 nm for Ag NPs (Maciollek and Ritter, 2014). Following an appropriate dilution in sdH_2O, absorbance measurements from 200nm – 900 nm were carried out at a resolution of 1 nm on the Jasco V-630 UV-Vis spectrophotometer (Jasco Analytical Instruments, MD, USA).

3.6.2 Differential Interference Contrast (DIC) Microscopy and Fluorescence Microscopy (FM)

All microscopic analysis was completed at the Wits Microscopy and Microanalysis unit. The assessment of the inherent fluorescent properties of metal NPs and their association with bacterial cells (for intracellular NP synthesis) was performed using DIC and FM. For analysis, 10 µL of each experiment or control reaction was drop-cast onto 50 µL of Entellan™ (Merck Millipore, Germany) on a glass slide, a cover slip added and dried overnight at 50 °C. The absorbance maxima obtained from UV-Vis spectroscopy were used as the excitation wavelength for FM using the Olympus BX63 Fluorescence Microscope (Olympus, Tokyo, Japan) fitted with an Olympus DP 80 camera (Olympus, Tokyo, Japan).

3.6.3 Scanning Electron Microscopy (SEM) and Energy-dispersive X-ray Spectroscopy (EDS)

The analysis of the surface morphology, topography and the chemical composition of the biosynthesized NPs was achieved through the use of SEM coupled with EDS. Samples were prepared by drop-casting 100 µl of each experiment or control reaction onto an aluminium stub and allowed to dry overnight at room temperature.

Cells used during synthesis of intracellular NPs were alternatively prepared through fixation. Each cell pellet was immersed in 2.5% glutaraldehyde (Sigma-Aldrich, MO, USA) buffered in a 0.1 M sodium phosphate buffer (pH 7.4) for 1 hour. The pellets were then washed three times in 0.1 M sodium phosphate buffer (pH 7.4) for 10 minutes each. They were further immersed in a 1% aqueous osmium tetroxide (Sigma-Aldrich, MO, USA) solution for 1 hour and washed as described previously. Dehydration of each pellet occurred through a graded alcohol series (30%, 50%, 70%, 90%, 98%, 100% ethanol, 15 min per step). Each sample was spread onto an aluminium stub and sputter coated to a thickness of 15 nm, with carbon (5 nm) using an Emitech K950X turbo pumped evaporator (Emitech Ltd, UK) and either Au/Pd or Cr (10 nm) using the Emitech K550X sputter coater (Emitech Ltd, UK). Cr was used to coat Au-containing samples, while samples containing PbS and Ag were coated with Au/Pd. Samples were analysed on the FEI Nova 600 Nanolab Dual Beam™ SEM/FIB (FEI Company, OR, USA) coupled with an Oxford Inca EDS detector (Oxford Instruments, Abingdon, UK) at 30 kV.

3.6.4 Transmission Electron Microscopy (TEM)

For the evaluation of size, shape and distribution of NPs, 10 µL of each experiment or control reaction was drop-cast onto a holey carbon-coated 200 mesh copper TEM grid (SPI, PA, USA) and dried in a desiccator overnight. TEM micrographs were taken on a FEI Tecnai T12 TEM (FEI Company, OR, USA) fitted with a TVIPS 4K CCD camera (Tietz Video and Image Processing Systems, Gauting, Germany) at 120 kV.

All microscopic images displayed are representative images chosen that include information found in several fields of view. Each image serves as the ‘average’ of multiple rendered images.

3.6.5 Particle Size Analysis

Image Processing

Particle size and distribution analysis was determined using the Particle Analysis tool in ImageJ Image Processing and Analysis Software (NIH, Maryland, USA) on the TEM micrographs (Schneider, Rasband and Eliceiri, 2012).

3.6.6 Powder X-ray Diffraction (PXRD)

Sample Preparation

All experiment and control reactions were flash frozen in liquid nitrogen and thereafter lyophilized using the VirTis BenchTop Pro Freeze Dryer (SP Scientific, Warminster, PA, USA). The resulting powdered samples were thoroughly agitated using the Vortex Genie 2 (Scientific Industries, NY, USA) for 1 minute to ensure even distribution and texture of powder particles.

Powder X-ray Diffraction (PXRD) Analysis

To evaluate the phase formation, crystalline nature, crystal type, purity as well as the structure of NPs, PXRD analysis was performed. Powder samples were loaded onto a zero-background Si sample holder (Rigaku Corporation, Tokyo, Japan). PXRD analysis was conducted at room temperature in a Rigaku MiniFlex600 Benchtop X-ray Diffractometer (Rigaku Corporation, Tokyo, Japan) fitted with a 600W (40Kv; 15 mA) X-ray generator, a counter monochromator to cut X-rays other than Cu Ka X-ray radiation (λ = 1.5406Å), and a high intensity D/tex Ultra high speed 1D detector. The diffractometer was operated at 30 kV with a current of 15 mA and a scanning speed of 1°(2θ) min^{-1}. PXRD patterns were obtained in the 2θ range of 10-90°. MATCH! Phase Identification Software (Crystal Impact, Bonn, Germany) was used for phase identification and comparison of samples to known elemental phases.

CHAPTER 4: RESULTS AND DISCUSSION

Increasing awareness among researchers and industry towards green chemistry and biological synthesis has led to development of environmentally friendly approaches for the production of NMs (Singh *et al*., 2016). When bacteria are incubated in the presence of toxic metals, both intra- and extracellular NPs can be generated as a result of the organisms' inherent defence mechanisms. These mechanisms can thus be exploited as an alternative yet green method for the commercial synthesis of advanced functional NMs (Suresh *et al*., 2010). Environmentally harmful surfactants, solvents and toxins are avoided, the method is highly reproducible, and results in NPs that are highly stable and of various morphologies and sizes. The current study sought to evaluate the propensity of *P. castaneae* for the synthesis of PbS, Ag and Au NMs.

4.1 Visual Confirmation of Nanoparticle Synthesis

The biological synthesis of NPs was accomplished by the separate addition of *P. castaneae* cell biomass and CFE to metal ion precursors. Colour changes or changes in opacity were noted by visual observation in each reaction flasks. Such colour transitions are indicative of an alteration in the metal ion oxidation state and the subsequent formation of NPs (Zhang, Shen and Gurunathan, 2016). The apparent colour of NPs in solution is caused by the LSPR; the interaction between free electrons on the NP surface and the incoming electromagnetic field (Liz-Marzán, 2004). The LSPR and subsequent apparent colour is not only highly dependent on NP size but also on the nature of metal, NP shape, surface chemistry, and aggregation state (Wiley *et al*., 2006). Visual confirmation of bacterial NP synthesis is thus the first point for characterization of metallic NPs. All experimental reactions showed a change in either colour or opacity, except for the Au-CFE reaction, as summarized in Table 4.1. The control reactions including: sdH_2O and biomass, sdH_2O and CFE, sdH_2O and metal ions, as well as LB broth and metal ions, showed no colour change, as expected.

Table 4.1. Confirmation of nanoparticle synthesis based on visual inspection.

Nanoparticle	Biological reagent	Visual traits	
		Before treatment	After treatment
PbS	Biomass	Translucent, white	Opaque, white precipitate
	CFE	Clear, pale yellow	Clearing, lightening
Au	Biomass	Translucent, milky white-yellow	Deep purple
	CFE	Clear, pale yellow	No change
Ag	Biomass	Translucent, white	Pale milky-yellow hue
	CFE	Clear, pale yellow	Yellow-brown

4.1.1 Lead Sulphide Nanoparticles Biosynthesized by *P. castaneae*

The production of a white precipitate in the PbS biomass reaction (inset of Figure 4.1) suggests the bacterial synthesis of a high concentration of larger PbS NPs. The high density of these NPs as well as the weak forces between the NPs and the surrounding medium thus leads to the settling of NM at the bottom of the reaction flask (Liyanage *et al*., 2016). These results are supported by the findings of Truong *et al*. (2011) in which large anisotropic PbS nanorods, nanobelts, nanovelvet-flowers and dendritic nanostructures with similar attributes were chemically synthesized. The increase in transparency of the PbS-CFE solution seen in the inset of Figure 4.1 is a characteristic of the synthesis of smaller (<50 nm) PbS NPs which absorb light in the UV region of the spectrum; thus showing no visible colour change. In a study by Ogawa *et al*. (1997) the chemical synthesis of 1.2 nm – 10 nm PbS NPs resulted in a clear and colourless solution. The changes in colour and opacity indicate that both the *P. castaneae* biomass and CFE could have successfully reduced metal ions to form metallic NPs.

4.1.2 Gold Nanoparticles Biosynthesized by *P. castaneae*

The colouration of a NP solution is dependent on many factors. For smaller (>30 nm) Au NPs, the LSPR causes an absorption of light in the blue-green region

of the spectrum (~450 nm) while light in the red regions of the spectrum (~700 nm) is reflected, yielding a rich red colour (Polte *et al*., 2010). As NP size increases, the SPR wavelength shifts to longer wavelength. Red light is then absorbed and blue-purple light is reflected, yielding solutions with a deep purple colour (Paul *et al*., 2015. As the particle size increases towards the bulk limit, SPR wavelengths move into the IR region and most visible light is reflected, causing a clear or translucent coloured NP solution (Dahanayaka *et al*., 2006). The dark purple colour of the Au NP biomass reaction was therefore indicative of larger particles that may have been polydisperse in nature (inset of Figure 4.2). Similar findings were reported when *Thermus scotodoctus* SA-01 was used for the bioreduction of Au^{3+} ions and yielded polydisperse Au NMs (Erasmus *et* al., 2014). Additionally, the purple colour of the Au-biomass NP solution could be as a result of the increased aggregation of smaller (<50 nm) Au NPs. To date, many morphologies of Au NPs have been bacteriologically produced, these include variably sized nanoplates, nanoprisms, nanorods, nanocubes as well as nanospheres (Murugan *et al*., 2014; Paul *et al*., 2015)

During particle aggregation, the effective particle shape, size, as well as dielectric environment also change, thus a change in the solution colour (Ghosh and Pal, 2007). The localization of the NPs on the *P. castaneae* cell wall can lead to an apparent purple coloured solution. This can occur even though Au NPs of the same size, but not attached to the bacterial cell, would exhibit a red colour. When Au NPs are closely packed within and/or on the bacterial biomass, in close proximity and in high concentration, a similar effect and deep purple colour are displayed (Murugan *et al*., 2014). Au^{3+} reduction is known to be a complex multistep process that is highly dependent on the conditions and kinetics of reaction (Dey *et al*., 2010). The Au-CFE shown in the inset of Figure 4.2 did not result in a colour change. It is likely that the CFE did not have the necessary, or high enough concentrations of bioreductant constituents to allow for Au NP synthesis, as compared to those present in the biomass. Due to a lack of colour/opacity change in the Au-CFE solutions, no further analyses were performed on these reactions.

4.1.3 Silver Nanoparticles Biosynthesized by *P. castaneae*

The yellow-brown colour changes (inset of Figure 4.3) observed in both the Ag-biomass and Ag-CFE solutions are indicative of the bioreduction of Ag^+ ions and the bacterial synthesis of Ag NPs (Gurunathan *et al*., 2009; Parikh *et al*., 2011). Ag NPs in solution display a yellow-brown colour due to a narrow LSPR absorbance band observable in the 350 nm – 600 nm regions (Hussain *et al*., 2011). A slight yellow hue in the Ag-biomass reaction as compared to the darker yellow-brown in the Ag-CFE reaction is consistent with the synthesis of a lower concentration of Ag NPs by the *P. castaneae* cells. If the bioreductants that are released into CFE by the bacteria are present in lower concentrations in the biomass reactions, the bacterial cells specifically, may not be able to efficiently reduce Ag^+ ions to form Ag NPs. Furthermore, the antibacterial properties of Ag and Ag NPs have been elucidated (Suresh *et al*., 2010). The exposure of *P. castaneae* cells to Ag^+ ions, at concentrations higher than the minimum inhibitory concentration (MIC), can thus lead to cell death and therefore decrease the production of the necessary bioreductants.

The formation of NPs only forms a part of the Ag resistance mechanism demonstrated by bacteria (Taylor *et al*., 2016). Gupta and coworkers (1999) described the *sil* operon, which is the genetic and molecular driving force behind Ag resistance found in *Salmonella typhimurium*. This mechanism allows for the efflux of Ag^+ ions into and out of the cells. The presence of such a mechanism in *P. castaneae* could then lead to the dual detoxification of Ag through metal efflux by the bacterial cells and also through NP formation by bioreductants excreted into the CFE. The constituents of the CFE and biomass of various microorganisms have been previously studied (Binupriya *et al*., 2010; Krishnan, Narayan and Chadha, 2016). The differences in the presence or absence of protein/peptide, carbohydrates, lipids and DNA, in varying concentrations in both the biomass and CFE are substantial (Erasmus *et al*., 2014). The dissimilarity of constituents of the bioreductants used plays an important role not only in whether or not metal ions are reduced, but also in the shape, size and aggregation state of the biosynthesized NPs (Binupriya *et al*., 2010).

4.2 Nanoparticle Characterization

4.2.1 Ultraviolet-visible (UV-Vis) Wavelength Scan

After performing visual observations for colour change, the reaction solutions were subjected to UV-Vis spectroscopy measurements to determine the absorbance maxima of metallic NPs biosynthesized by *P. castaneae*.

Lead Sulphide Nanoparticles Biosynthesized by *P. castaneae*

PbS material in its bulk form exhibits absorption in the IR region of the electromagnetic spectrum with an onset at 3020 nm (Cao *et al*., 2006). Two distinct features were observed in the PbS NP UV-Vis spectra; well-defined peaks were centred at ~320 nm and ~550 nm, respectively (Figure 4.1). This suggests that the overall population of PbS nanoparticles was composed of polydispersed particles with a diverse range of distinct sizes and/or morphologies. This feature has been observed previously in biologically synthesized PbS NPs (Kowshik *et al*., 2002). The colour change and change in opacity (inset of Figure 4.1) are consistent with the LSPR peaks.

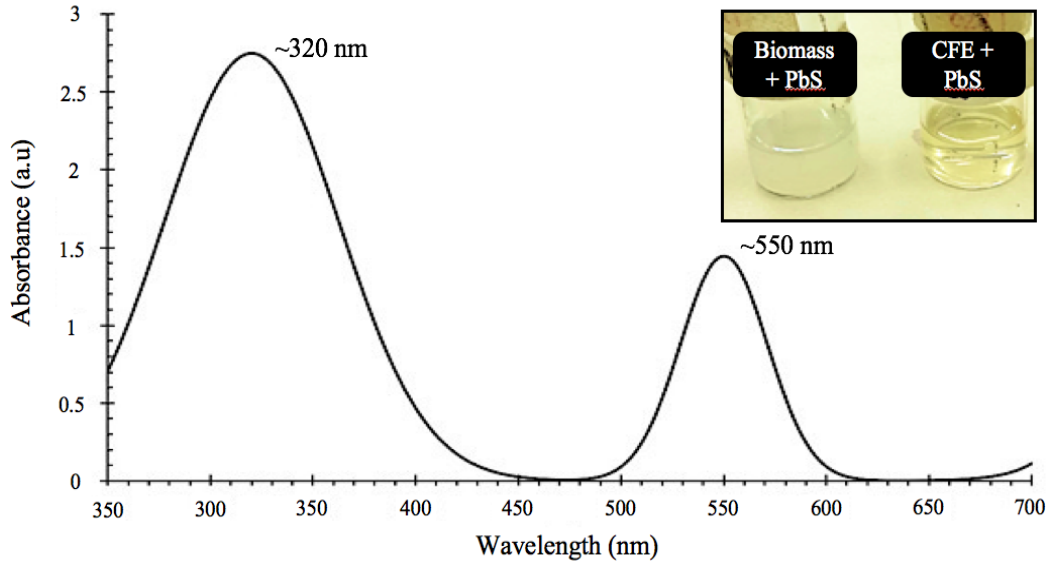

Figure 4.1. UV-Vis absorbance spectrum of the PbS NPs synthesized by *P. castaneae*. The spectrum shows two distinct absorbance peak maxima at ~320 nm and ~550 nm, respectively, after exposure to 1 mM metal ion precursors. Inset: Photograph of PbS-biomass and PbS-CFE reactions after 72 h of incubation.

Gold Nanoparticles Biosynthesized by *P. castaneae*

Figure 4.2 shows the UV-Vis spectra of as-synthesized Au NPs displaying a broad LSPR band centred at ~ 595 nm. The red shift in the LSPR band, as compared to small spherical Au NPs (~525 nm for 18 nm NPs), indicates the polydisperse nature, increased size and/or increase in aggregation of the Au NPs (Ankamwar, Chaudhary and Sastry, 2005). This absorption maxima correlates with the deep purple colour observed in the Au-biomass reaction (inset of Figure 4.2) which is characteristic of large polydisperse Au NPs, as demonstrated by Paul *et al*. (2015).

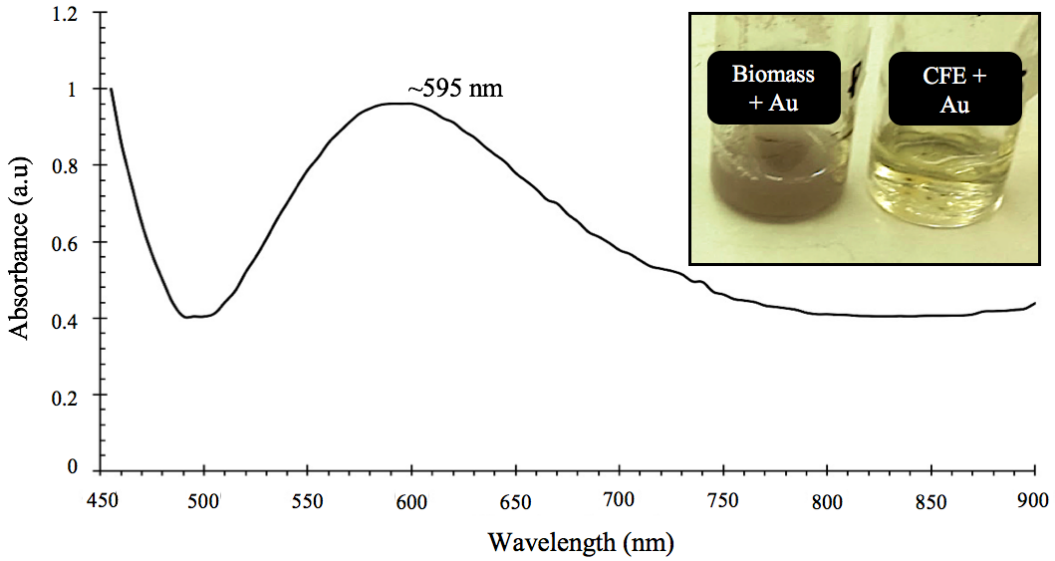

Figure 4.2. UV-Vis absorbance spectrum of the Au NPs synthesized by *P. castaneae*. The spectrum shows a distinct absorbance peak maxima at ~595 nm after exposure to 1 mM metal ion precursors. Inset: Photograph of Au-biomass and Au-CFE reactions after 72 h of incubation.

Silver Nanoparticles Biosynthesized by *P. castaneae*

In the UV-Vis spectra shown in Figure 4.3, Ag NPs showed a narrow LSPR band centred at ~440 nm, comparable to the LSPR shown in the work of Dhas *et al*. (2014). The shift to a higher wavelength indicates a sharp increase in size or overall surface roughness of the NPs (Verma *et al*., 2013). The position of the absorption edges is strongly shifted to higher energies. Relative to bulk material, the LSPR peaks of the as-synthesized Ag NPs is significantly blue shifted from the NIR into the visible and near-UV regions with decreasing particle size (Cao *et al*., 2006).

This indicates the great influence of quantum confinement of charge carriers on the NP surface (Wu and Ding, 2006). The peak shift is attributed to the transition from bulk material to NPs in the presence of the biomass/CFE (Dhas *et al*., 2014). The LSPR peak correlates with the colour change as shown in the inset of Figure 4.3.

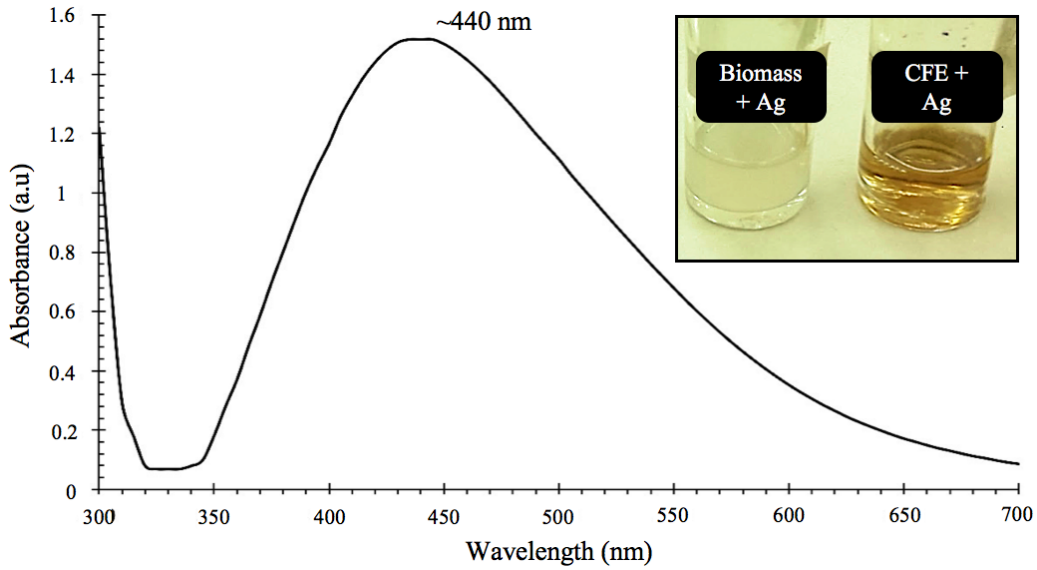

Figure 4.3. UV-Vis absorbance spectrum of the Ag NPs synthesized by *P. castaneae*. The spectrum shows distinct absorbance peak maxima at ~440 nm after exposure to 1 mM metal ion precursor. Inset: Photograph of Ag-biomass and Ag-CFE reactions after 72 h of incubation.

According to Gans theory (Gans, 1915), polarizability, and therefore the LSPR wavelength, is highly dependent on both the size and shape of NPs (Eustis and El-Sayed, 2006). When symmetry is broken, as illustrated in anisotropic NPs, a particle gains additional modes of plasmon resonance (Nehl and Hafner, 2008). The uneven surfaces of anisotropic NPs cause a red shift in the LSPR peaks and thus a larger enhancement of the electromagnetic field at the NP edge in comparison to that of the isotropic NPs (Wiley *et al*., 2006). As an example, nanorods are more easily polarized longitudinally, showing a LSPR peak of a higher wavelength and thus a lower energy. With an increasing aspect ratio of a nanorod, for a fixed diameter, only the transverse LSPR will be affected. Dong *et al*. (2006) demonstrated this phenomenon in the surfactant-assisted fabrication of PbS nanorods, nanobelts, nanoflowers as well as dendritic nanostructures.

4.2.2 Differential Interference Contrast (DIC) Microscopy and Fluorescence Microscopy (FM)

DIC and FM (Figure 4.4) were used as preliminary tools to assess the presence of NMs before further study. The absorbance peak found in the UV-Vis analysis was used as the reference for the excitation wavelength in FM for all NPs. Although the absorbance peak for PbS NPs was measured at 325 nm, radiation within the UV range is known to destroy the structure of bacterial cells (Arrieta, Weinbauer and Herndl, 2000). The excitation wavelength was therefore adjusted to 375 nm to effectively avoid the antimicrobial effects of UV-B and -C light. This then maintained the integrity of the as-synthesized PbS NPs in the presence of the *P. castaneae* cells to evaluate any associations between them. Multiple rod-shaped bacteria with prominent morphological changes can be observed (white arrows in Figure 4.4a). Such changes are common in those of heavy metal-stressed bacterial cells. Either elongation or shortening of bacterial cells is observed (Nepple, Flynn and Bachofen, 1999). Even though morphological changes occur, as well as possible cell lysis, viable bacterial cells were still present. This was indicated by movement of motile cells though the use of light microscopy, brightfield microscopy and DIC. As seen under the light microscope, motile cells are identified through their consistent directional movement, as opposed to Brownian motion, which is visualized as a vibrational movement. *P. castaneae* has also been previously characterized to be a motile bacterium (Valverde *et al*., 2008).

PbS NPs showed bright pink fluorescence when excited at this wavelength, as shown in Figure 4.4b. This is consistent with results from Srivastava and Kowshik (2017) who used these fluorescent properties for *in situ* bio-sensing applications. For Au and Ag NPs, excitation wavelengths of 550 nm and 450 nm were used, respectively (Figure 4.4e and 4.4h). Both Au and Ag NPs showed either gold or bright blue fluorescence respectively. He *et al*. (2008) demonstrated the high anti-photobleaching capacity of fluorescent Au NPs under strong light illumination. Similar properties are demonstrated by Ag NPs which show fluorescent properties that are independent of size (Ashenfelter *et al*., 2015).

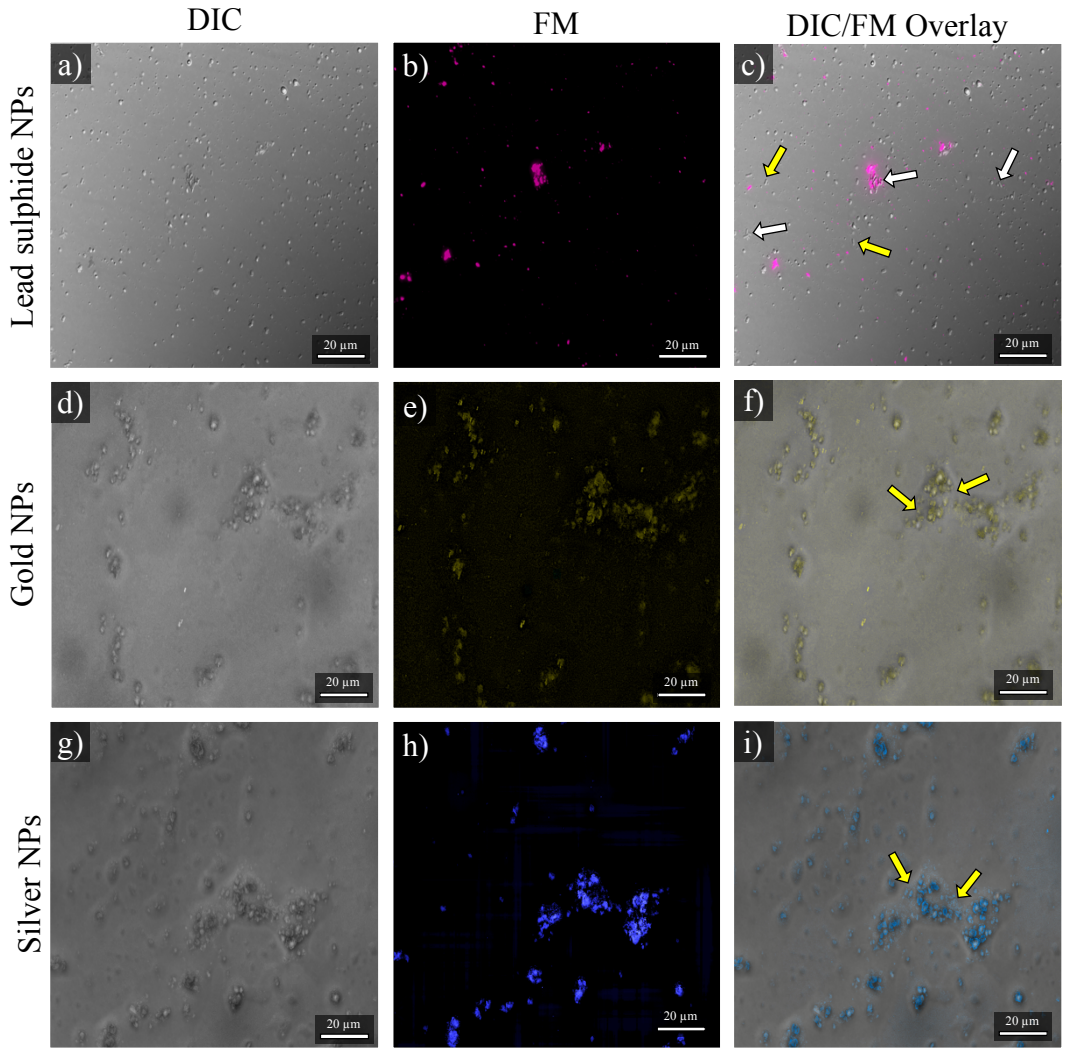

Figure 4.4. DIC, FM and DIC/FM overlay images showing the distribution of PbS, Au and Ag NPs in relation to *P. castaneae* cells or cell remnants. Images show the localization of NPs in the exterior environment in large clusters is clear after the exposure of metal ion precursors to *P. castaneae* cells for 72 h. Micrographs show the isolated channel for PbS, Au and Ag NP detection with excitations wavelengths of 375 nm, 550 nm and 450 nm respectively. DIC images of a) PbS, d) Au and g) Ag NPs. FM images of b) PbS, e) Au and h) Ag NPs. DIC/FM overlay images of c) PbS, f) Au and i) Ag NPs. Yellow arrows indicate the presence *P. castaneae* cells with a normal morphology, whereas white arrows indicate shrunken cells with distinct features of toxin-stress (Note: observable in the original image). The localization of NPs show their presence in large clumps either on the exterior of the cells or in close proximity to the cells.

4.2.3 Powder X-ray Diffraction (PXRD) and Energy-dispersive X-ray Spectroscopy (EDS)

EDS provides an elemental analysis of metallic NPs and serves as a supplementary technique to verify the nature and composition of the NPs synthesized. This analysis was localized to a specific area on the surface of a metal NP when viewed under the electron microscope. Using PXRD analysis, the phase composition, phase structure and crystallinity of the lyophilized NP powder was obtained. Samples with different morphologies but identical composition will all exhibit the same EDS and XRD spectral patterns (Song *et al*., 2013). Therefore, only one EDS and XRD pattern is displayed per metal, respectively.

Lead Sulphide Nanoparticles Biosynthesized by *P. castaneae*

Figure 4.5 shows the EDS spectra of PbS NPs, which revealed a strong signal for Pb and S present in the sample. Weak signals for C, O and P are also found, which are attributed to the biological material present, as well as Ca, which was present in the sulphur precursor metal salt. Biologically synthesized PbS NPs have been shown to induce a strong signal peak around 2.4 keV (Zhou *et al*., 2009).

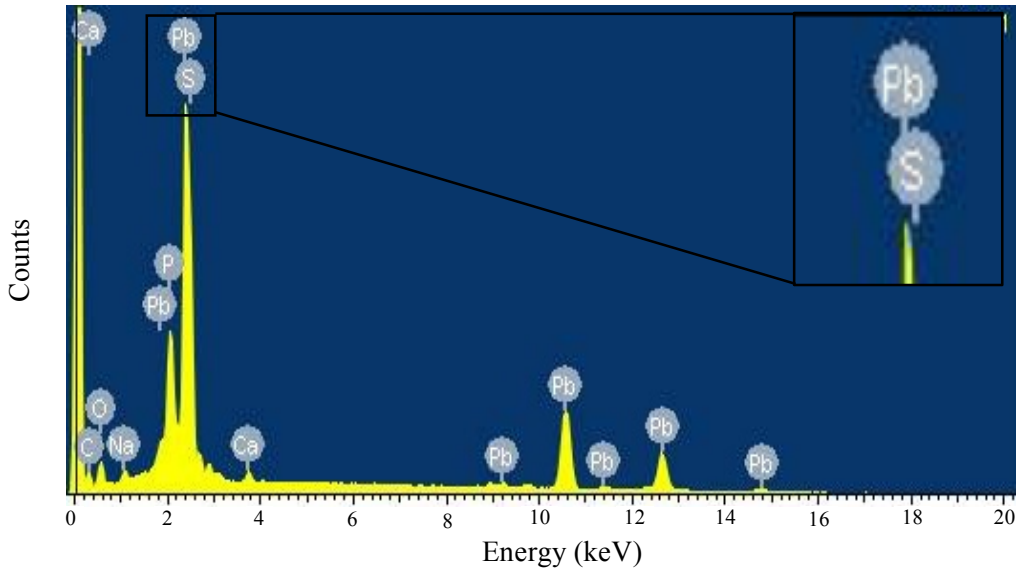

Figure 4.5. EDS spectrum of PbS NPs synthesized by *P. castaneae*. The bacterially produced PbS NPs show a strong signal for Pb and S, while also displaying weak signals for Na, O, P, C and Ca. The weak signals are attributed to the presence of biological material.

As shown in Figure 4.6, all peaks can be readily indexed as the face-centred-cubic (fcc) PbS structure, in agreement with the literature standards (JCPDS card no. 5-529) (Li *et al*., 2007). A large number of intense Bragg reflections are observed originating from the lyophilized PbS NP powder. The reflection peaks of {111}, {200}, {220}, {311}, {222}, {331} and {420} crystal planes were clearly distinguished. The presence of organic material from the bacterial cells and culture media resulted in an increase of background noise, widening of peaks as well as the occurrence of additional peaks. This has been previously reported for biologically synthesized PbS NPs (Kowshik *et al*., 2002; Seshadri, Saranya and Kowshik, 2011; Kaur *et al*., 2014).

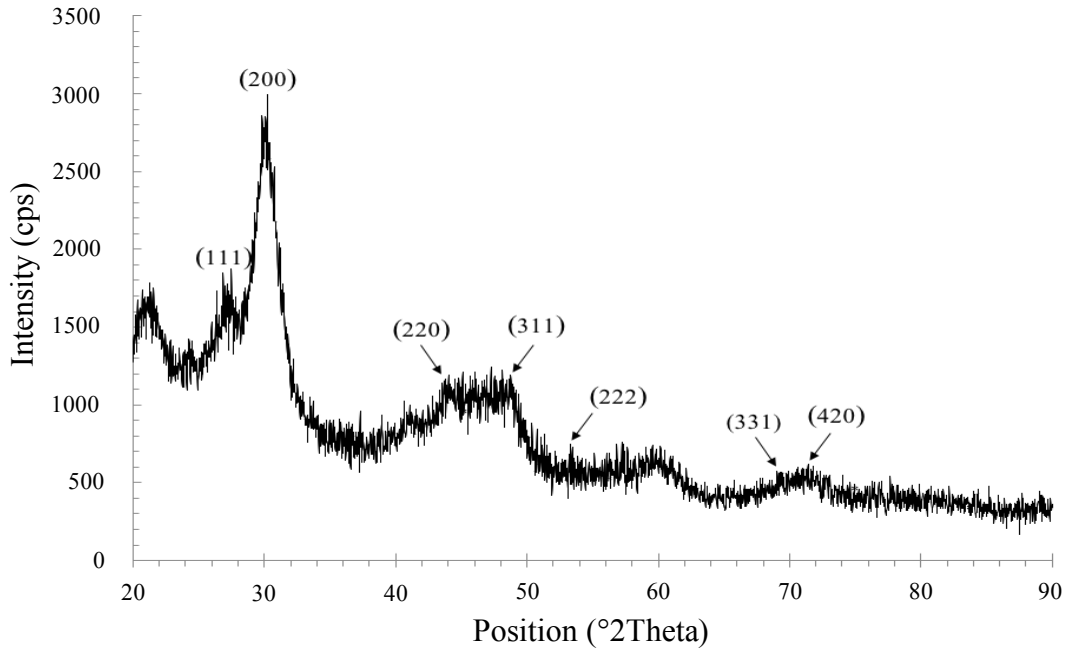

Figure 4.6. PXRD diffractogram of lyophilized powder of PbS NPs synthesized by *P. castaneae*. Intense reflection peaks for the {111}, {200}, {220}, {311}, {222}, {311} and {420} crystal planes are observed. The appearance of very broad peaks could be indicative of larger microstructures which have dimensions outside of the 1 nm – 100 nm range as well as the presence of biological material (Seshadri, Saranya and Kowshik, 2011).

Gold Nanoparticles Biosynthesized by *P. castaneae*

The EDS spectra for Au NPs shows a strong signal for Au as well as Cu (originating from the Cu sample loading grid) as shown in Figure 4.7. Weak peaks for C and O represent the organic nature of biological material attached to the surface of Au NPs.

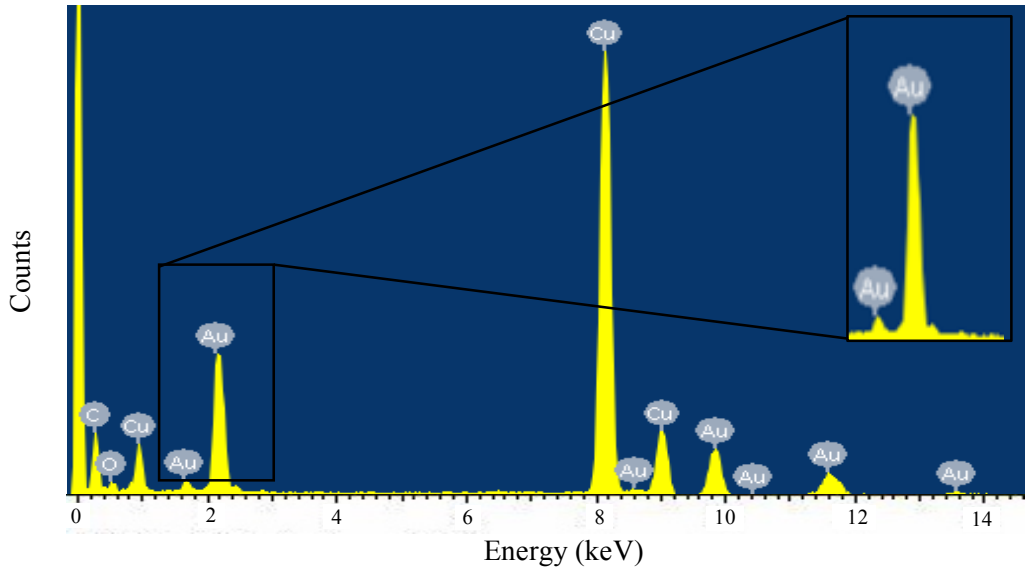

Figure 4.7. EDS spectrum of Au NPs synthesized by *P. castaneae*. The biologically synthesized Au NPs show a strong signal for Au, while also displaying weak signals for O and C. The weak signals are attributed to the presence of biological material either in close proximity to the NPs or capping the NPs. Strong signals from Cu are also observed, attributed to the Cu sample loading grids.

The XRD pattern in Figure 4.8 was obtained from the Au NP powder and corresponds to the fcc crystal structure of elemental gold. The XRD pattern exhibits five peaks corresponding to the {111}, {200}, {220}, {311} and {222} diffraction peaks of metal gold respectively (JCPDS Card No. 4-0783). The peak at 38.12° of 2θ was found to be at maximum which suggests the NPs are predominantly aligned towards the {111} facet, commonly reported for large 2-D anisotropic Au NMs (Fazal *et al*., 2014). The presence of the purple colour in the reaction solution due to the SPR band at 595 nm as well as increased stabilization at the {111} facet is indicative of Au NPs with an anisotropic and polydispersed nature, as shown by Anuradha, Abbasi and Abbasi (2015). Also present are peaks of contamination that

are indexed to halite (JCPDS No. 05-0628). The halite (NaCl) rock salt, detected in the sample, precipitated out of solution during the lyophilization process. The NaCl ions originated from the culture media used for bacterial growth. The reflections shown represent the {100}, {200}, {220}, {222}, {400} and {420} reflection peaks of standard halite (Wahed *et al*., 2015).

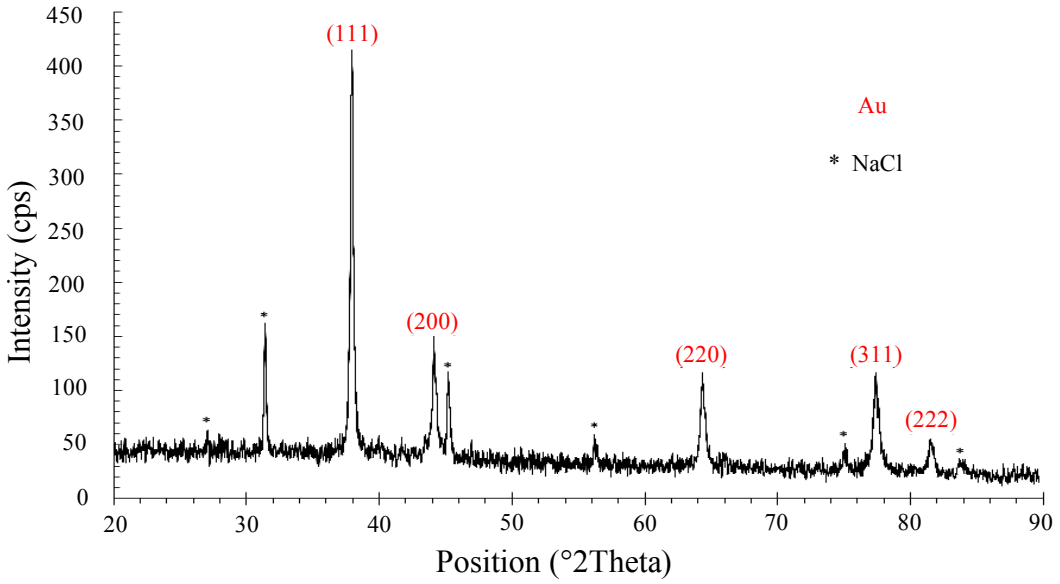

Figure 4.8. PXRD diffractogram of lyophilized powder of Au NPs synthesized by *P. castaneae*. Intense reflection peaks for the {111}, {200}, {220}, {311} and {222} crystal planes are observed. The observed peak broadening is indicative of crystalline material with nanometre dimensions. Contaminant peaks belonging to NaCl, which originated from the culture media, are also observed. Crystallization of NaCl occurred during the lyophilization process.

Silver Nanoparticles Biosynthesized by *P. castaneae*

The EDS analysis for biological Ag NPs is shown in Figure 4.9, which confirms the occurrence of Ag NPs. A strong signal for Ag and Cl are shown. Peaks from common contaminants (Si and Cd) are also observed. This is consistent with other biologically synthesized NPs that are silver in nature (Dhas *et al*., 2014; Kumar *et al*., 2016).

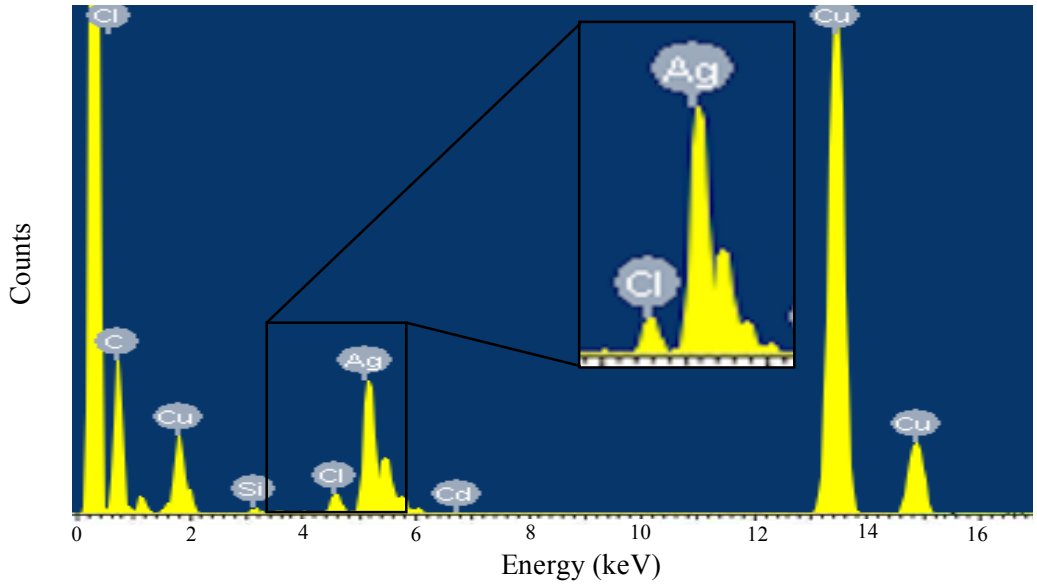

Figure 4.9. EDS spectrum of Ag NPs synthesized by *P. castaneae*. The biological Ag NPs show a strong signal for Ag, while also displaying weaker signals for Cl and C. The weak signals are attributed to the presence of biological material either in close proximity to the NPs or capping the NPs. Strong signals from Cu are also observed, and attributed to the Cu sample loading grids.

Figure 4.10 shows the XRD pattern of the as-prepared Ag NPs. Reflection peaks matched well with the standard reflection peaks of metallic silver in the {111}, {200} and {220} planes of the fcc structure (JCPDS file: 65-2871). These peaks coexist with those of the AgCl standards; corresponding to the {111}, {200}, {220}, {311}, {222}, {400}, {331}, {420}, and {422} planes of the cubic phase of AgCl (JCPDS file: 31-1238). Cl^- ions are likely to have originated from the culture media used, thus the formation of both Ag and AgCl NPs. It is unclear whether metal alloys, individual metallic NPs or combinations of these were formed. The broadening of peaks indicates the nano-sized nature of all NP samples (Fazal *et al*., 2014). The biological synthesis of Ag/AgCl NPs is common, although not well explained (Dhas *et al*., 2014; Hu *et al*., 2009; Kumar *et al*., 2016). Using *B. subtilis*, Paulkumar *et al*. (2013) showed the synthesis of polydisperse AgCl NPs ranging from 20 nm – 60 nm; this without the addition of Cl^- ions. The enzyme responsible for reduction of Ag^+ ions was hypothesized to be a membrane bound 37 kDa nitrate reduction enzyme.

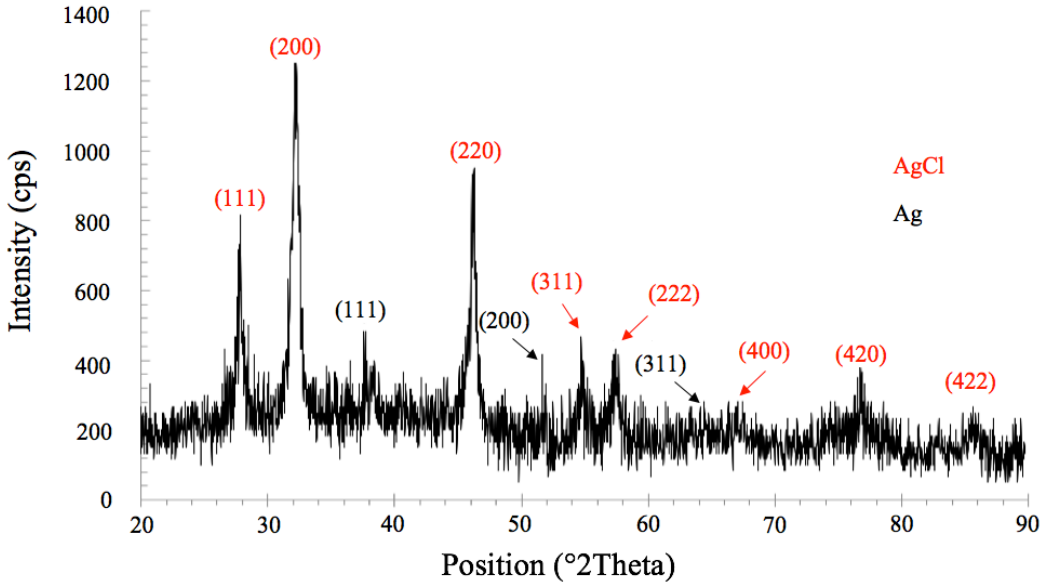

Figure 4.10. PXRD diffractogram of lyophilized powder of Ag/AgCl NPs synthesized by *P. castaneae*. Intense reflection peaks for the {111}, {200}, {220}, {311} and {222} crystal planes indexed to AgCl are observed. The observed peak broadening is indicative of crystalline material with nm dimensions. Reflection peaks for {111}, {200} and {311} crystal planes indexed to Ag are also present. This indicates the synthesis of a mixed population of Ag and AgCl NPs.

4.2.4 Scanning Electron Microscopy (SEM) and Transmission Electron Microscopy (TEM) Analysis

Lead Sulphide Nanoparticles from *P. castaneae* Cell-free Extract

When the CFE of *P. castaneae* was used to synthesize PbS NPs, a general uniformity in spherical particle structure and morphology was observed using electron microscopy. Figure 4.11 shows a well-defined porous network of globular aggregates. These aggregates appear similar through-out, suggesting uniformity in particle dimensions in terms of shape and size. The close packing of NPs as well as drying effects and uneven surface covering during sputter coating, originating from sample preparation, can result in the appearance of apparent non-spherical NPs, as indicated by the yellow arrows in Figure 4.11 (Patel, Mighri and Ajji, 2012). Although unlikely, the pre-existing spherical particles under the stress of high energy electron beam can also act as nucleating agents for the initial growth of non-spherical NPs (Chen, Palmer and Wilcoxon., 2006).

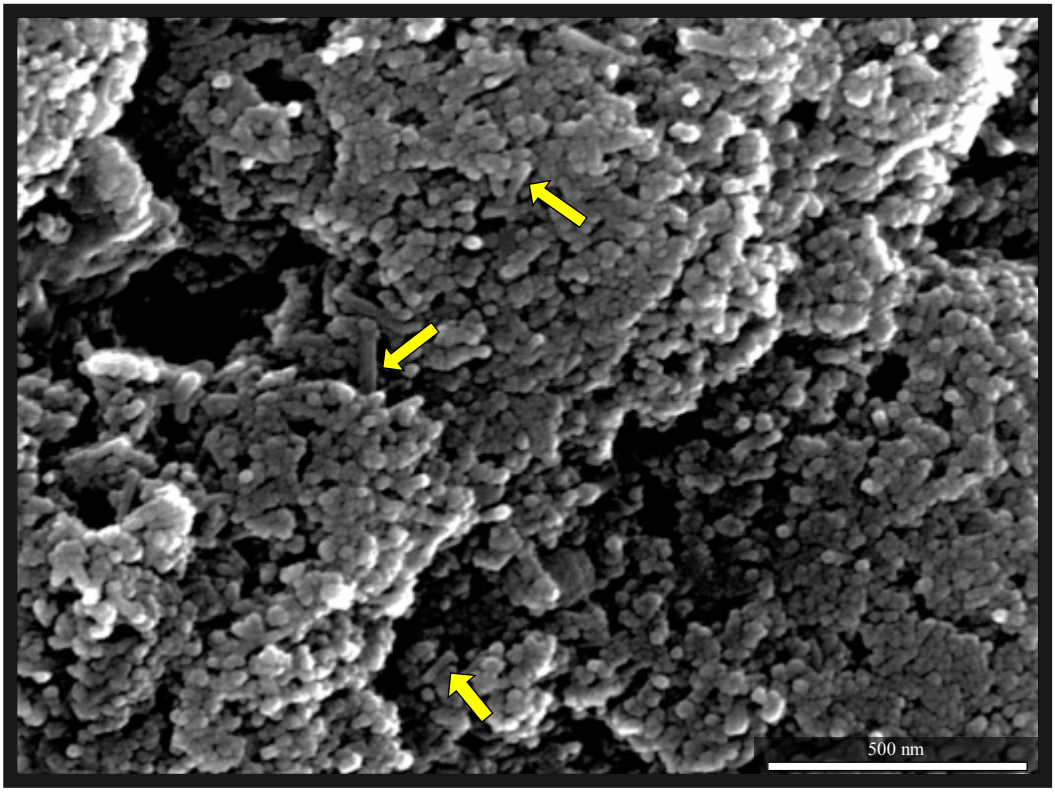

Figure 4.11. SEM micrograph of *P. castaneae* CFE-synthesized PbS NPs. The micrograph shows the close-packing of spherical PbS NPs synthesized after the exposure of *P. castaneae* CFE to Pb and S metal ion precursor solutions for 72 h. Yellow arrows indicate the appearance of apparent non-spherical PbS NPs, likely present due to sample preparation effects.

In the TEM micrograph, non-aggregated spherical PbS NPs ranging from 4 nm – 22 nm in diameter are observed (Figure 4.12). The PbS NPs show considerable contrast in surface characteristics (inset of Figure 4.12). Twinning across multiple planes suggests the synthesis of NPs with a decahedral penta-twinned crystal structure. This results in a three-dimensional quasi-spherical shape with highly truncated edges. The level of truncation and inherent shape is dependent on the concentration and nature of both the precursor metal ions as well as of the surfactant/capping agent (Zhang *et al*., 2010). The twinned morphology suggests the preferential binding of presumptive biological capping agents onto the surface of the PbS NPs.

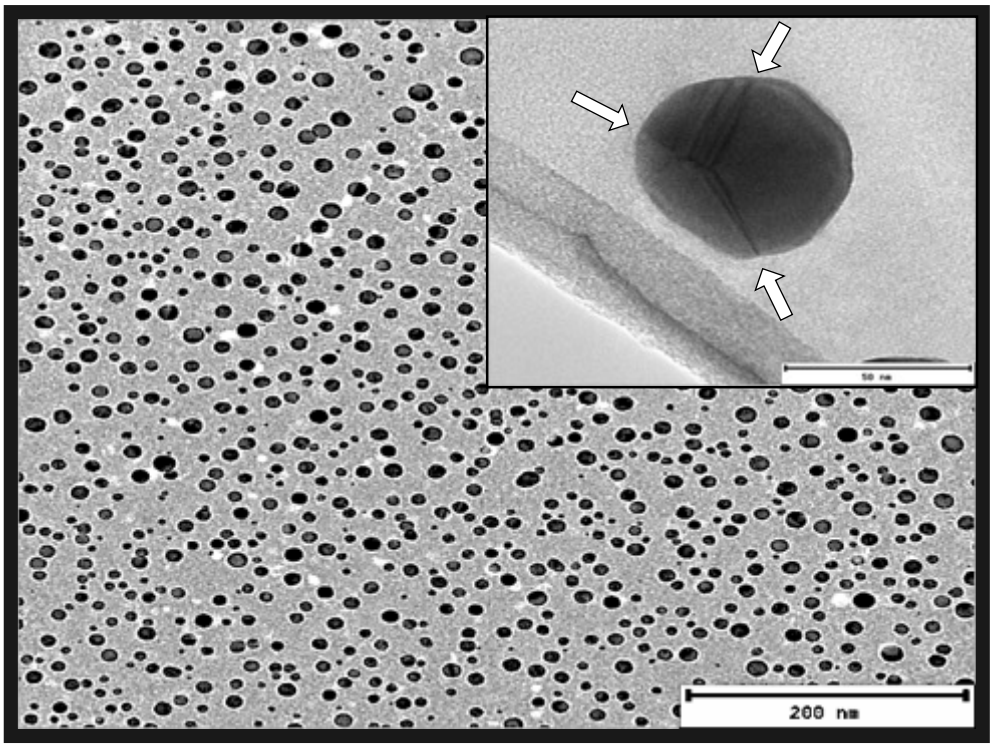

Figure 4.12. TEM micrograph of *P. castaneae* CFE-synthesized PbS NPs. The micrograph shows well-dispersed spherical PbS NPs synthesized after the exposure of *P. castaneae* CFE to Pb and S metal ion precursor solutions for 72 h. Inset: A high magnification TEM micrograph of a PbS NP with a decahedral penta-twinned crystal structure. White arrows indicate twinning planes in which the directionality of the crystal lattice changes. Scale bar represents 10 nm.

As compared to SEM micrographs, well-dispersed PbS NPs are present in TEM micrographs. This is due to a lack of sample preparation required for this technique. Using the ImageJ particle analysis tool (Schneider, Rasband and Eliceiri, 2012), a narrow size distribution of 12 nm ± 2 nm was calculated (Figure 4.13a). The high magnification TEM image of spherical PbS NPs (Figure 4.13b) shows dark halos surrounding the electron-dense PbS NP core. These halos represent presumptive biomolecules which are excreted into the CFE by *P. castaneae* and involved in the stabilization/capping of the PbS NPs. Protein-capped Ag NPs synthesized by Jain *et al*. (2015) using *Aspergillus* sp. NJP02 showed a similar core-shell appearance. These results are consistent with the narrow LSPR band shown in the UV spectra as well as the colour and opacity changes upon visual inspection, definitively confirming PbS NP formation.

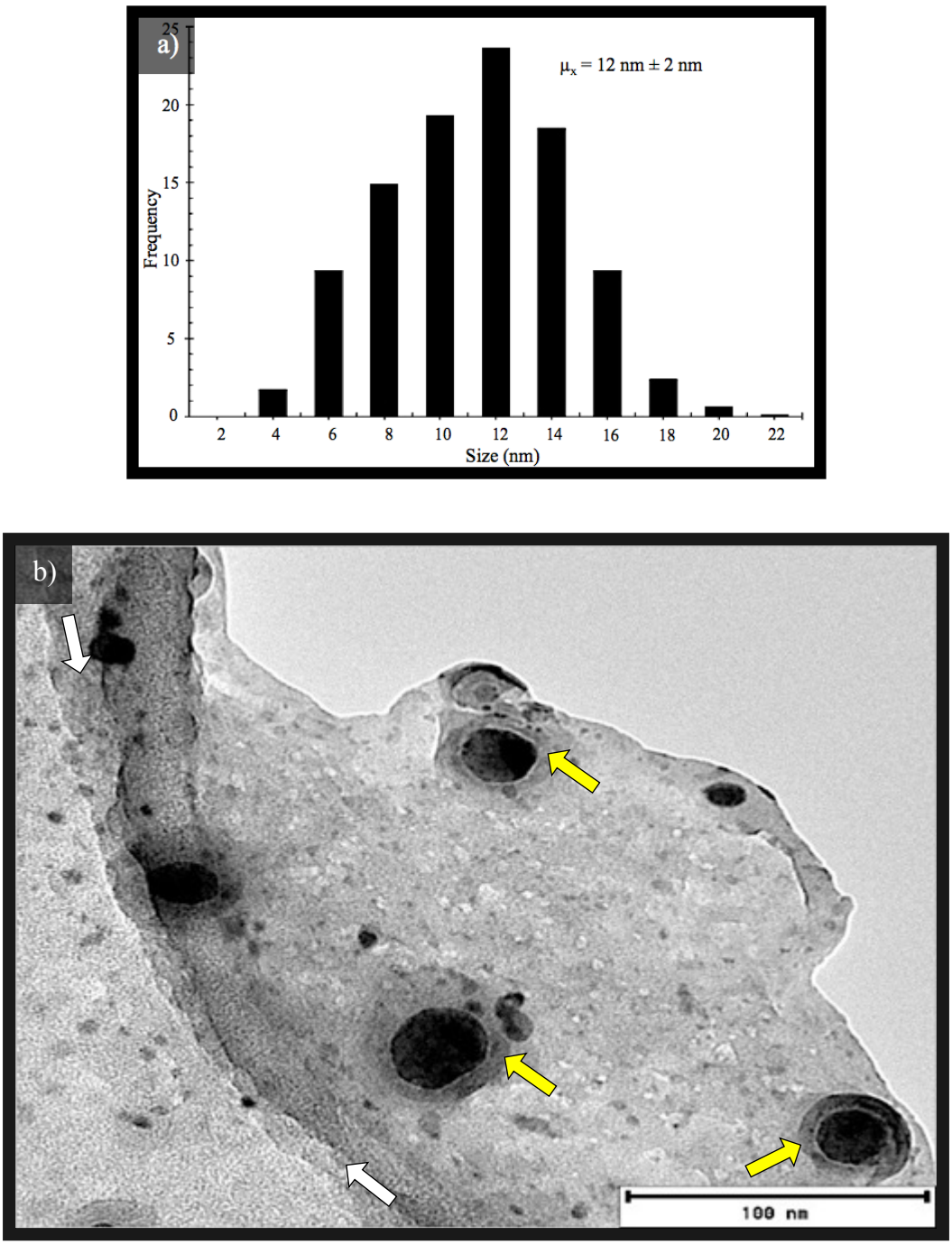

Figure 4.13. Size distribution graph and TEM micrograph of *P. castaneae* CFE-synthesized PbS NPs. a) Size distribution histogram of PbS NPs showing an average size of 12 nm ± 2 nm, calculated using ImageJ particle analysis tool (Schneider, Rasband and Eliceiri, 2012). b) High magnification TEM micrograph of 30 nm – 40 nm spherical PbS NPs synthesized after the exposure of *P. castaneae* CFE to Pb and S metal ion precursor solutions for 72 h. The NPs are surrounded by presumptive biological capping molecules. Yellow arrows indicate the 10 nm – 15 nm layer of biomolecules surrounding the NPs.

Lead Sulphide Nanoparticles from *P. castaneae* Cell Biomass

The particle structure and morphology of the PbS NPs synthesized by the *P. castaneae* biomass were analysed using SEM and TEM. Distinct changes in cell morphology and surface characteristics were observed in metal-exposed cells when compared to that of unexposed cells. *P. castaneae* biomass which was not exposed to metal ions show a creased and corrugated cell surface (Figure 4.14). Untreated cells show no signs of cell damage or lysis. The 'rough' surface characteristics are consistent with the high-energy electron beam used as well as dehydration during the fixation process (Patel, Mighri and Ajji, 2012).

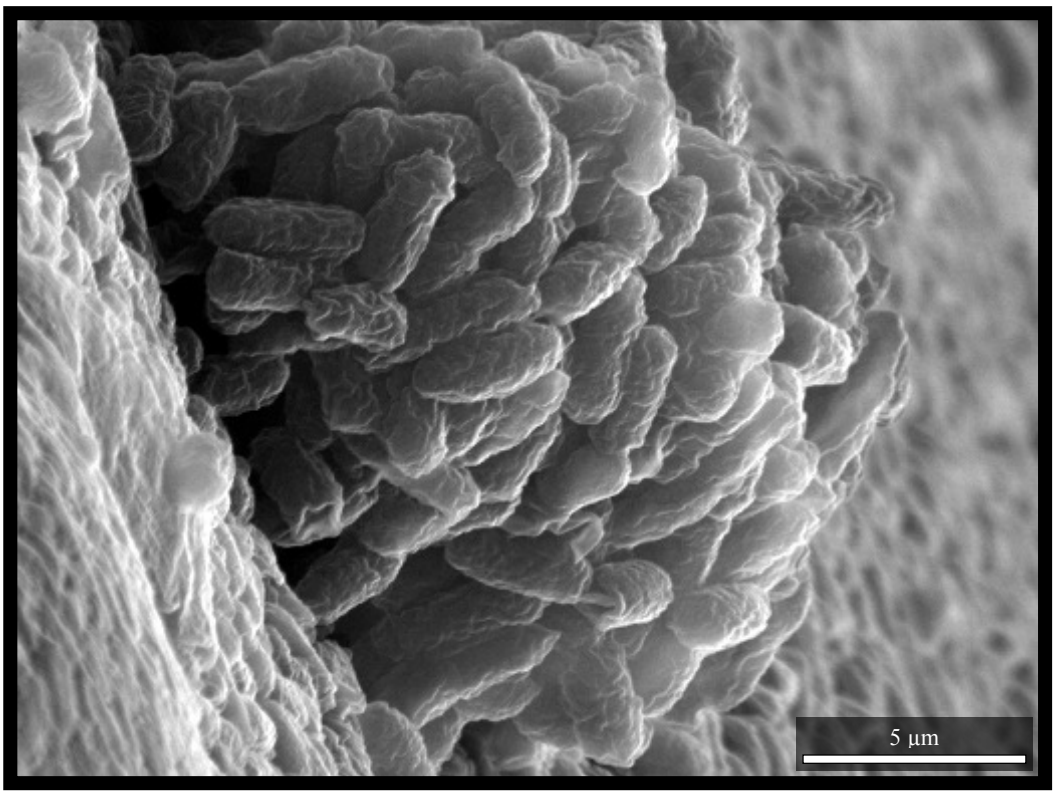

Figure 4.14. SEM micrograph of *P. castaneae* cells before exposure to PbS metal ion precursors. *P. castaneae* cells before exposure to metal ion precursors show no signs of cell damage or lysis but do show a creased cell surface due to the effects of the dehydration that occurred during sample preparation. Cells were incubated without metal ion precursors for 72 h.

Upon exposure to PbS precursors ions, the bacterial cell surface becomes rough, uneven and pitted. Large clusters of spherical PbS NPs on the surface of cells is

shown in Figure 4.15. The granular appearance indicates the presence of individual NPs which are superimposed to form larger clusters. PbS NP clusters are possibly formed intracellularly within vesicles or on the cell surface within the periplasmic space. The damaging effects of heavy-metal ions are also apparent (Thakkar, Mhatre and Parikh, 2010). These include multiple invaginations, membrane blebbing and cell shrinkage; leading to possible cell lysis (white arrows).

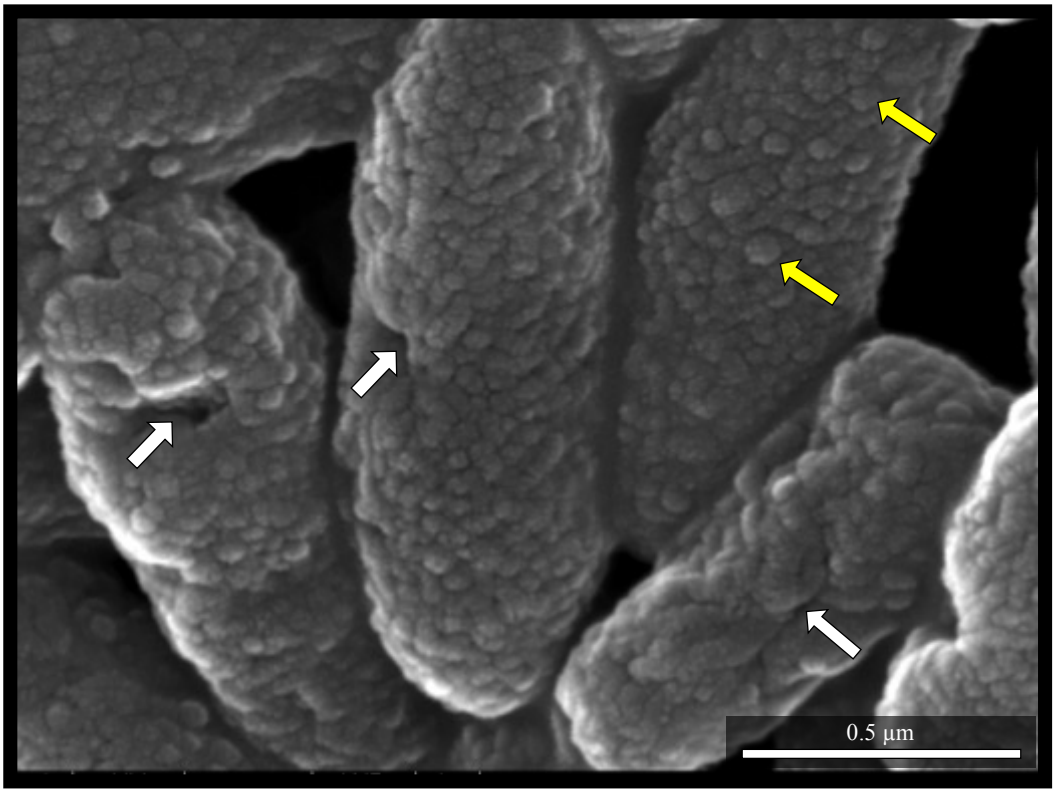

Figure 4.15. SEM micrographs of *P. castaneae* cells after exposure to Pb and S metal ion precursors. *P. castaneae* cells after the exposure of *P. castaneae* biomass to Pb and S metal ion precursor solutions for 72 h, show the synthesis of clusters of small (4 nm – 20 nm) spherical PbS NPs (yellow arrow) as well as many signs of cell damage. This includes cell shrinkage, blebbing and cell wall invagination (white arrows).

Multiples sizes, shapes and morphologies are produced through the exposure of the biomass to PbS metal ions in solution. These include filamentous nanoflowers with core sizes of ~1.5 µm and filaments with an approximate diameter of 60 nm (white arrows) and aspect ratios of length/diameter between 2 and 10 (Figure 4.16). Also

visible are 80 nm – 150 nm truncated nanorods (yellow arrows) with aspect ratios between 5 and 12.

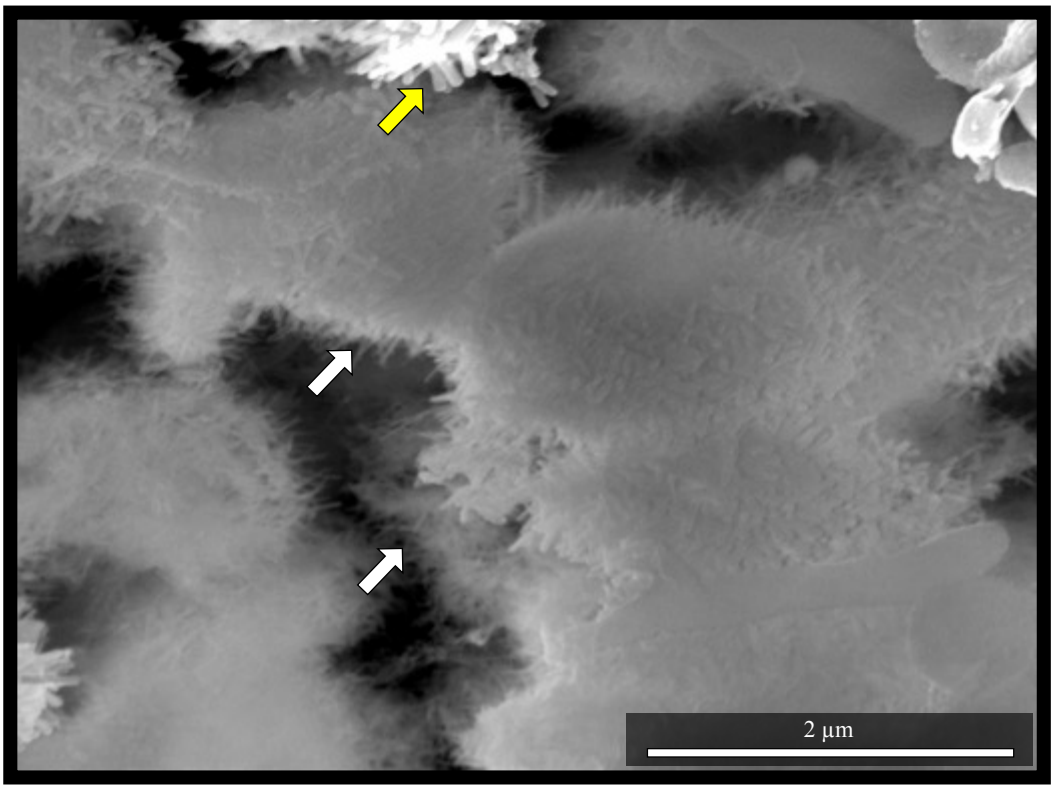

Figure 4.16. SEM micrograph of anisotropic PbS nanoflowers and nanorods synthesized by *P. castaneae* biomass. Filamentous nanoflowers with core diameters of ~1.5 µm with filaments extending radially. Smaller (~60 nm) nanofilaments (white arrows) can be observed alongside larger (80 nm – 150 nm) nanorods (yellow arrow) in large clumps. These NMs were produced extracellularly after the exposure of cell biomass to Pb and S metal ion precursor solution.

Clusters of truncated and/or rounded penta-twinned nanorods of 80 nm – 150 nm were also produced in large clusters (Figure 4.17). Quantum dot-sized (2 - 18 nm) spherical NPs are also shown to coat the surface of the nanorods (inset of Figure 4.17). Whether the spherical NPs were formed on the surface of the nanorods or within solution and deposited onto the surface is unclear. Although ZnO and Te nanorods have been synthesized extracellularly by the fungus *Fusarium solani* (Venkatesh *et al*., 2013) and *Pseudomonas pseudoalcaligenes* (Forootanfar *et al*.,

2015) respectively, published literature on the microbial synthesis of nanorods is limited. The exact mechanisms of nanorod biosynthesis are not yet known.

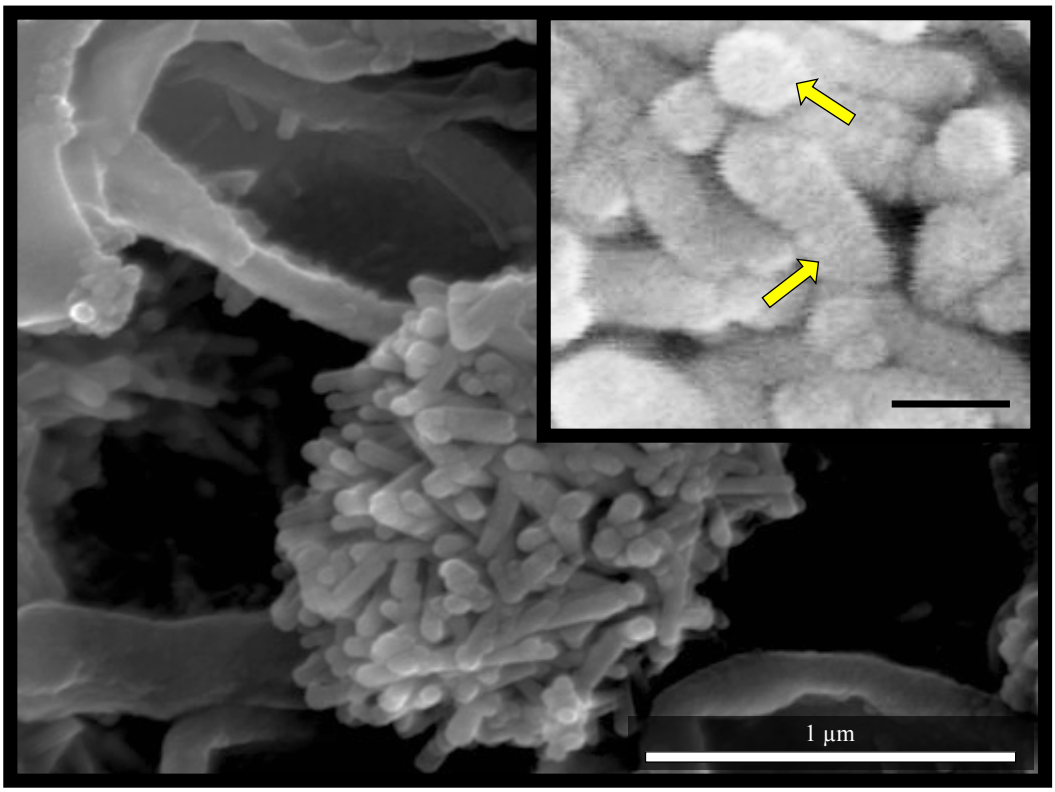

Figure 4.17. SEM micrographs of anisotropic PbS NMs synthesized by *P. castaneae* biomass. A large cluster of truncated and/or rounded penta-twinned PbS nanorods covered in PbS quantum dots (2 - 18 nm) NPs (yellow arrow in inset) were synthesized by the *P. castaneae* biomass after exposure to Pb and S metal ion precursor solutions for 72 h. Scale bar in inset represents 100 nm.

Figure 4.18 shows low magnification SEM image of anisotropic PbS NPs. The close association between bacterial cells and nanorods is demonstrated wherein lysed bacterial cells cover large (10 µm) mounds of PbS NM. Cell lysis is possibly observed due to the exposure to concentrations of metal ions at higher than the MIC. Nanorods between 20 nm – 90 nm with aspect ratios range between 10 and 30 are observed. NMs with these aspect ratios have often been referred to as nanowires (Zhang *et al*., 2005a). PbS nanowires have until now only been produced chemically and have shown implications for use in gate-tunable superconducting quantum interference devices (SQUIDs) (Kim *et al*., 2016).

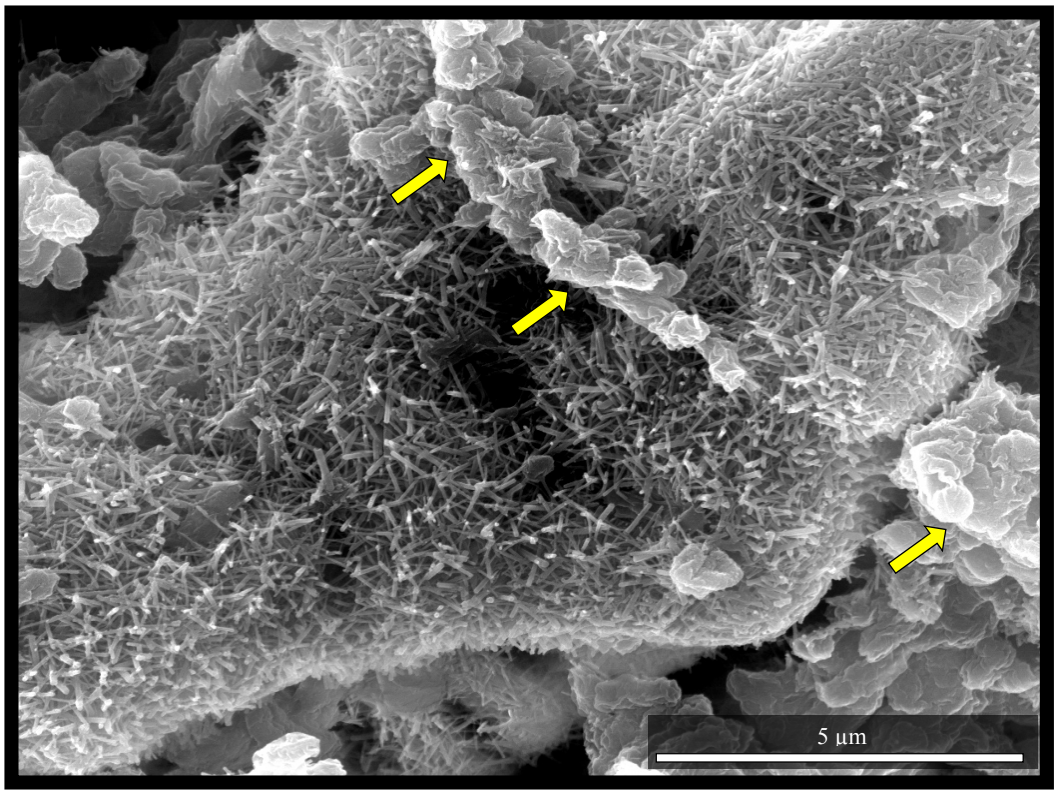

Figure 4.18. SEM micrograph of PbS nanorods and nanowires synthesized by *P. castaneae* biomass. Damaged *P. castaneae* cells (yellow arrows) in close association with large mounds of PbS nanorods and nanowires. NM materials was produced on the exterior of cells after exposure to Pb and S metal ion precursor solutions for 72 h.

Figure 4.19 shows well-defined 5-fold twinned pentagonal nanorods. These nanorods are clustered tightly together to form porous structures which are often covered in bacteria or bacterial artefacts. Three types of 1-D PbS NMs are observed; these include rod-shaped prisms with either (i) irregular pentagonal, (ii) quadrilateral or (iii) hexagonal cross-sections. In the present study, the length of the longest nanorods reached ~5 µm with varying aspect ratios of between 4 and 8. The longest nanowires reached ~6 µm with varying aspect ratios between 10 and 40. The well-defined geometry of the nanorods suggests the highly preferential binding of presumptive biomolecules to the NP surface, stabilizing the morphology.

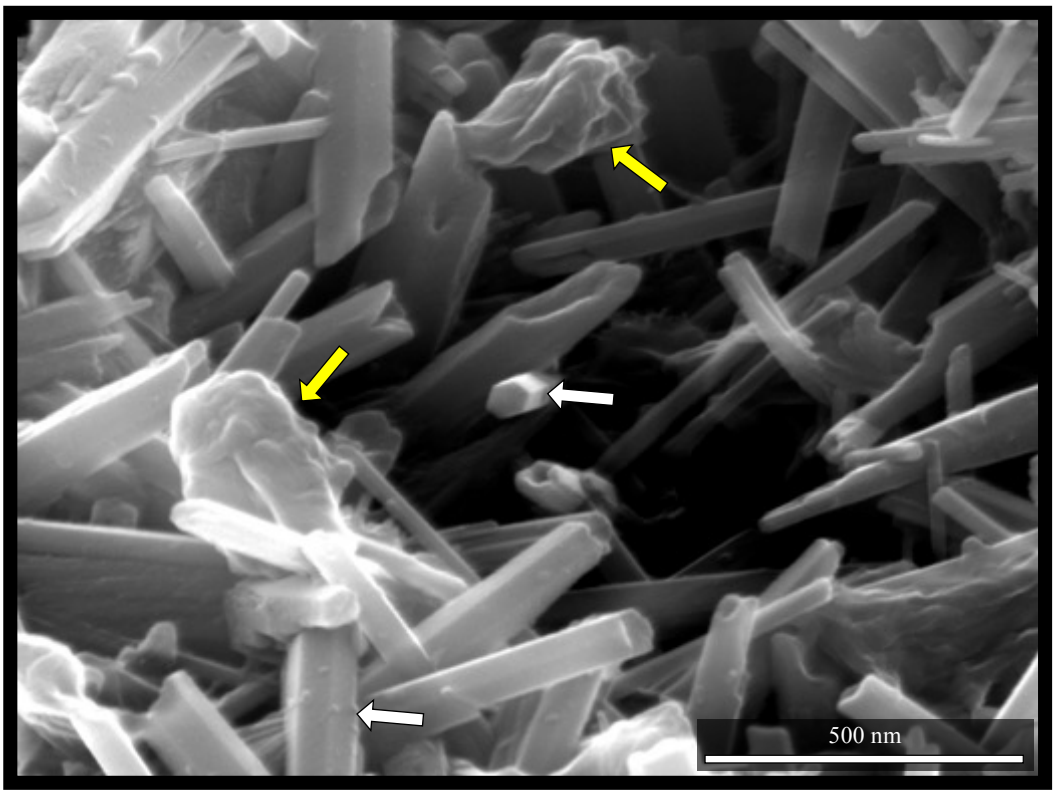

Figure 4.19. SEM micrograph of well-defined PbS nanorods synthesized by *P. castaneae* biomass. Nanorods showing sharp edges and definite geometries with variable sizes and aspect ratios. Well-defined 5-fold twinned pentagonal nanorods (white arrow) that form a porous network are shown surrounded by bacterial cell remnants/artefacts (yellow arrows). Broken edges are likely due to the high force used in centrifugation during sample preparation.

P. castaneae cells, under TEM analysis, that have not been exposed to heavy-metal ions show no signs of cell damage or lysis (Figure 4.20). Biological material is represented by light greyed electron dense areas under TEM (white arrows). The double membraned structures found in the image represent the holey carbon-coated copper TEM grid onto which the as-synthesized samples were loaded (yellow arrows).

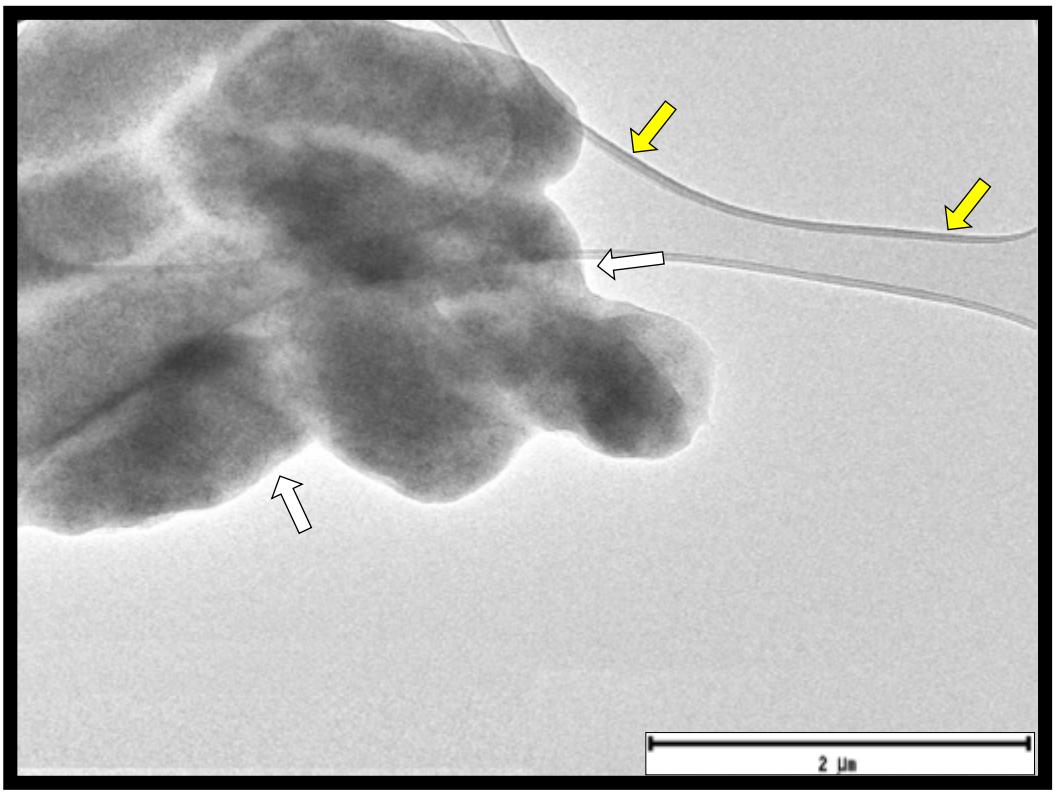

Figure 4.20. TEM micrograph of *P. castaneae* cells before exposure to Pb and S metal ion precursors. *P. castaneae* cells were incubated without metal ion precursors for 72 h and show no signs of cell damage or lysis (white arrows). Yellow arrows represent the holey carbon-coated copper TEM grid onto which the as-synthesized samples were loaded.

In contrast, cells that have been exposed to heavy-metal ions shown a considerably more electron dense area at the cell surface. The increase in opacity is indicative of the presence of heavy metals (Williams, Aderhold and Edyvean, 1998). The TEM micrograph shows the polydisperse nature of PbS NPs synthesized by *P. castaneae* cells; as opposed to the monodisperse nature of NPs synthesized by the CFE. Various anisotropic PbS NPs are shown in clusters surrounding, within and/or on the surface of the bacterial cells (Figure 4.21). The origin of larger (~80 nm) spherical NPs and nanorods is shown to be the bacterial cell surface (inset of Figure 4.21). The accumulation of NPs on the cell surface is also indicative of synthesis that occurs on the cell surface by periplasmic enzymes within the membrane. This has been demonstrated by Lin, Lok and Che (2014) using the nitrate reductase c-type cytochrome subunit NapC. NPs are found in higher concentration within

electron-dense areas that are likely to be extracellular polymeric substance (EPS), indicated by the red arrows in Figure 4.21.

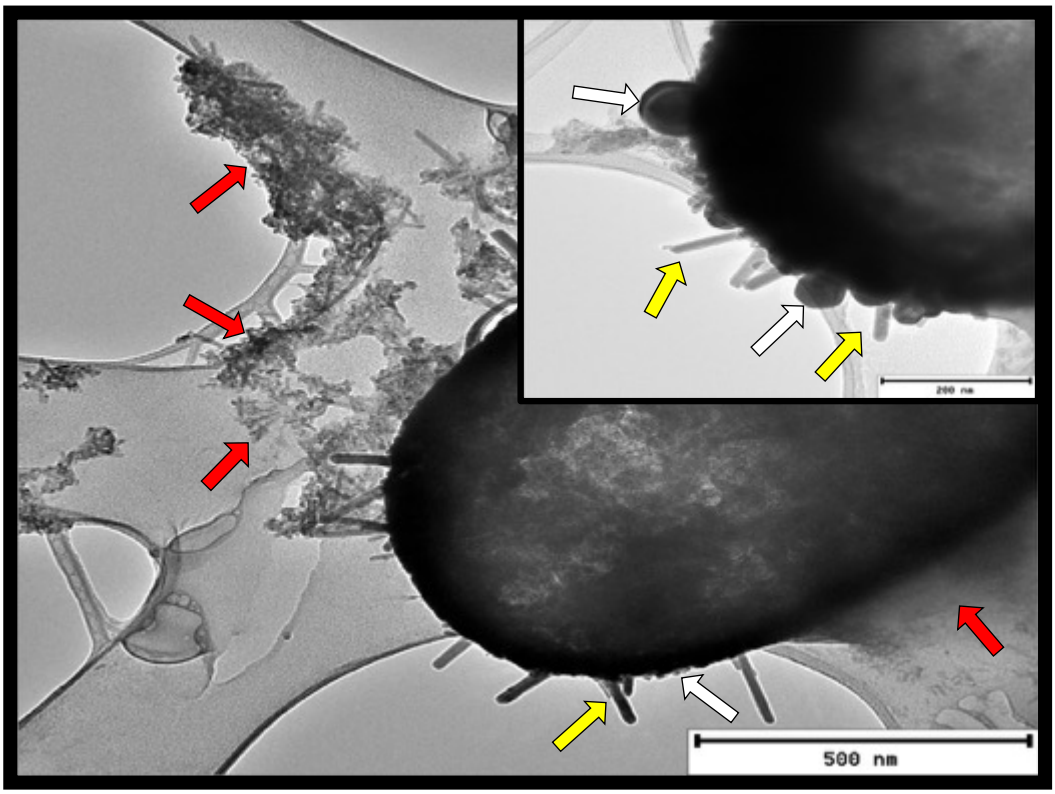

Figure 4.21. TEM micrographs of *P. castaneae* cells after exposure to Pb and S metal ion precursors. Bacterial cells covered in differently shaped and sized PbS NPs. Nanorods (white arrow) and nanospheres (yellow arrow) are shown to completely cover the bacterial cell surface. Also shown are aggregates of multiple-morphology NPs within an electron-dense area likely to be EPS (red arrows). Inset: high magnification image of bacterial cells with nanorods (white arrow) and nanospheres (yellow arrow) protruding from the cell surface. Scale bar represents 200 nm.

Figure 4.22 represents a low magnification TEM image of biologically synthesized filamentous nanoflowers. The nanoflowers are composed of a large number of nano- and microfilaments that extend radially from the core to form a rock crystal-like structure. The length of the filaments ranges between 40 nm and 80 nm for nanofilaments, and between 150 nm and 1.5 μm for microfilaments. According to Dong *et al*. (2006), PbS nanoflowers are formed through the crossing of bundles of nano- and microfilaments as well as nanospheres.

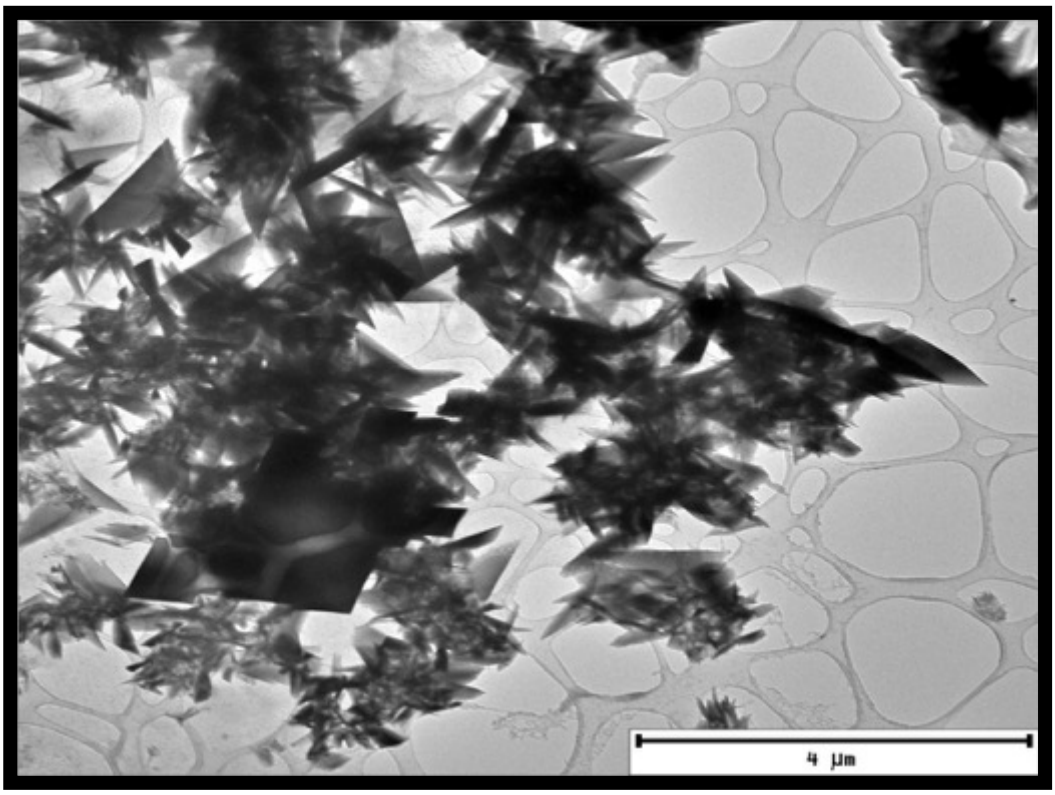

Figure 4.22. Low magnification TEM micrograph of *P. castaneae* biomass-synthesized PbS nanoflowers. Filamentous and sheet-like PbS nanoflowers composed and multiple nano- and microfilaments. are shown to be extracellularly produced after the exposure of cell biomass to Pb and S metal ion precursors for 72 h.

The presence of spherical PbS NPs is also seen in close proximity to the fibrous ends of the nanoflower (Figure 4.23). This suggests the attachment of spherical NPs to each other through Ostwald ripening to form larger porous microstructures. However, without a time-based study to elucidate the formation of these nanoflowers it is not possible to definitively confirm whether the quantum dots are part of the formation process or merely synthesized in solution and are in close proximity to the nanoflowers. The formation of large filamentous nanostructures is highly dependent on the presence, concentration and preferential binding of capping agents. The use of oleic acid and CTAB as surfactants and a change of reactions conditions during chemical synthesis have been used to produce similar anisotropic PbS NPs (Dong *et al*., 2006; Wang *et al*., 2011).

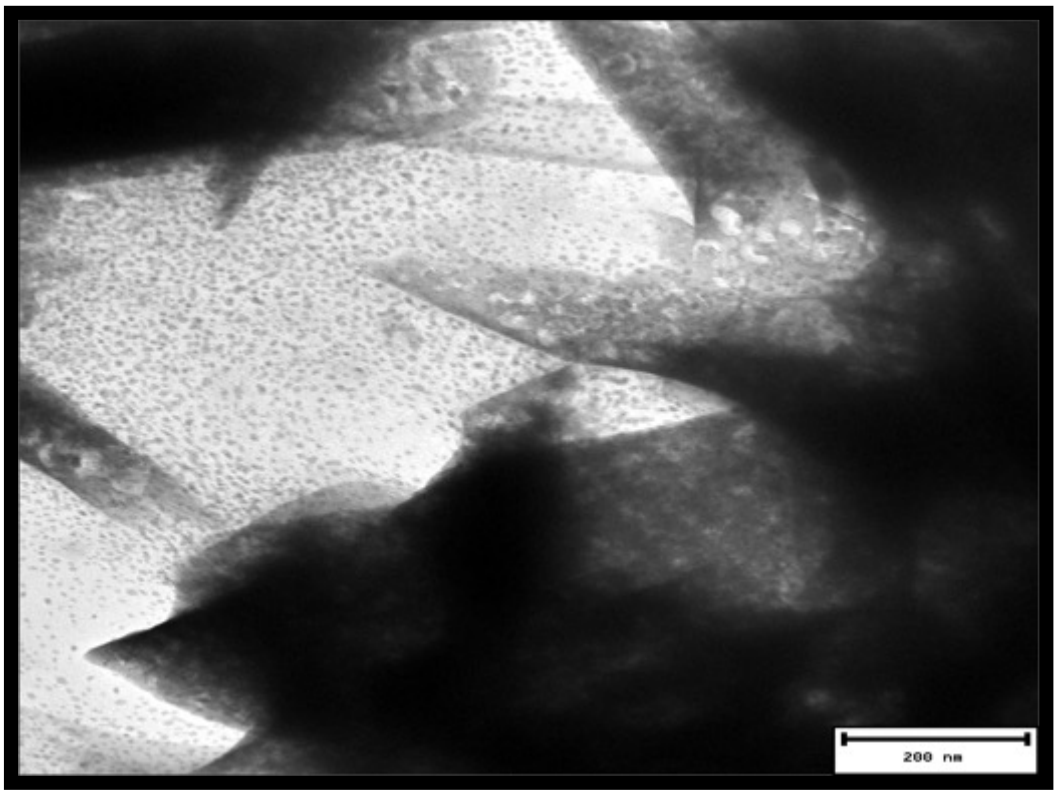

Figure 4.23. High magnification TEM micrograph of *P. castaneae* biomass-synthesized PbS nanoflowers and quantum dots. Fibrous edges of PbS nanoflowers which are in close proximity to PbS quantum dots. The formation of nanoflowers could occur through the Ostwald ripening of smaller quantum dots which redissolve into solution to be deposited onto the surface of the nanoflowers.

The low magnification TEM micrograph in Figure 4.24 shows the presence of quasi-spherical NPs on the surface of *P. castaneae* cells as well as NPs that have been extruded into the extracellular environment. The NPs are seen covering the holey carbon layer with diameters ranging between 20 nm – 50 nm. Larger NPs are found both on the cell surface and intracellularly while smaller (~15 nm) NPs are only found in the extracellular environment (yellow arrows in Figure 4.24). The polydispersed nature of the larger (~80 nm) NPs can be seen as well as the complete covering of *P. castaneae* cells by quasi-spherical PbS NPs. El-Shanshoury *et al*. (2012) used *Bacillus anthracis* PS2010 in the extracellular synthesis of similar spherical PbS NPs. This research also demonstrated the direct correlation between the amount of EPS produced and the amount of metal which was deposited within the EPS (El-Shanshoury *et al*., 2012). At higher magnification, many PbS quantum

dots (3 nm – 18 nm) NPs are also seen coating the surface of the holey carbon grid (inset of Figure 4.24).

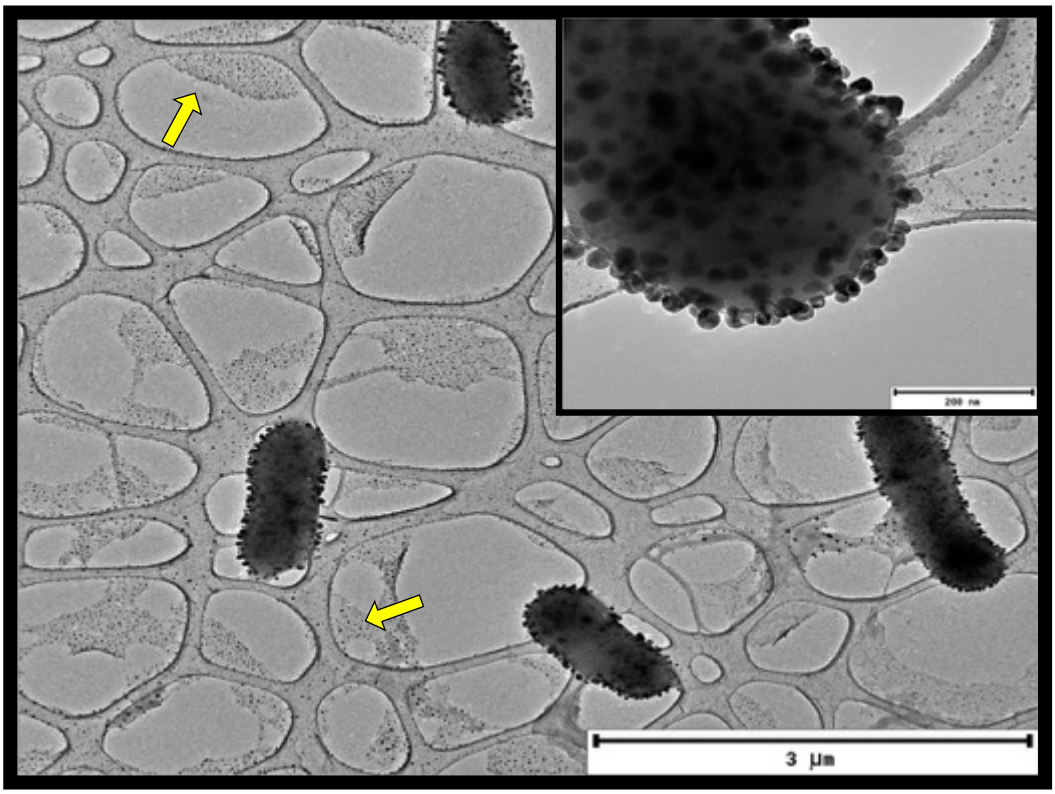

Figure 4.24. Low and high magnification TEM micrographs of *P. castaneae* biomass-synthesized spherical PbS NPs. *P. castaneae* cells are covered in multiple large amorphously shaped and near-spherical PbS NPs. Smaller NPs are localized in an electron-dense area presumed to be EPS (yellow arrows). Inset: High magnification TEM image showing the polydispersed nature of large PbS NPs on the bacterial cell surface as well as smaller PbS quantum dots in the exterior environment. Scale bar represents 200 nm.

The distinct localization of NPs with different sizes and morphologies provides evidence for a different mechanism of synthesis for the different types of PbS NPs. Smaller NPs are either synthesized and released extracellularly or synthesized extracellularly by the same bioreductants found in the CFE. The extracellular layer of biomolecules, are presumably EPS that are composed of polysaccharides, proteins, lipids and genetic material. EPS is represented as a more electron dense "gel-like" area covering the holey carbon substrate that is visibly saturated with variously sized and shaped PbS NPs (Figure 4.25). The inset of Figure 4.25 shows

a high magnification micrograph of PbS NPs within the EPS. These include quantum gots with diameters between 3 nm – 10 nm with aspect ratios between 3 and 20, quantum rods and nanorods between 18 nm – 37 nm with similar aspect ratios. Quasi-spherical quantum dots with particles sized between 2 nm – 15 nm, as well as various irregularly shaped nanoprisms with sizes between 20 nm – 80 nm were also produced.

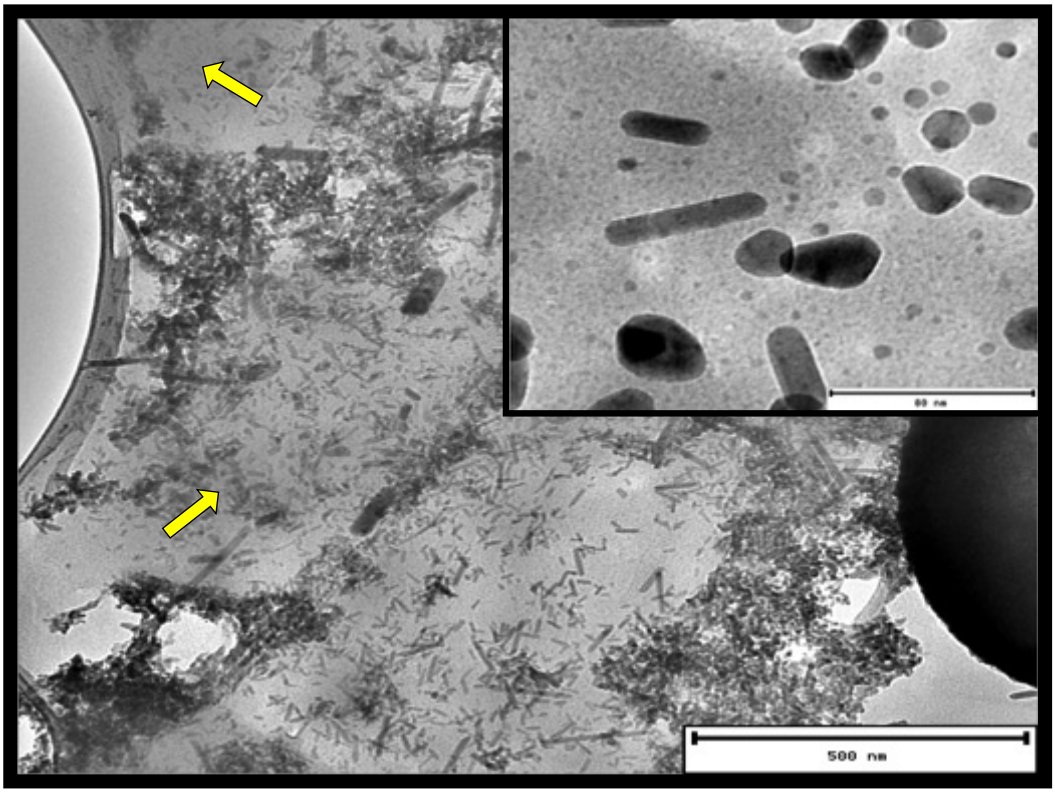

Figure 4.25. Low and high magnification TEM micrographs of *P. castaneae* biomass-synthesized isotropic and anisotropic PbS NPs. Differently sized PbS nanorods and nanospheres aggregated within the presumed EPS layer (yellow arrow) after 72 h of incubation with Pb and S metal ion precursors. Inset: High magnification TEM image of PbS quantum rods, nanorods, amorphously-shaped NPs and nanospheres with the presumed EPS layer. Scale bar represents 40 nm.

All the constituents of the bacterial EPS are known to be involved in the bioreduction and stabilization of metal NPs by bacteria (Kang, Alvarez and Zhu, 2013; Li *et al*., 2016; Raj *et al*., 2016). Many other *Paenibacillus* species have been shown to produce increased amounts of EPS (Pal and Paul, 2008). *P. polymyxa*

(Prado Acosta *et al*., 2005) and *P. jamilae* (Morillo *et al*., 2006) are known to produce EPS that shows a strong binding affinity towards heavy metals. Anisotropic PbS NPs could either be dispersed within the EPS and/or synthesized within the EPS.

The synthesis of larger NPs only at the cell surface or within the cell to later be transported to the cell surface suggests that the concentrations of precursors and capping agents are found in a higher concentration at this localization. Concentrations are much lower in the extracellular environment and thus the production of smaller sized NPs. This mechanism was first proposed by Beveridge and Fyfe (1985) in their investigation of metal mineralization by bacteria. A two-step mechanism was shown involving anionic sites on the cell wall that, through electrostatic interactions, acted as sites for nucleation. Consequently, this led to the metal reduction and precipitation of nanoscale crystals within and on the cell wall.

In the crystalline equivalent of PbS systems, Cho *et al.* (2005) discovered that truncated PbSE ~10 nm nanocubes are formed through the evolution of ~5 nm cuboctahedrons. Further investigation suggested that the {110} facets are more highly reactive and as such, are preferentially consumed in order to satisfy the lowest thermodynamic energy required. This results in growth perpendicular to the {111} facets. Similarly, the as-synthesized PbS nanorods show growth in the same direction and stabilization of the same facets. The SEM/TEM analysis of PbS NPs are in agreement with the strong absorption peaks in the NIR range observed for the CFE and biomass-prepared PbS NPs. These peaks are thefefore due to the formation of highly anisotropic NMs and not due to the self-assembly or packing of quasi-spherical NPs as demonstrated by Ankamwar, Chaudhary and Sastry (2005).

Gold Nanoparticles from *P. castaneae* Cell Biomass

Figure 4.26 shows a SEM micrograph of spherical Au NPs of various sizes arranged in clusters on the surface of a larger nanotriangle synthesized by the *P. castaneae* biomass. Individual NPs have diameters of 15 nm – 30 nm with

clusters ranging from 30 nm – 600 nm. Larger clusters (150 nm- 250 nm) of Au NPs are known as soft particle aggregates and have been implicated in the formation of large anisotropic Au NMs (Shankar *et al*., 2004). A truncated nanotriangle (white arrow) as well as a larger nanotriangle folding over clusters of Au NPs (red arrows) are visible. The presence of truncated or snipped-edged nanotriangle is owed to the very thin dimensions of these 2-D NMs (Verma *et al*., 2013).

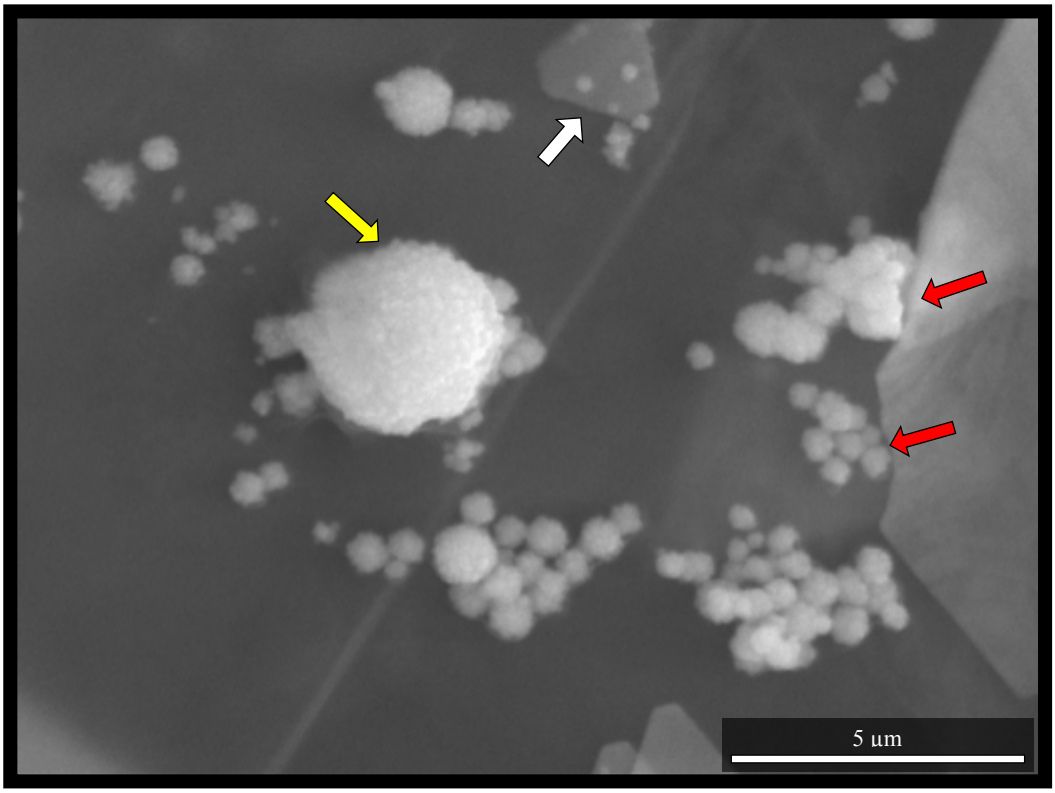

Figure 4.26. High magnification SEM micrograph of multiple Au NPs synthesized by *P. castaneae* biomass. Clusters of ~15 nm Au nanospheres covering the surface of a larger nanotriangle. A soft nanoparticle cluster (yellow arrow) can be observed. Smaller truncated nanotriangles, covered in small clusters are shown (white arrow). The propensity of large nanoplates to bend due to their extremely thin dimensions is observed as the nanoplates fold and contort over smaller clusters (red arrows). Production of anisotropic Au NPs occurred after the 72 h incubation of cell biomass with Au ion precursor in solution.

The polydisperse nature of Au NPs is illustrated in Figure 4.27 with the presence of >5 µm nanoplates including nanotriangles, nanohexagons and nanotrapezoids (white arrows) in close association with *P. castaneae* cells (yellow arrows). The

synthesis of 2-D Au NM is proposed to involve the rapid reduction of Au^{3+} ions and the room-temperature sintering of 'liquid-like' (soft aggregates) spherical Au NPs (Shankar *et al*., 2004). Regardless of the horizontal and vertical lengths, the thickness of the Au nanoplates does not exceed 50 nm. The reorganization of Au atoms and soft NP aggregates, to form the most thermodynamically stable shape, is responsible for the limitation in thickness (Ha, Koo and Chung, 2007).

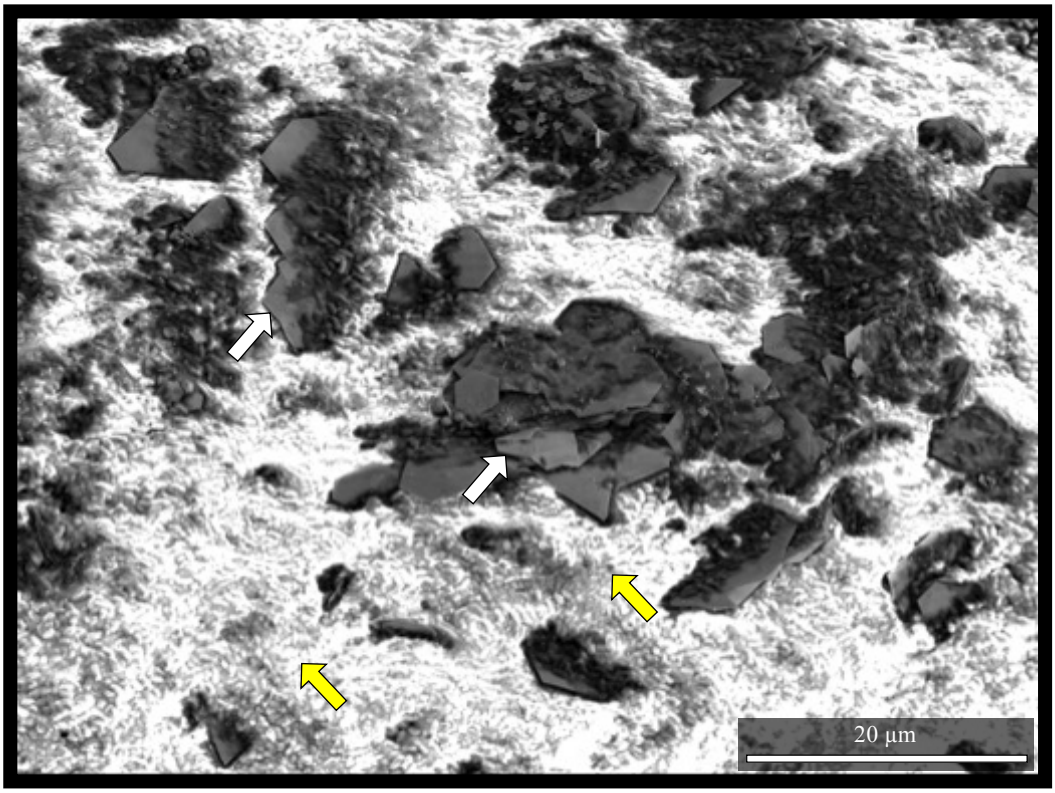

Figure 4.27. Low magnification SEM micrograph of multiple Au NPs synthesized by *P. castaneae* biomass. Large anisotropic Au nanoplates (white arrow) are shown covered by a high concentration of *P. castaneae* cells (yellow arrow). Production of anisotropic Au NPs occurred after the 72 h incubation of cell biomass with Au ion precursor in solution.

Figure 4.28 displays several stacked large nanoplates as well as multiple irregularly shaped nanoprisms (50 nm – 600 nm) covered in 'fluid-like' organic matter, cell remnants and/or EPS. The susceptibility of the Au nanoplates to bend is also demonstrated. Erasmus *et al*. (2014) demonstrated the ability of the ABC transporter, peptide binding protein from *Thermus scotoductus* SA-01, to reduce

Au^{3+} ions to yield a high percentage of thin, flat, single-crystalline Au nanotriangles. This research showed that varying the concentration of the Au ion precursor can produce similar anisotropic Au NPs of various shapes and sizes.

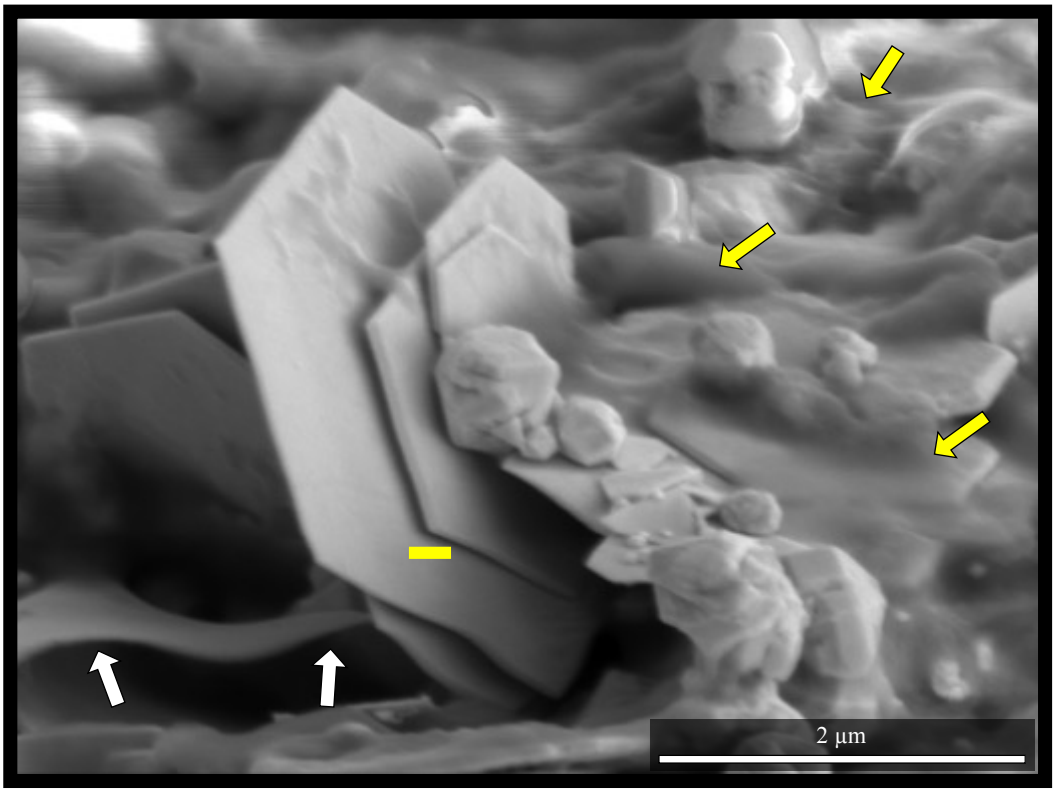

Figure 4.28. SEM micrographs of polydisperse Au NMs produced by *P. castaneae* cell biomass. Stacked Au nanohexagons covered by multiple irregularly shaped Au nanoprisms. Fluid-like organic material (yellow arrows) surrounds much of the NM. The propensity of Au nanoplates to bend and contort under stress is shown by the white arrows. Yellow scale bar represents 40 nm. Production of anisotropic Au NPs occurred after the 72 h incubation of cell biomass with Au ion precursor in solution.

Various other 2-D and 3-D Au NMs were also produced by *P. castaneae* cells (Figure 4.29). Pentagonal and hexagonal nanoprisms with definite and truncated edges are shown in the inset Figure 4.29. Although 2-D nanoplates have frequently been biologically synthesized (Erasmus *et* al., 2014; He *et al*., 2007; Varia *et al*., 2016), the bacterial synthesis of 3-D nanoprisms of this nature and size have not yet been reported in literature. Large nanoprisms have however been produced using plant extracts (Shankar *et al*., 2004), fungal extracts (Goswami and Ghosh,

2013) and chemical reduction using 3-butenoic acid (Casado-Rodriguez *et al*., 2016).

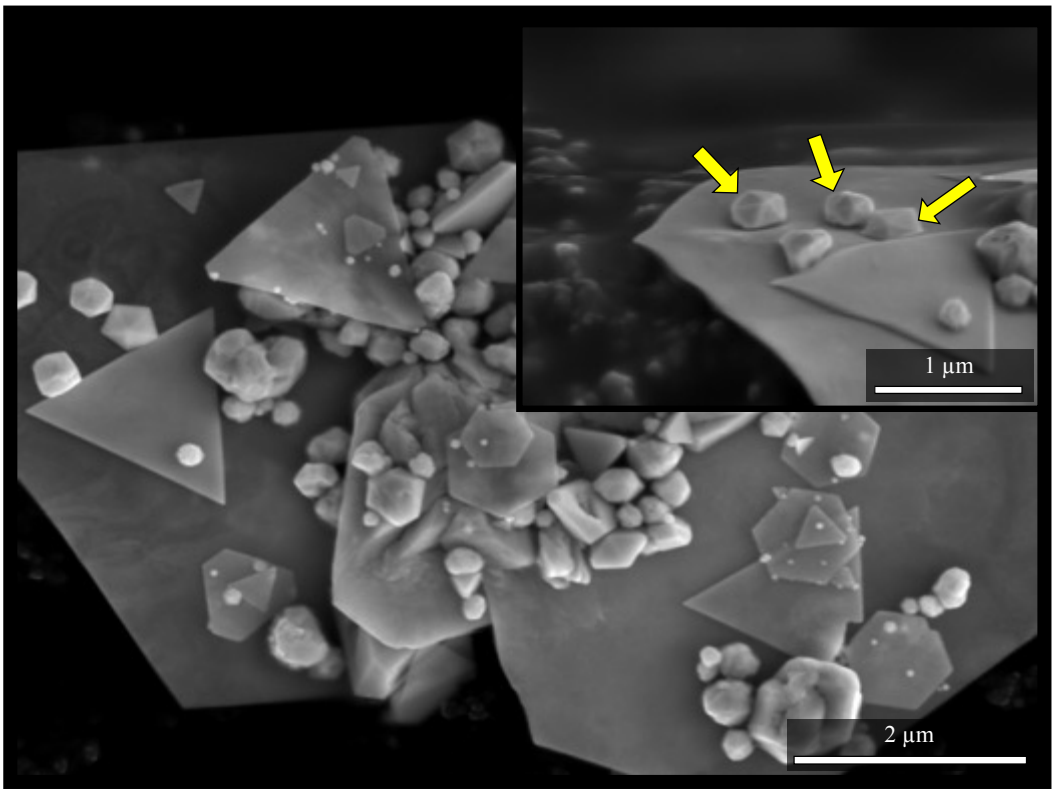

Figure 4.29. Low and high magnification SEM micrographs of polydisperse Au NMs produced by *P. castaneae* cell biomass. Variously shaped and sized 1-D, 2-D and 3-D Au NMs in close association with each other. Inset: 3-D Pentagonal Au nanoprisms in close association with other Au NMs. Production of anisotropic Au NPs occurred after the 72 h incubation of cell biomass with Au ion precursor in solution.

Figure 4.30 shows a TEM micrograph of penta-twinned and spherical Au NPs that originate from within the bacterial cell surface. Distinct differences in the nanoparticle shapes are evident, even though they all originate from within the cell and are in close proximity. This suggests the binding of presumptive biomolecules to the NP surface occurs on an atom-by-atom level. These Au NP chains are comparable to the Fe_3O_4 NPs produced by magnetotactic bacteria within their highly specialized magnetosome organelles (Yan *et al*., 2012). The mechanism of formation is a highly complex process that involves multiple discrete steps;

including vesicle formation, Fe uptake and transport, and biologically controlled mineralization to form NPs (Bazylinski and Schübbe, 2007).

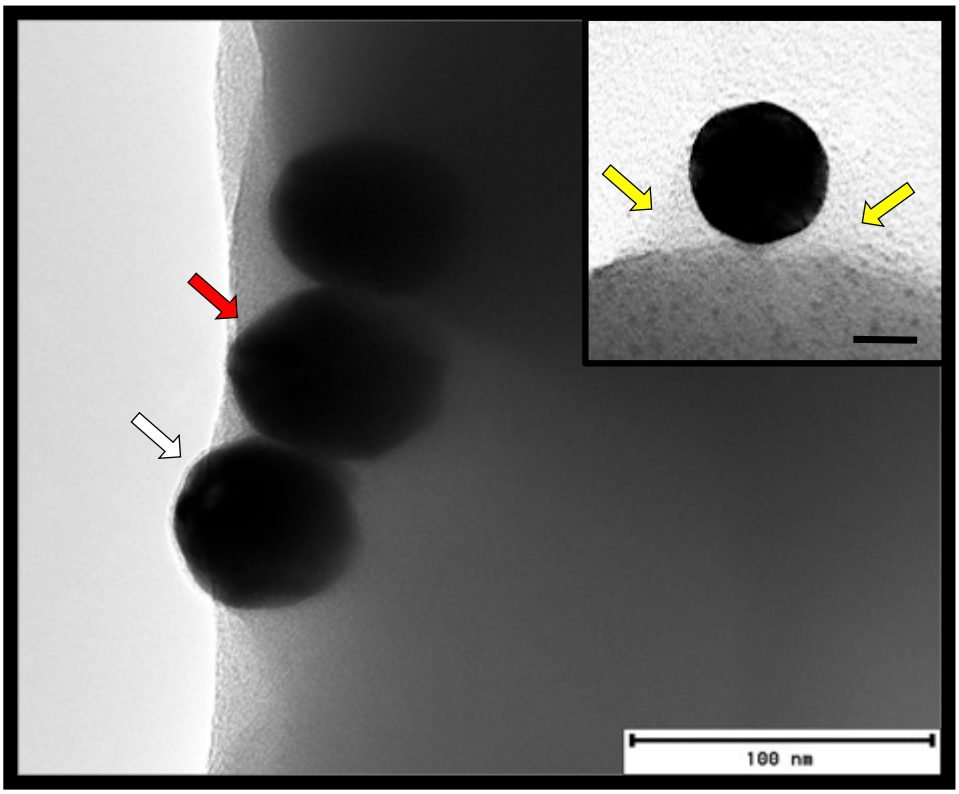

Figure 4.30. TEM micrographs of *P. castaneae* biomass-synthesized Au NPs of distinct morphologies. A chain of spherical (white arrow) and penta-twinned (red arrow) Au NPs within the cell surface of a *P. castaneae* cell. Production of the Au NPs occurred after the incubation of cell biomass with Au ion precursor in solution for 72 h. Inset: Spherical Au NP in the process of being extruded into the extracellular environment. The covering of the NP by the cell wall in evident in the grey electron dense area surrounding the NP (yellow arrows).

Nanoanisotropes are also shown to be coated with presumptive biomolecules (Figure 4.31). These biomolecules are hypothesized to be involved in both the reduction and capping of the Au NMs. A Fourier Transform InfraRed (FTIR) spectroscopy analysis of the biomolecules associated with Au NPs by Murugan *et al*. (2014), indicated the presence of proteins and/or peptides which were shown to be responsible for the stabilization of the Au NPs. The high magnification TEM micrograph (inset of Figure 4.31) shows the uneven surface coating of Au NPs by

biomolecules from *P. castaneae*. The diameter of the coating varies between 0.5 nm – 3.5 nm.

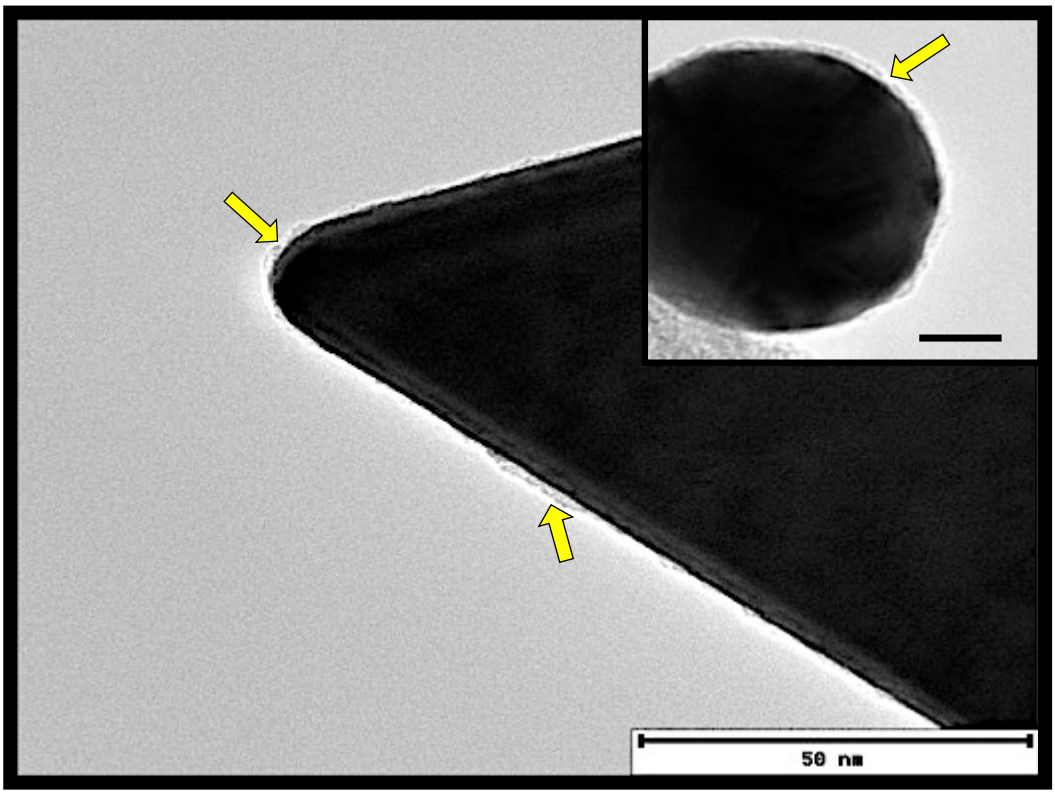

Figure 4.31. High magnification TEM micrographs of *P. castaneae* biomass-synthesized Au NPs covered in biomolecules. The surface of a Au nanotriangle showing surface coatings by presumptive bacterially-derived biomolecules (yellow arrow). Inset: High magnification TEM micrograph showing the uneven surface coating of a 0.5 nm – 3.5 nm layer of presumptive biomolecules (yellow arrow). Scale bar represents 10 nm.

The TEM micrograph in Figure 4.32 shows the polydisperse nature as well as both the smooth and rough surface morphology of Au NPs synthesized by *P. castaneae*. Multiple 1-D, 2-D and 3-D Au NMs are shown in close association with each other; 2 μm truncated nanotriangles are shown covered in smaller nanotriangles as well as nanohexagons, nanoprisms and nanospheres. The production of polydispersed Au NPs is a common characteristic of biologically synthesized Au NMs. These results are consistent with those of other biologically synthesized Au NPs (Ankamwar, Chaudhary and Sastry, 2005; Murugan *et al*., 2014; Paul *et al*., 2015;

Varia *et al*., 2016; Verma *et al*., 2013; Zhang, Shen and Gurunathan, 2016). The polydisperse nature of biologically synthesized Au NPs is owed to the availability of contrasting bioreductants as well as stabilizing biomolecules in various concentrations. These can therefore use a diverse range of different multi-step mechanisms (Erasmus *et al*., 2014).

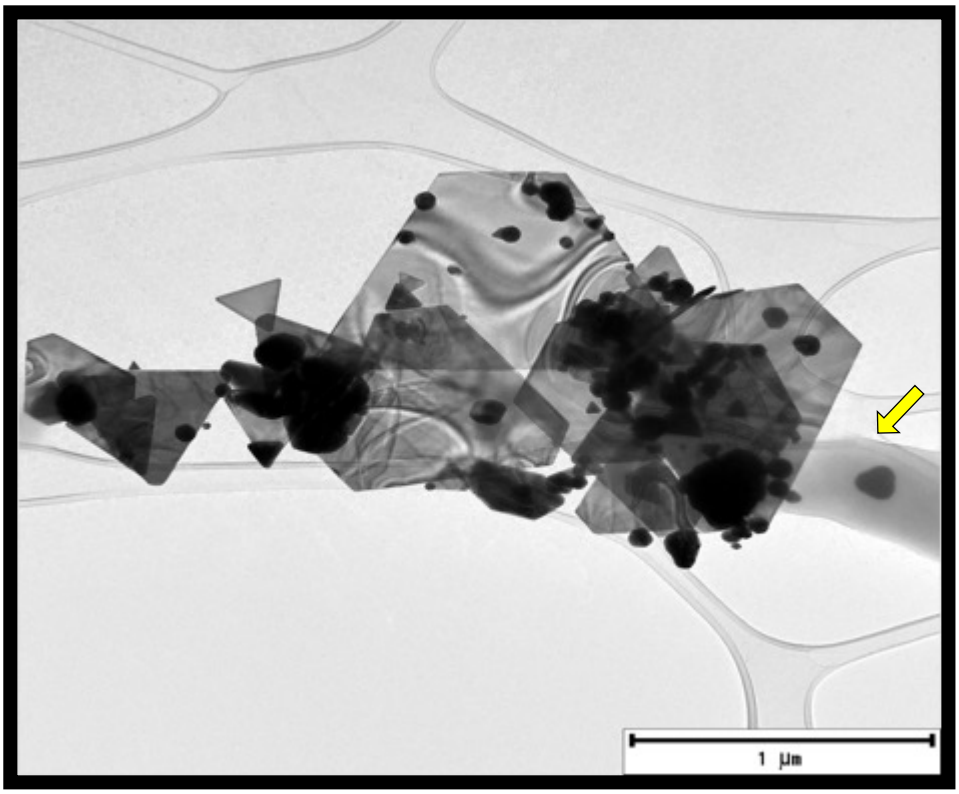

Figure 4.32. TEM micrograph of polydisperse Au NM produced by *P. castaneae* cell biomass. Multiple anisotropic Au NPs in close association. Production of anisotropic Au NPs occurred after the 72 h incubation of cell biomass with Au ion precursor in solution. A single bacterial cell (yellow arrow) with a truncated Au nanotriangle either within or on the surface of the cell can be observed.

Figure 4.33 represents side-by-side TEM micrographs taken at 0° and 20° angles showing the ~30 nm thickness of Au nanotriangles. The Au NPs are shown protruding through the surface of *P. castaneae* cells; either biosynthesized at the site of protrusion or biosorbed onto the bacterial cell surface.

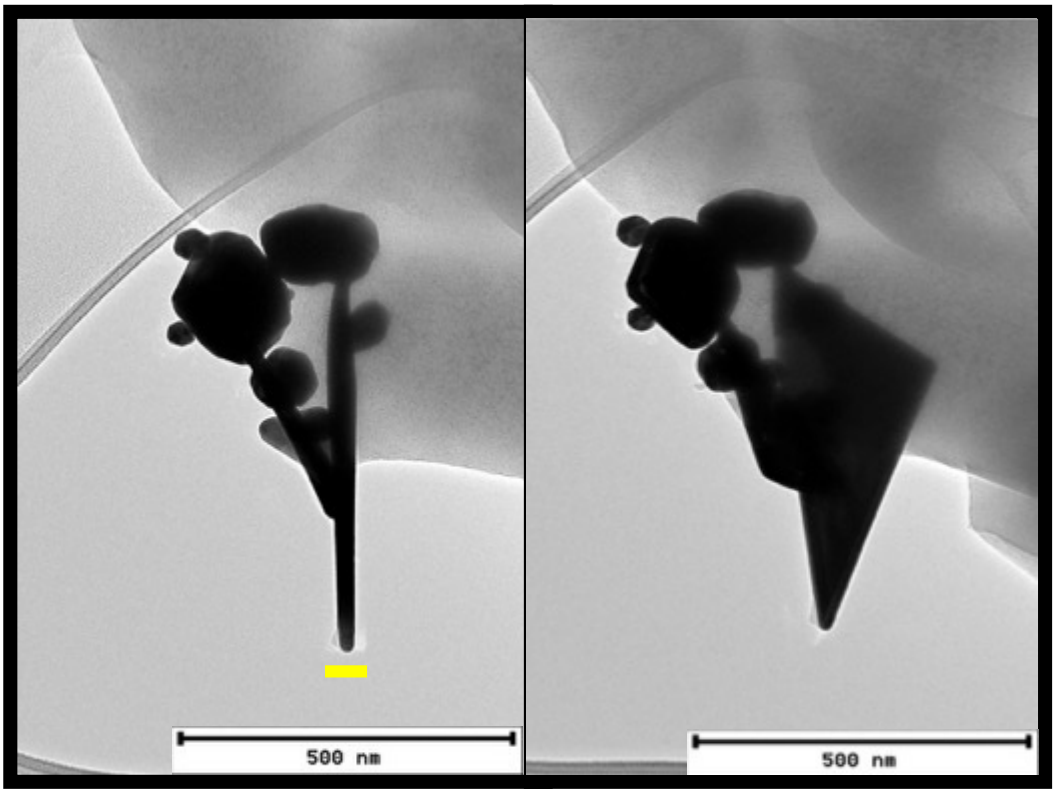

Figure 4.33. TEM micrographs of polydisperse Au NM produced by *P. castaneae* cell biomass showing nanoplates thickness. Side-by-side TEM micrographs of Au NPs taken at 0° and 20° angles, respectively. Yellow scale bar represents 45 nm.

Figure 4.34 shows a low magnification TEM micrographs of Au NP aggregates. Aggregates are composed of 10 nm – 20 nm quasi-spherical Au NPs surrounded by a dense layer of *P. castaneae*-derived biomolecules. These aggregates have previously been described as nanoperiwinkles (Jena and Raj, 2007) or soft NP aggregates (Shankar *et al*., 2004). These NP clusters are hypothesized to form using a different mechanism compared to that of the spherical NPs and are generally considered to be the initial form in the production of Au nanoplates (Li and Shi, 2005). Agglomeration of Au NP aggregates and the preferential binding of biomolecules to the {111} facets thus leads to perpendicular growth of Au nanoplates (Zhou *et al*., 2015).

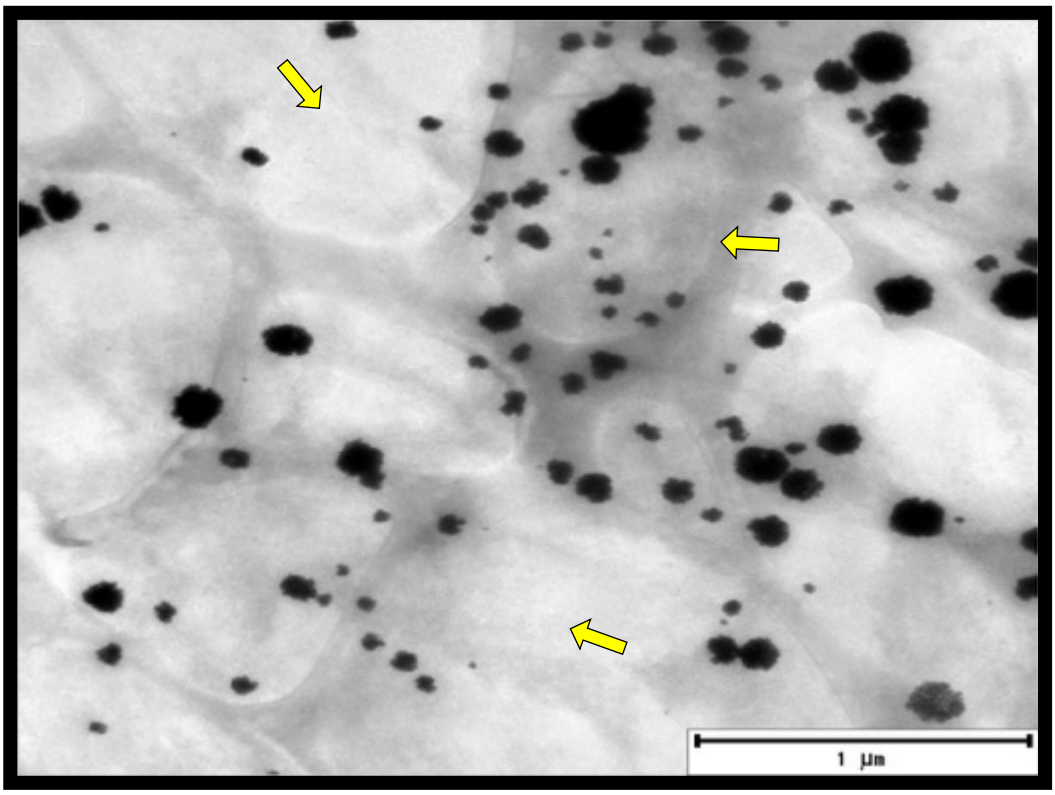

Figure 4.34. Low magnification TEM micrograph of Au NP aggregates produced by *P. castaneae* cell biomass. Low magnification images of soft NP aggregates or nanoperiwinkles on a layer of presumptive EPS (yellow arrow). Aggregates are composed of 10 nm – 20 nm quasi-spherical Au NPs.

Kerr and Yan (2016) demonstrated the importance of reactions conditions in the synthesis of Au nanotriangles. The effects of temperature, order and manner of addition of reducing agent, and ratio of metal ion precursor to reducing agent were shown to be extremely important. Figure 4.35 shows the high magnification TEM micrograph of Au NP soft aggregates. The shape and morphology are similar to previously reported aggregates, deemed as the initial starting point for Au nanoanisotrope synthesis (Kerr and Yan, 2016).

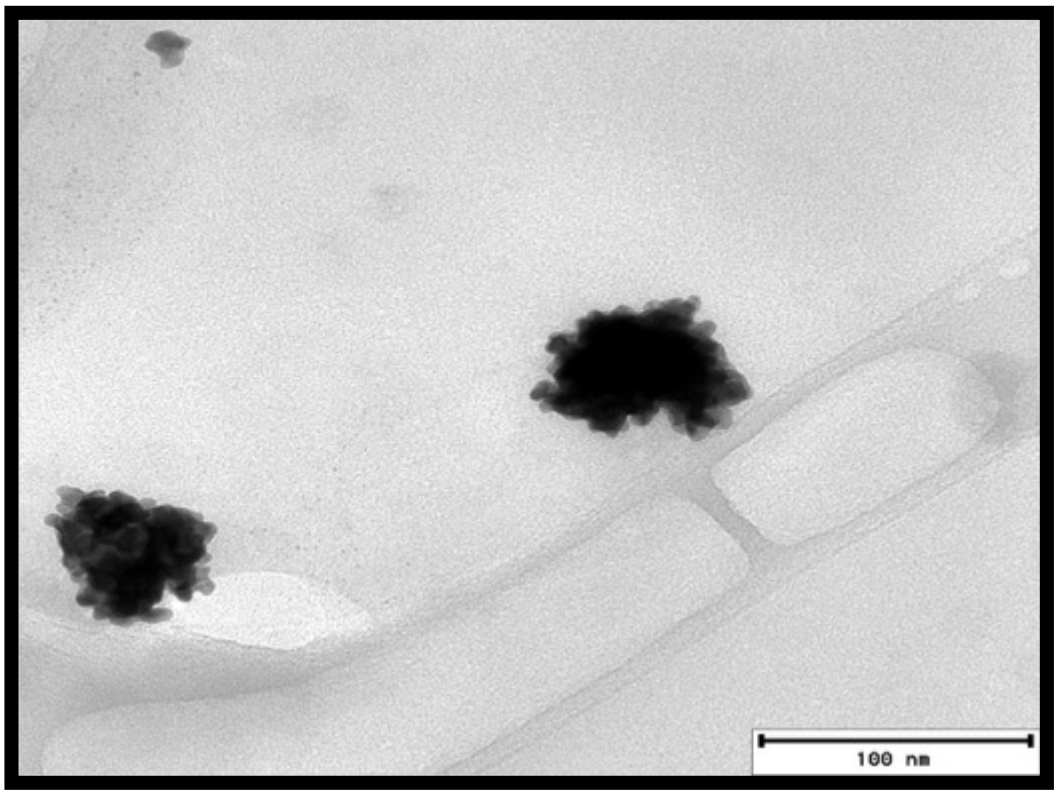

Figure 4.35. High magnification TEM micrograph of Au NP aggregates produced by *P. castaneae* cell biomass. High magnification images of soft NP aggregates or nanoperiwinkles on a layer of presumptive EPS. Aggregates are composed of 10 nm – 20 nm quasi-spherical Au NPs.

It is proposed that Au^{3+} ions bind to biomass through functional groups on the cell wall peptides or proteins which carry a more positive charge (Sanghi and Verma, 2010). Tight binding to non-reducing molecules therefore weakens the reducing power of the bioreductants. This allows the ions to get closer to the binding sites causing the reduction rate to be decreased. A slow reduction rate directly contributes to the formation of anisotropic Au NMs whereas fast reduction leads to spherical NPs (Varia *et al*., 2016). Also implicated is the concentration and nature of the precursor ions, as well as capping or stabilizing agents, in this case proposed as biomolecules from *P. castaneae*. The fact that the resulting Au NPs synthesized by *P. castaneae* are stable for very long periods of time despite the absence of any additives, indicates that the particles are electrostatically stabilized.

Silver/Silver Chloride Nanoparticles from *P. castaneae* Cell-free Extract

Ag/AgCl NPs produced from the CFE tended more towards monodispersity than other metal NPs synthesized by *P. castaneae*. The high magnification SEM micrograph in Figure 4.36 shows large clumps of spherical Ag/AgCl NPs. Close-packing from drying effects in sample preparation for SEM analysis of Ag/AgCl NPs produced aggregates with granular appearance made up of many spherical NPs ranging between 15 nm and 25 nm. These results are consistent with the narrow absorption band of ~440 nm as well as the broadening of Bragg reflections in the PXRD analysis. Kumar *et al*. (2016) showed the synthesis of a mixture of Ag and AgCl NPs, synthesized through the use of an extract from needles of *Pinus densiflora*, with an absorption band of ~438 nm and similar PXRD spectral patterns.

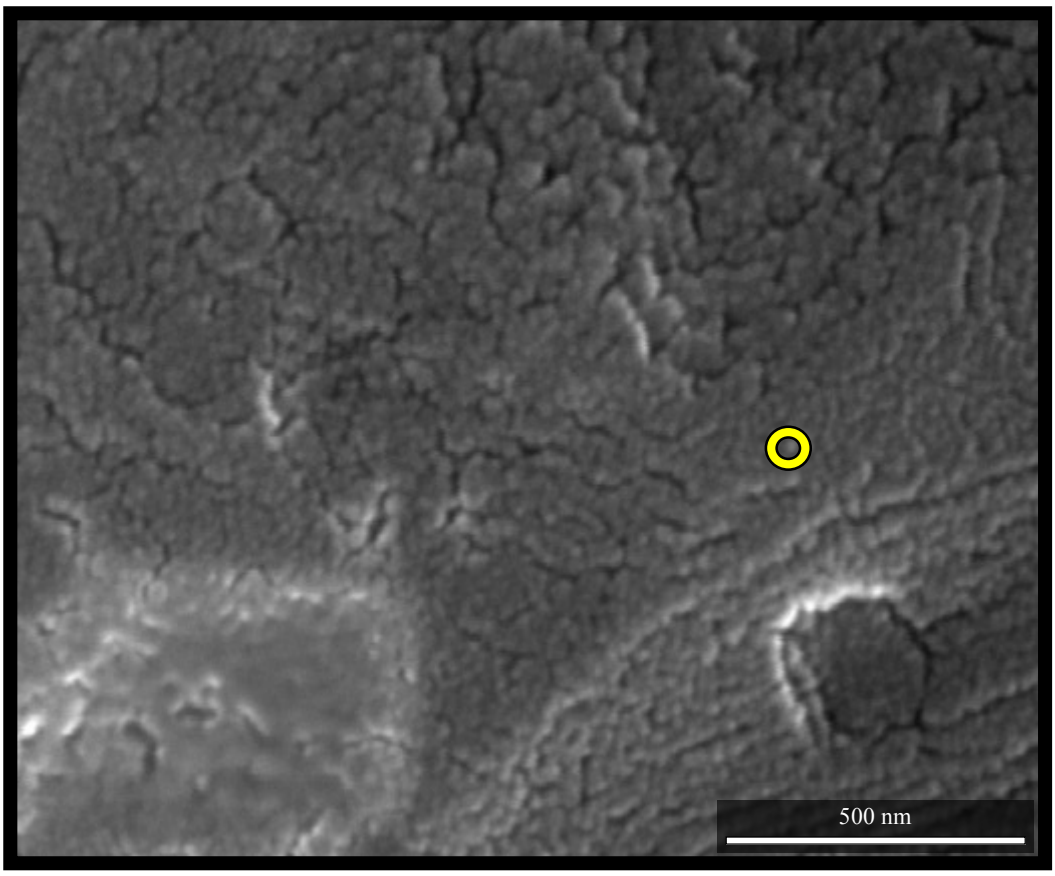

Figure 4.36. High magnification SEM micrographs of spherical Ag/AgCl NPs produced by *P. castaneae* CFE. High magnification SEM micrographs of densely packed spherical Ag/AgCl NPs ranging between 15 nm – 25 nm. Yellow circle represents 25 nm.

Although most NPs range between 8 nm and 20 nm, a small percentage of large (<40 nm) NPs were also synthesized (Figure 4.37). This is a feature common in the biological synthesis of Ag/AgCl NPs (Dhas *et* al., 2014; Hu *et al*., 2009; Kumar *et al*., 2016).

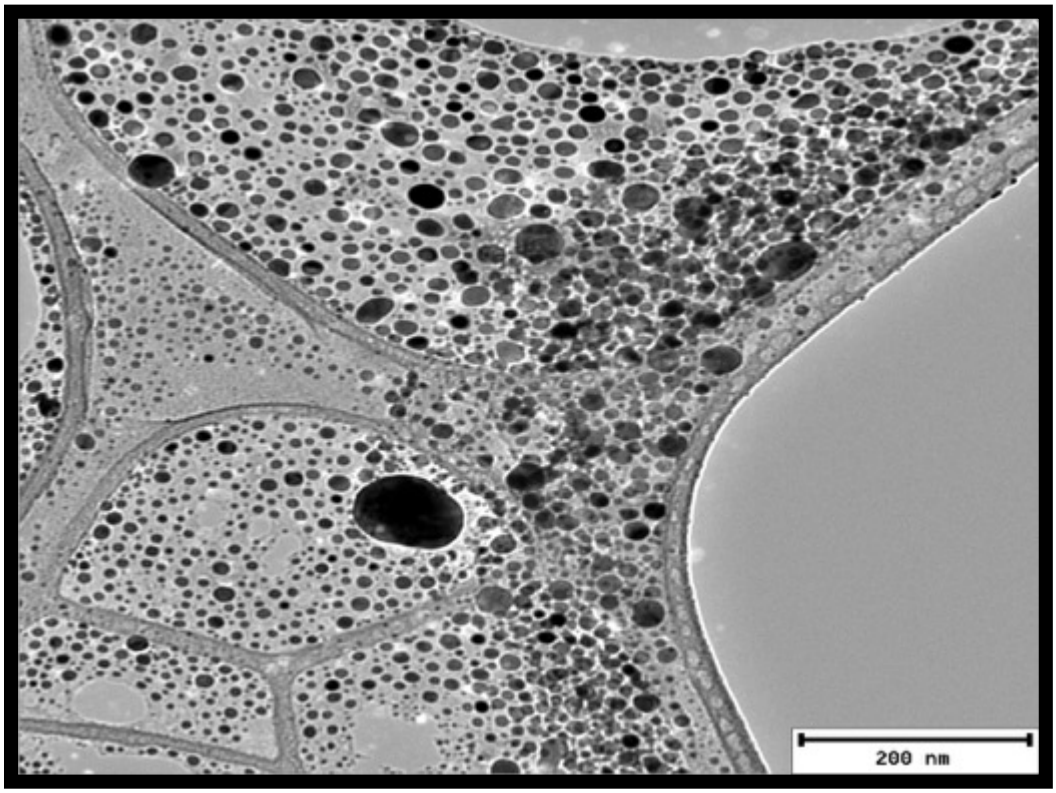

Figure 4.37. Low magnification TEM micrograph of spherical Ag/AgCl NPs produced by *P. castaneae* CFE. Low magnification TEM micrograph of well-dispersed spherical Ag/AgCl NPs. NPs mostly range between 8 nm – 20 nm with the synthesis of large (> 50 nm) quasi-spherical NPs.

Figure 4.38 shows the increased surface roughness of Ag/AgCl NPs produced by the CFE of *P. castaneae*. Such a high degree of surface roughness has yet to be published in literature for biosynthesized Ag/AgCl NPs, but is common in the chemical synthesis of Ag NPs (Chen *et* al., 2013). The "rough" Ag NPs have

received much attention in the plasmonic industry as enhanced SERS substrates as each crevice acts as a site for catalysis or as a plasmonic hotspot (Lu *et al*., 2013).

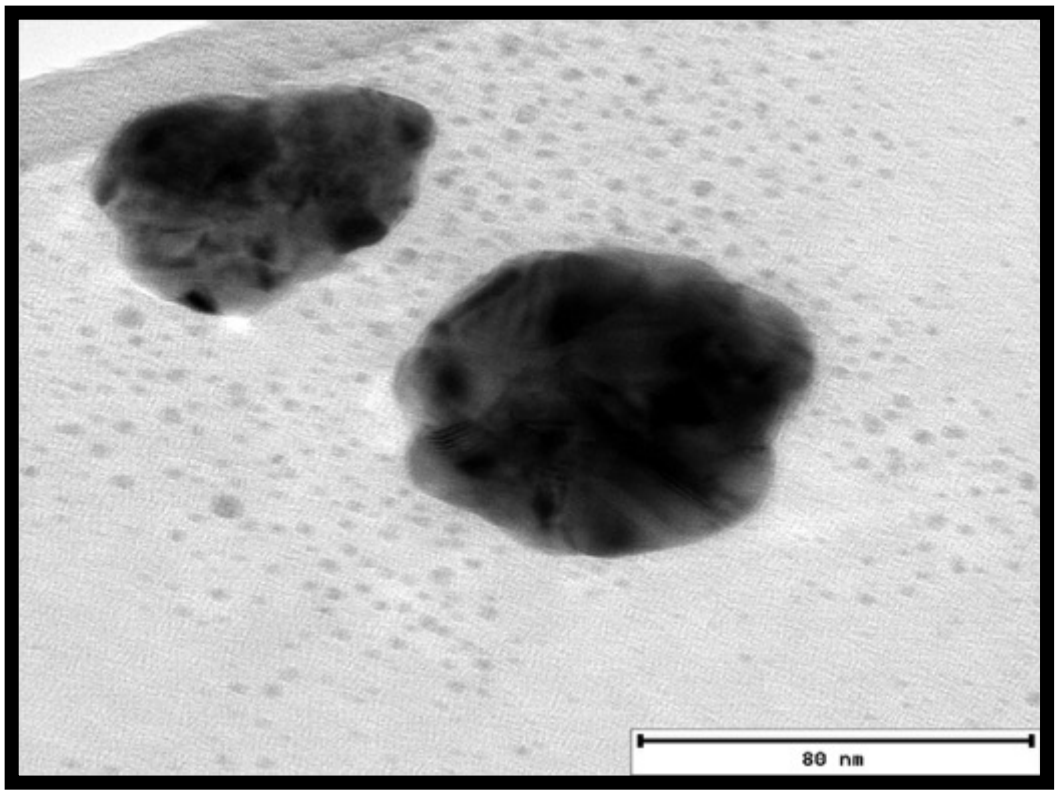

Figure 4.38. High magnification TEM micrograph of spherical "rough" Ag/AgCl NPs produced by *P. castaneae* CFE. High magnification TEM micrograph of quasi-spherical Ag/AgCl NPs showing the rough surface morphology.

Silver Nanoparticles from *P. castaneae* Cell Biomass

Although silver ions are generally considered toxic to bacteria (Taylor *et al*., 2016), *P. castaneae* biomass was still capable of producing Ag/AgCl NPs. Figure 4.39 shows bacterial cells that show no signs of lysis or cell death that are in close association with a large cluster of Ag/AgCl NPs.

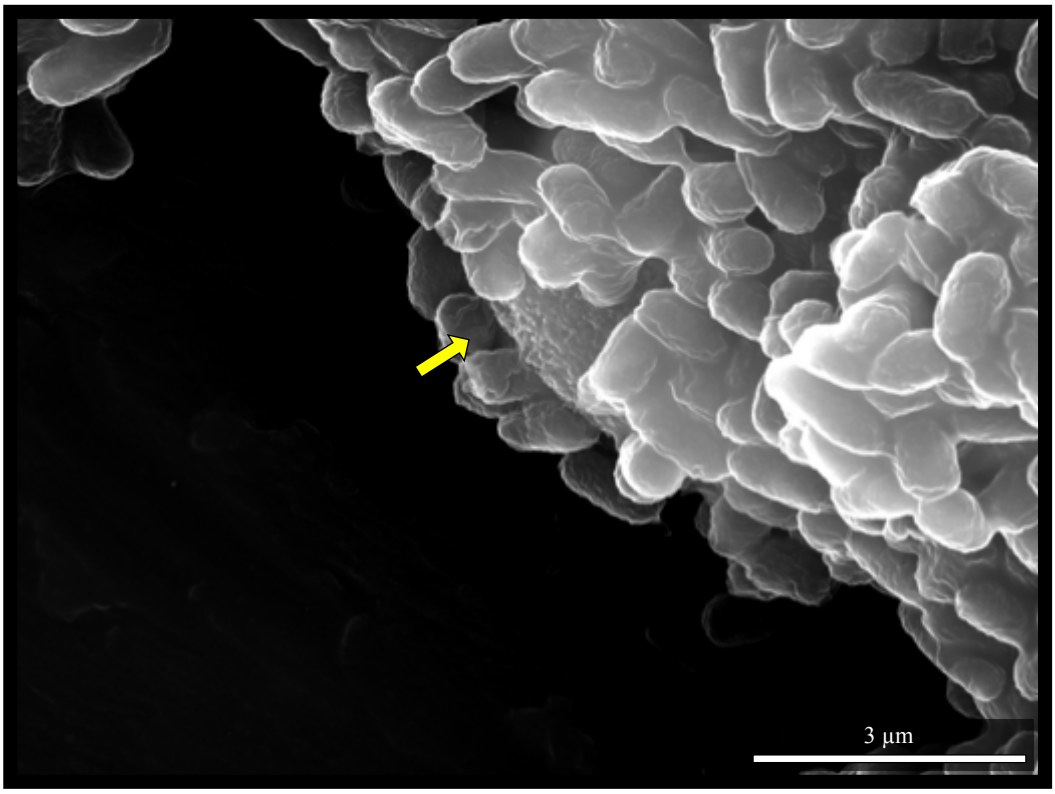

Figure 4.39. SEM micrograph of Ag/AgCl NPs produced by *P. castaneae* biomass. A cluster of spherical Ag/AgCl NPs (yellow arrow) covered by a layer of bacterial cells which show no signs of cell damage or lysis.

Many bacterial species have shown resistance to toxic heavy metal-based antimicrobials such as Ag and AgCl (Dibrov *et* al., 2002; Nair and Pradeep, 2002; Zhang *et al*., 2005b). This is due to the detoxification mechanisms used by bacteria to quell the stress caused by these metals; one such mechanism is the formation of NPs. Although resistance is high, some bacterial cells within the population are still susceptible to cell shrinkage and lysis. Ag^- ions as well as Ag/AgCl NPs are still able to cause cell lysis in *P. castaneae* as shown in Figure 4.40.

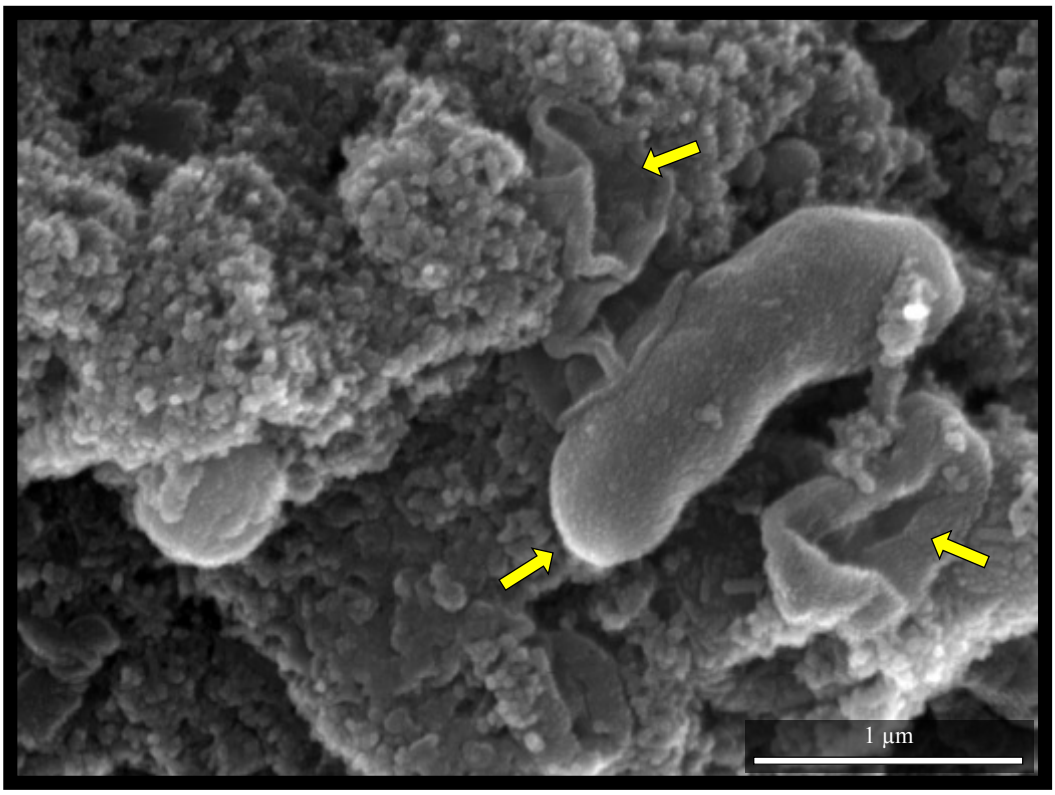

Figure 4.40. SEM micrograph of Ag/AgCl NPs produced by *P. castaneae* biomass with evidence of cell lysis. Aggregates of densely packed spherical Ag/AgCl NPs in close proximity to lysed and damaged bacterial cells (yellow arrows).

Ag/AgCl NPs are well-distributed through-out the cell biomass, on the surface of *P. castaneae* cells (Figure 4.41). Ag/AgCl NPs are found in either large (60 nm – 200 nm) clusters or well-distributed within biomolecules which are hypothesized to be EPS (inset of Figure 4.41). Compared to non-exposed cells (Figure 4.16a), Ag^{+} ion-stressed *P. castaneae* cells appear to be shrunken and rounded and produce substantially more EPS, possibly as a defence mechanism to bind these toxic ions.

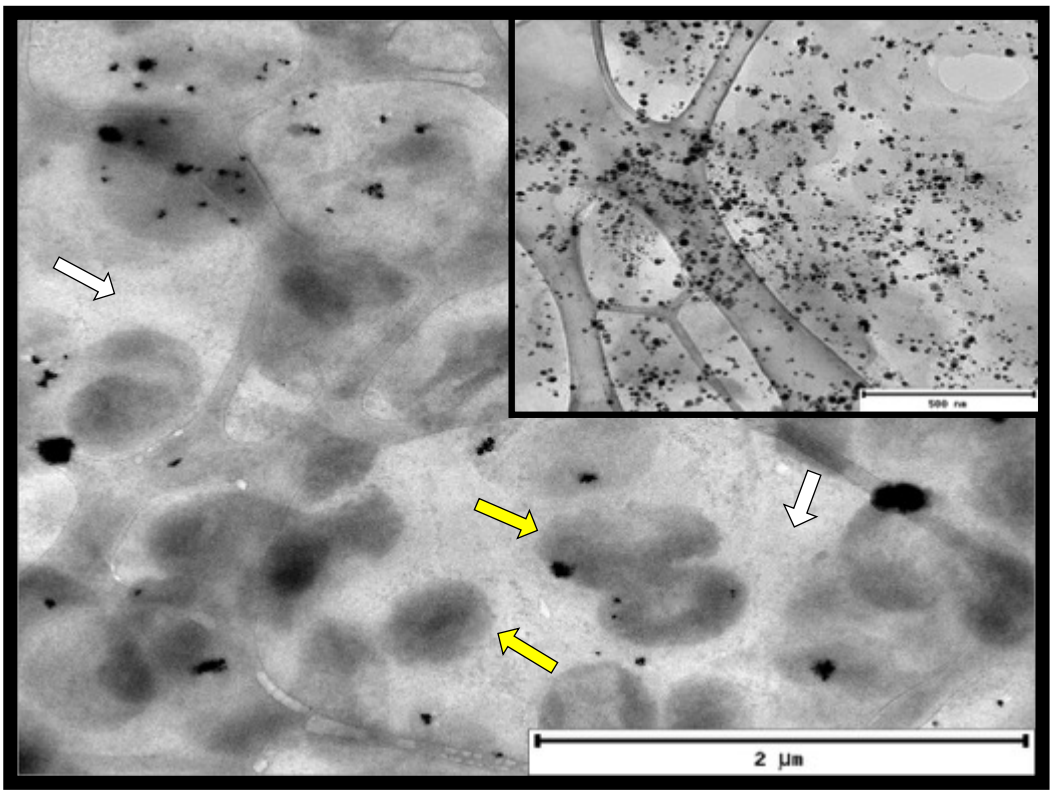

Figure 4.41. TEM micrographs of Ag/AgCl NPs produced by *P. castaneae* biomass. Ag/AgCl NPs distributed in aggregates on the surface of the bacterial cells. Cells also shows signs of toxin-stress, including cell shrinkage and a rounded shape (yellow arrow). High amounts of EPS are produced as shown in the spaces between bacterial cells (white arrow). Inset: Ag/AgCl NPs well-distributed within biomolecules which are hypothesized to be EPS.

Ag NPs were not noted in the interior of bacterial cells, indicating the extracellular synthesis either on the cell surface or by molecules extruded by bacterial cells. This is consistent with only a slight colour change in biomass-Ag reactions compared to CFE-Ag reactions. Bioreductants capable of Ag^{+} ion reduction are therefore found in a higher concentration at the bacterial cell wall or released into the extracellular environment. These results are consistent with previously biologically synthesized Ag/AgCl NPs (Dhas *et* al., 2013; Hu *et al*., 2009).

4.3 Possible Mechanism for Nanoparticle Growth and Synthesis

The exact mechanism of formation of both the isotropic and anisotropic metal NPs in microbial systems are not fully understood. From the current research it appears that the bacterial synthesis of metallic NPs might be easily manipulated so as to control the synthesis of specific NPs with predefined shapes. The bacterial synthesis of metal NPs for discrete commercial use by *P. castaneae* is therefore an exciting prospect. In the production of metallic NPs via established chemical techniques, the morphology and size of NPs is highly sensitive to any kind of additive. Small changes in the type or amount of additive therefore lead to a distinct change in particles shape and size (Gerdes *et al*., 2015). The presence of multiple morphologies and sizes in the bacterial synthesis of metallic NPs thus suggest the reduction and stabilization of NPs occurs through several different routes.

Biological synthesis however, does not require the addition of additives such as acetic acid, dichloroethane, polyvinyl alcohol, CTAB, hydroxylpropyl methylcellulose or sodium dodecyl sulfate (Dong *et* al., 2006; Lu *et al*., 2013). This is due to the fact that, in bacterial synthesis, the required molecules are already present and produced by the bacteria themselves (Singh *et al*., 2016). Previous studies have reported that the biotransformation of metal ions into elemental metal involves the presence or secretion of biomolecules such as NADH-dependent reductases (Kaur *et al*., 2014), small peptides (Parikh *et al.,* 2011), quinines (Seshadri, Saranya, and Kowshik, 2011), lipids, enzymes (Kowshik et al., 2002), reducing sugars in the EPS (Kang, Alvarez and Zhu, 2013; Raj *et al*., 2016) as well as soluble electron-shuttles (Li *et al*., 2016; Suresh *et al*., 2010).

These results are consistent with the 3-D diffusion controlled mechanism modelled by Varia *et al*. (2016). In this model, $AuCl^{4-}$ ions diffuse through a stagnant aqueous thin film bordering the *S. putrefaciens* cell wall. The ions are then transported through the cell wall's lipopolysaccharide layer to the protein/enzyme metal recognition peptide motifs sorption and nucleation sites. Reduction occurs through electron transfer to the $AuCl^{4-}$ ions, located at redox active sites on membrane

proteins, such as cytochromes and hydrogenase (Varia *et al*., 2014). Au NP synthesis is facilitated through the phase change of $AuCl^{4-}$ to Au^{0}.

In the current study, similar mechanisms for the biosynthesis of metal NMs are hypothesized. Successful reduction of precursor metal ions into PbS, Au and Ag/AgCl NPs was shown to occur both intra- and extracellularly at various localizations. These being within the cell, on the cell surface, within the EPS as well as extracellularly in solution. As concentrations of both the reducing agents and surfactants/capping agents varies in these localization, so too does the shape, morphology and nature of the subsequently synthesized metal NPs. For anisotropic NMs, the synthesis of various shapes demonstrates the preferential binding of different surfactants to specific crystal facets. The subsequent stabilization of these facets and thus the perpendicular growth along that facet is possible as long as the required precursors are present (Kuang *et al*., 2013).

The mechanism of NPs formation is dependent on the presence of both bioreductants and biologically-derived capping/stabilizing agents from *P. castaneae* cells. The ability of biomolecules to serve as both reductant and capping agents have been well documented (Krishnan, Narayan and Chadha, 2016; Murugan *et* al., 2014; Park, Lee and Lee, 2016). From the results of this study, it is hypothesized that there are shared mechanisms, and therefore shared biomolecules, for the synthesis of spherical and non-spherical NPs, respectively. Spherical NPs of PbS and Ag/AgCl were produced using a CFE of *P. castaneae*, therefore a similar mechanism using the same biomolecules is likely. The production of large anisotropic PbS NPs using the *P. castaneae* biomass suggests the presence of the same bioreductant, but a different biological capping agent. This capping agent then preferentially binds to certain PbS facets causing the preferential and directional anisotropic growth (Lu *et al*., 2009). The synthesis of Au NPs only occurred with the use of bacterial biomass and thus a different mechanism and bioreductant was responsible for this. It is known that the reduction of Au^{+} ions occurs in a complex multistep process (Dey *et al*., 2010) and thus the use of shared bioreductant/s for the synthesis of Au NPs. However, large anisotropic Au NPs

require a different capping agent than spherical Au NPs and hence their polydisperse nature.

Notwithstanding these facts, the concentration of the precursor ions, bioreductants and capping agents at each specific localization (intracellular, extracellular or within the EPS) could play a major role in directing the synthesis of each specific NP type. This was shown by Erasmus *et al*. (2014), using *Thermus scotoductus* SA-01 for the synthesis of Au NPs, in which a change in the concentration of the ion precursor led to the formation of NPs with different shapes and sizes. From the initial studies on *P. castaneae* NP synthesis, a 2-step mechanism is proposed for metal NP formation, as summarized in Figure 4.42.

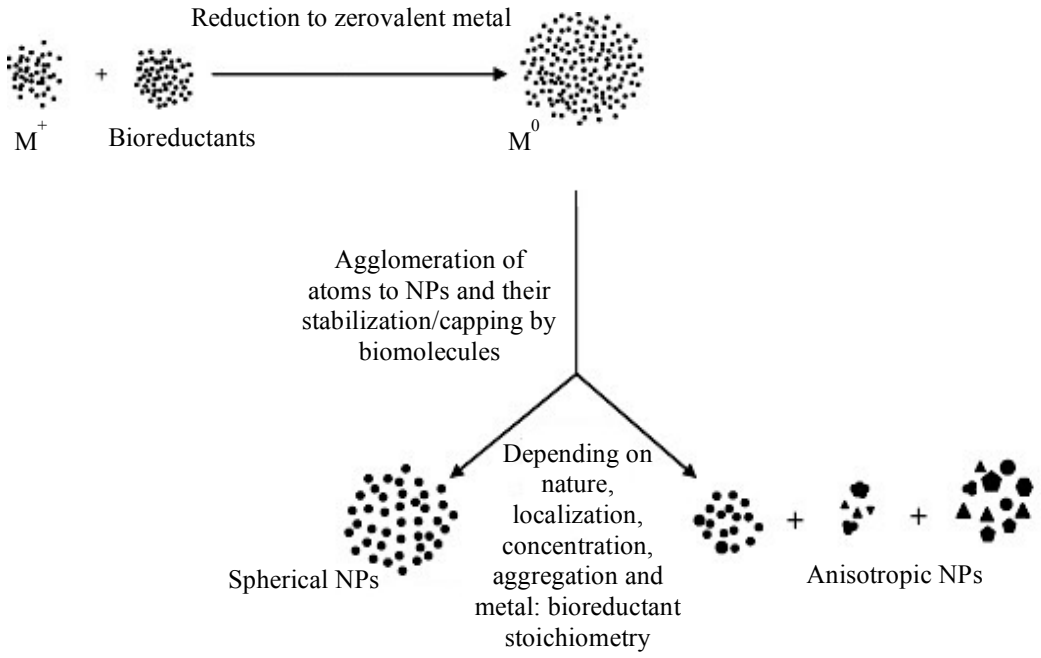

Figure 4.42. Mechanism of metallic nanoparticle formation by *P. castaneae*. The proposed mechanism shows the reduction of valent metal ions (M^+) by bioreductants to form zerovalent metal ions (M^0). Upon agglomeration, Ostwald ripening and orientated attachment, biomolecules also stabilize and cap the NP clusters. Depending on the nature of the biomolecules present as well as concentrations of precursors, either spherical (isotropic) or non-spherical (anisotropic) NPs will be produced.

PbS, Au and Ag/AgCl NPs with multiple shapes, sizes and morphologies were successfully synthesized using *P. castaneae* biomass and CFE. The synthesis method was shown to be facile and reproducible. NMs were also produced in a sustainable and green manner. As a consequence of the unique physical, chemical, electrical and optical properties of each respective metallic NP, they have direct technological and industrial potential in various fields (Hesto *et al*., 2016). This method can therefore be easily up-scaled and optimized for the commercial biosynthesis of metallic NPs. This is the first report of the synthesis of metallic NPs by *P. castaneae*, thus expanding on the limited knowledge surrounding the biological synthesis of NPs.

CHAPTER 5: CONCLUSION AND RECOMMENDATIONS

The ability of a heavy metal-resistant isolate of the bacteria, *P. castaneae*, to not only remove metal ions from solution but also reduce ions to their zerovalent forms in the synthesis of PbS, Au and Ag/AgCl NPs has been successfully shown. The green synthesis of the noble- and transition metal NPs was accomplished through the exposure of excess metal ion precursors in solution to *P. castaneae* cell biomass and CFE (pH 7). This is the first report of NP synthesis using the heavy metal-resistant isolate of *P. castaneae* as well as the first report of the bacterial synthesis of PbS nanorods and nanowires and nanorods covered in quantum dots, 3-D Au nanoprisms and 'rough' quasi-spherical Ag/AgCl NPs. Based on comparisons to previously published research (Husseiny *et al*., 2007; Jena *et* al., 2014; Narayanan and Sakthivel, 2010;), this biological synthesis method has proven to be facile, highly efficient, cost-effective as well as environmentally friendly and scalable.

In order to establish a commercially viable NM synthesis method, it is thus necessary to determine the exact mechanism of formation as well as the biomolecules involved in reduction and stabilization of metallic NPs. Upon identification of distinct mechanisms for the synthesis of specific metal NP types and morphologies, the optimization of the methods can then ensue. Depending on the required application, the optimization of the reaction conditions can lead to the synthesis of tunable monodisperse (or polydisperse) metallic NPs of high purity and crystallinity. These include adjustments to parameters such as temperature, concentration and mixing ratios of bioreductants, stabilizers and metal ion precursors, aeration, pH, growth phase, growth medium as well as incubation time. A highly optimized bacterial synthesis process can then be implemented in the commercial synthesis of various metallic NMs.

REFERENCES

Ahemad, M., and Kibret, M. (2013). Recent trends in microbial biosorption of heavy metals: a review. *Biochemistry and Molecular Biology*, *1*(1), 19-26.

Ahmad, A., Senapati, S., Khan, M. I., Kumar, R., and Sastry, M. (2003). Extracellular biosynthesis of monodisperse gold nanoparticles by a novel extremophilic actinomycete, *Thermomonospora* sp. *Langmuir*, *19*(8), 3550-3553.

Albanese, A., Tang, P. S., and Chan, W. C. (2012). The effect of nanoparticle size, shape, and surface chemistry on biological systems. *Annual Review of Biomedical Engineering*, *14*, 1-16.

Alshehri, A. H., Jakubowska, M., Młożniak, A., Horaczek, M., Rudka, D., Free, C., and Carey, J. D. (2012). Enhanced electrical conductivity of silver nanoparticles for high frequency electronic applications. *ACS Applied Materials and Interfaces*, *4*(12), 7007-7010.

Amendola, V., Polizzi, S., and Meneghetti, M. (2007). Free silver nanoparticles synthesized by laser ablation in organic solvents and their easy functionalization. *Langmuir*, *23*(12), 6766-6770.

Anastas, P. T., and Warner, J. C. (1998) *Green Chemistry: Theory and Practice* (pp. 30). New York: Oxford University Press

Anastas, P., and Eghbali, N. (2010). Green chemistry: principles and practice. *Chemical Society Reviews*, *39*(1), 301-312.

Ankamwar, B., Chaudhary, M., and Sastry, M. (2005). Gold nanotriangles biologically synthesized using tamarind leaf extract and potential application in vapor sensing. *Synthesis and Reactivity in Inorganic, Metal-Organic and Nano-Metal Chemistry*, *35*(1), 19-26.

Anuradha, J., Abbasi, T., and Abbasi, S. A. (2015). An eco-friendly method of synthesizing gold nanoparticles using an otherwise worthless weed pistia (*Pistia stratiotes* L.). *Journal of Advanced Research*, *6*(5), 711-720.

Arrieta, J. M., Weinbauer, M. G., and Herndl, G. J. (2000). Interspecific variability in sensitivity to UV radiation and subsequent recovery in selected isolates of marine bacteria. *Applied and Environmental Microbiology*, *66*(4), 1468-1473.

Ashenfelter, B. A., Desireddy, A., Yau, S. H., Goodson III, T., and Bigioni, T. P. (2015). Fluorescence from molecular silver nanoparticles. *The Journal of Physical Chemistry C*, *119*(35), 20728-20734.

Aslan, K., Lakowicz, J. R., and Geddes, C. D. (2004). Nanogold-plasmon-resonance-based glucose sensing. *Analytical Biochemistry*, *330*(1), 145-155.

Ateeq, M., Shah, M. R., ul Ain, N., Bano, S., Anis, I., Faizi, S., and Naz, S. S. (2015). Green synthesis and molecular recognition ability of patuletin coated gold nanoparticles. *Biosensors and Bioelectronics*, *63*, 499-505.

Bai, H. J., and Zhang, Z. M. (2009). Microbial synthesis of semiconductor lead sulfide nanoparticles using immobilized *Rhodobacter sphaeroides*. *Materials Letters*, *63*(9), 764-766.

Bai, H. J., Zhang, Z. M., Guo, Y., and Yang, G. E. (2009). Biosynthesis of cadmium sulfide nanoparticles by photosynthetic bacteria *Rhodopseudomonas palustris*. *Colloids and Surfaces B: Biointerfaces*, *70*(1), 142-146.

Baldan, A. (2002). Review progress in Ostwald ripening theories and their applications to nickel-base superalloys Part I: Ostwald ripening theories. *Journal of Materials Science*, *37*(11), 2171-2202.

Baughman, R. H., Zakhidov, A. A., Gregg, G.S., and de Heer, W. A. (2002). Carbon nanotubes--the route toward applications. *Science*, *297*(5582), 787-792.

Bazylinski, D. A., and Schübbe, S. (2007). Controlled biomineralization by and applications of magnetotactic bacteria. *Advances in Applied Microbiology*, *62*, 21-62.

Beveridge, T. J., and Fyfe, W. S. (1985). Metal fixation by bacterial cell walls. *Canadian Journal of Earth Sciences*, *22*(12), 1893-1898.

Bhadwal, A. S., Tripathi, R. M., Gupta, R. K., Kumar, N., Singh, R. P., and Shrivastav, A. (2014). Biogenic synthesis and photocatalytic activity of CdS nanoparticles. *RSC Advances*, *4*(19), 9484-9490.

Bharde, A., Wani, A., Shouche, Y., Joy, P. A., Prasad, B. L., and Sastry, M. (2005). Bacterial aerobic synthesis of nanocrystalline magnetite. *Journal of the American Chemical Society*, *127*(26), 9326-9327.

Binupriya, A. R., Sathishkumar, M., Vijayaraghavan, K., and Yun, S. I. (2010). Bioreduction of trivalent aurum to nano-crystalline gold particles by active and inactive cells and cell-free extract of *Aspergillus oryzae* var. *viridis*. *Journal of Hazardous Materials*, *177*(1), 539-545.

Brown, S. D., Nativo, P., Smith, J. A., Stirling, D., Edwards, P. R., Venugopal, B., and Wheate, N. J. (2010). Gold nanoparticles for the improved anticancer drug delivery of the active component of oxaliplatin. *Journal of the American Chemical Society*, *132*(13), 4678-4684.

Cao, H., Wang, G., Zhang, S., and Zhang, X. (2006). Growth and photoluminescence properties of PbS nanocubes. *Nanotechnology*, *17*(13), 3280.

Casado-Rodriguez, M. A., Sanchez-Molina, M., Lucena-Serrano, A., Lucena-Serrano, C., Rodriguez-Gonzalez, B., Algarra, M., and Contreras-Caceres, R. (2016). Synthesis of vinyl-terminated Au nanoprisms and nanooctahedra mediated by 3-butenoic acid: direct Au@pNIPAM fabrication with improved SERS capabilities. *Nanoscale*, *8*(8), 4557-4564.

Chandran, S. P., Chaudhary, M., Pasricha, R., Ahmad, A., and Sastry, M. (2006). Synthesis of gold nanotriangles and silver nanoparticles using *Aloe vera* plant extract. *Biotechnology Progress*, *22*(2), 577-583.

Chen, Y., Palmer, R. E., and Wilcoxon, J. P. (2006). Sintering of passivated gold nanoparticles under the electron beam. *Langmuir*, *22*(6), 2851-2855.

Chen, X., Jia, B., Saha, J. K., Stokes, N., Qiao, Q., Wang, Y., and Gu, M. (2013). Strong broadband scattering of anisotropic plasmonic nanoparticles synthesized by controllable growth: effects of lumpy morphology. *Optical Materials Express*, *3*(1), 27-34.

Cho, K. S., Talapin, D. V., Gaschler, W., and Murray, C. B. (2005). Designing PbSe nanowires and nanorings through oriented attachment of nanoparticles. *Journal of the American Chemical Society*, *127*(19), 7140-7147.

Cobbett, C., and Goldsbrough, P. (2002). Phytochelatins and metallothioneins: roles in heavy metal detoxification and homeostasis. *Annual Review of Plant Biology*, *53*(1), 159-182.

Dahanayaka, D. H., Wang, J. X., Hossain, S., and Bumm, L. A. (2006). Optically transparent Au {111} substrates: Flat gold nanoparticle platforms for high-resolution scanning tunneling microscopy. *Journal of the American Chemical Society*, *128*(18), 6052-6053.

Dahl, J. A., Maddux, B. L., and Hutchison, J. E. (2007). Toward greener nanosynthesis. *Chemical Reviews*, *107*(6), 2228-2269.

Dai, L. (2006). From conventional technology to carbon nanotechnology: The fourth industrial revolution and the discoveries of C60, carbon nanotube and nanodiamond. In *Carbon nanotechnology* (pp. 3-11) Amsterdam: Elsevier.

Daraio, C., and Jin, S. (2012). Synthesis and patterning methods for nanostructures useful for biological applications. In *Nanotechnology for Biology and Medicine* (pp. 27-44). New York: Springer.

Das, M., Shim, K. H., An, S. S. A., and Yi, D. K. (2011). Review on gold nanoparticles and their applications. *Toxicology and Environmental Health Sciences*, *3*(4), 193-205.

Department of Science and Technology (DST). Republic of South Africa. The national nanotechnology strategy. Pretoria: Government Gazette, 2007.

Dey, G. R., El Omar, A. K., Jacob, J. A., Mostafavi, M., and Belloni, J. (2010). Mechanism of trivalent gold reduction and reactivity of transient divalent and monovalent gold ions studied by gamma and pulse radiolysis. *The Journal of Physical Chemistry A*, *115*(4), 383-391.

Dhand, C., Dwivedi, N., Loh, X. J., Ying, A. N. J., Verma, N. K., Beuerman, R. W., Lakshminarayanan, R., and Ramakrishna, S. (2015). Methods and strategies for the synthesis of diverse nanoparticles and their applications: a comprehensive overview. *RSC Advances*, *5*(127), 105003-105037.

Dhas, T. S., Kumar, V. G., Karthick, V., Angel, K. J., and Govindaraju, K. (2014). Facile synthesis of silver chloride nanoparticles using marine alga and its antibacterial efficacy. *Spectrochimica Acta Part A: Molecular and Biomolecular Spectroscopy*, *120*, 416-420.

Dibrov, P., Dzioba, J., Gosink, K. K., and Häse, C. C. (2002). Chemiosmotic mechanism of antimicrobial activity of Ag+ in *Vibrio cholerae*. *Antimicrobial Agents and Chemotherapy*, *46*(8), 2668-2670.

Ding, W., Zhang, P., Li, Y., Xia, H., Wang, D., and Tao, X. (2015). Effect of latent heat in boiling water on the synthesis of gold nanoparticles of different sizes by using the Turkevich method. *ChemPhysChem*, *16*(2), 447-454.

Dong, L., Chu, Y., Liu, Y., Li, M., Yang, F., and Li, L. (2006). Surfactant-assisted fabrication PbS nanorods, nanobelts, nanovelvet-flowers and dendritic nanostructures at lower temperature in aqueous solution. *Journal of Colloid and Interface Science*, *301*(2), 503-510.

Drexler, K. E. (2013). *Radical abundance: How a revolution in nanotechnology will change civilization*. (pp.135). New York: Public Affairs.

Du, L., Jiang, H., Liu, X., and Wang, E. (2007). Biosynthesis of gold nanoparticles assisted by *Escherichia coli* DH5α and its application on direct electrochemistry of hemoglobin. *Electrochemistry Communications*, *9*(5), 1165-1170.

Duan, H., Wang, D., and Li, Y. (2015). Green chemistry for nanoparticle synthesis. *Chemical Society Reviews*, *44*(16), 5778-5792.

Dunn, P. J. (2012). The importance of green chemistry in process research and development. *Chemical Society Reviews*, *41*(4), 1452-1461.

El-Nour, K. M. A., Eftaiha, A. A., Al-Warthan, A., and Ammar, R. A. (2010). Synthesis and applications of silver nanoparticles. *Arabian Journal of Chemistry*, *3*(3), 135-140.

El-Shanshoury, A. R., Elsilk, S. E., Ateya, P. S., and Ebeid, E. M. (2012). Synthesis of lead nanoparticles by *Enterobacter* sp. and avirulent *Bacillus anthracis* PS2010. *Annals of microbiology*, *62*(4), 1803-1810.

Elcey, C. D., Kuruvilla, A. T., and Thomas, D. (2014). Synthesis of magnetite nanoparticles from optimized iron reducing bacteria isolated from iron ore mining sites. *International Journal of Current Microbiology and Applied Sciences*, *3*(8), 408-417.

Erasmus, M., Cason, E. D., van Marwijk, J., Botes, E., Gericke, M., and van Heerden, E. (2014). Gold nanoparticle synthesis using the thermophilic bacterium *Thermus scotoductus* SA-01 and the purification and characterization of its unusual gold reducing protein. *Gold Bulletin*, *47*(4), 245-253.

Eustis, S., and El-Sayed, M. A. (2006). Why gold nanoparticles are more precious than pretty gold: noble metal surface plasmon resonance and its enhancement of the radiative and nonradiative properties of nanocrystals of different shapes. *Chemical Society Reviews*, *35*(3), 209-217.

Faraday, M. (1857). The Bakerian lecture: experimental relations of gold (and other metals) to light. *Philosophical Transactions of the Royal Society of London*, *147*, 145-181.

Fazal, S., Jayasree, A., Sasidharan, S., Koyakutty, M., Nair, S. V., and Menon, D. (2014). Green synthesis of anisotropic gold nanoparticles for photothermal therapy of cancer. *ACS Applied Materials and Interfaces*, *6*(11), 8080-8089.

Feng, Y. Y., Zhang, J., Zhou, P., Lu, G. F., Bao, J. C., Wang, W., and Xu, Z. (2004). A facile method to prepare PbS nanorods. *Materials Research Bulletin*, *39*(13), 1999-2005.

Fernández, E. J., Garcia-Barrasa, J., Laguna, A., López-de-Luzuriaga, J. M., Monge, M., and Torres, C. (2008). The preparation of highly active antimicrobial silver nanoparticles by an organometallic approach. *Nanotechnology*, *19*(18), 185602.

Fletcher, T. (2002). Neighborhood change at Love Canal: contamination, evacuation and resettlement. *Land Use Policy*, *19*(4), 311-323.

Flynn, T. M., O'Loughlin, E. J., Mishra, B., DiChristina, T. J., and Kemner, K. M. (2014). Sulfur-mediated electron shuttling during bacterial iron reduction. *Science*, *344*(6187), 1039-1042.

Forootanfar, H., Amirpour-Rostami, S., Jafari, M., Forootanfar, A., Yousefizadeh, Z., and Shakibaie, M. (2015). Microbial-assisted synthesis and evaluation the cytotoxic effect of tellurium nanorods. *Materials Science and Engineering: C*, *49*, 183-189.

Gaikwad, S., Ingle, A., Gade, A., Rai, M., Falanga, A., Incoronato, N., and Galdiero, M. (2013). Antiviral activity of mycosynthesized silver nanoparticles against herpes simplex virus and human parainfluenza virus type 3. *International Journal of Nanomedicine*, *8*, 4303-4314.

Gans, R. (1915). Über die form ultramikroskopischer silberteilchen. *Annalen der Physik*, *352*(10), 270-284.

Gardner, J. (2015). Nanotechnology in medicine and healthcare: Possibilities, progress and problems. *South African Journal of Bioethics and Law*, *8*(2), 50-53.

Gauteng Department of Agricultural and Rural Development, (2016), 9th Annual Agricultural Research Symposium: Research Agenda Report 2015/2016. Johannesburg: GDARD.

Ge, L., Li, Q., Wang, M., Ouyang, J., Li, X., and Xing, M. M. (2014). Nanosilver particles in medical applications: synthesis, performance, and toxicity. *International Journal of Nanomedicine*, *9*, 2399.

Gerdes, F., Volkmann, M., Schliehe, C., Bielewicz, T., and Klinke, C. (2015). Sculpting of lead sulfide nanoparticles by means of acetic acid and dichloroethane. *International Journal of Research in Physical Chemistry and Chemical Physics*, *229*(1-2), 139-151.

Ghosh, S. K., and Pal, T. (2007). Interparticle coupling effect on the surface plasmon resonance of gold nanoparticles: from theory to applications. *Chemical Reviews*, *107*(11), 4797-4862.

Glezer, A. M. (2011). Structural classification of nanomaterials. *Russian Metallurgy (Metally)*, *2011*(4), 263-269.

Gopinath, V., Priyadarshini, S., Priyadharsshini, N. M., Pandian, K., and Velusamy, P. (2013). Biogenic synthesis of antibacterial silver chloride nanoparticles using leaf extracts of *Cissus quadrangularis* Linn. *Materials Letters*, *91*, 224-227.

Goswami, A. M., and Ghosh, S.K. (2013). Biological synthesis of colloidal gold nanoprisms using *Penicillium citrinum* MTCC9999. *Journal of Biomaterials and Nanobiotechnology*, *4*, 20-27

Grimalt, J. O., Ferrer, M., and Macpherson, E. (1999). The mine tailing accident in Aznalcollar. *Science of the Total Environment*, *242*(1), 3-11.

Gupta, A., Matsui, K., Lo, J. F., and Silver, S. (1999). Molecular basis for resistance to silver cations in *Salmonella*. *Nature medicine*, *5*(2), 183-188.

Guria, M. K., Majumdar, M., and Bhattacharyya, M. (2016). Green synthesis of protein capped nano-gold particle: An excellent recyclable nano-catalyst for the reduction of nitro-aromatic pollutants at higher concentration. *Journal of Molecular Liquids*, *222*, 549-557.

Gurunathan, S., Kalishwaralal, K., Vaidyanathan, R., Venkataraman, D., Pandian, S. R. K., Muniyandi, J., and Eom, S. H. (2009). Biosynthesis, purification and characterization of silver nanoparticles using *Escherichia coli*. *Colloids and Surfaces B: Biointerfaces*, *74*(1), 328-335.

Ha, T. H., Koo, H. J., and Chung, B. H. (2007). Shape-controlled syntheses of gold nanoprisms and nanorods influenced by specific adsorption of halide ions. *The Journal of Physical Chemistry C*, *111*(3), 1123-1130.

Harikrishnan, H., Shine, K., Ponmurugan, K., Moorthy, I. G., and Kumar, R. S. (2014). In vitro eco-friendly synthesis of cadmium sulfide nanoparticles using heterotrophic *Bacillus cereus*. *Journal of Optoelectronic and Biomedical Materials*, *6*(1), 1-7.

Harrison, J. J., Ceri, H., and Turner, R. J. (2007). Multimetal resistance and tolerance in microbial biofilms. *Nature Reviews Microbiology*, *5*(12), 928-938.

He, S., Guo, Z., Zhang, Y., Zhang, S., Wang, J., and Gu, N. (2007). Biosynthesis of gold nanoparticles using the bacteria *Rhodopseudomonas capsulata*. Materials Letters, 61(18), 3984-3987.

He, H., Xie, C., and Ren, J. (2008). Nonbleaching fluorescence of gold nanoparticles and its applications in cancer cell imaging. *Analytical Chemistry*, *80*(15), 5951-5957.

Heller, K. J. (2001). Probiotic bacteria in fermented foods: product characteristics and starter organisms. *The American Journal of Clinical Nutrition*, *73*(2), 374-379.

Hesto, P., Lourtioz, J. M., Dupas-Haeberlin, C., Lahmani, M., and Dubouchet, T. (2016). Nanotechnology and Industry. In *Nanosciences and Nanotechnology* (pp. 339-356). Switzerland: Springer International Publishing.

Hirsch, L. R., Stafford, R. J., Bankson, J. A., Sershen, S. R., Rivera, B., Price, R. E., and West, J. L. (2003). Nanoshell-mediated near-infrared thermal therapy of tumors under magnetic resonance guidance. *Proceedings of the National Academy of Sciences U.S.A*, *100*(23), 13549-13554.

Hirsch, R. J., Narurkar, V., and Carruthers, J. (2006). Management of injected hyaluronic acid induced Tyndall effects. *Lasers in Surgery and Medicine*, *38*(3), 202-204.

Hu, X., and Chan, C. T. (2004). Photonic crystals with silver nanowires as a near-infrared superlens. *Applied Physics Letters*, *85*(9), 1520-1522.

Hu, W., Chen, S., Li, X., Shi, S., Shen, W., Zhang, X., and Wang, H. (2009). *In situ* synthesis of silver chloride nanoparticles into bacterial cellulose membranes. *Materials Science and Engineering: C*, *29*(4), 1216-1219.

Hugenholtz, J., Sybesma, W., Groot, M. N., Wisselink, W., Ladero, V., Burgess, K., and Savoy, G. (2002). Metabolic engineering of lactic acid bacteria for the production of nutraceuticals. In *Lactic Acid Bacteria: Genetics, Metabolism and Applications* (pp. 217-235). Netherlands: Springer.

Hulkoti, N. I., and Taranath, T. C. (2014). Biosynthesis of nanoparticles using microbes—A review. *Colloids and Surfaces B: Biointerfaces*, *121*, 474-483.

Husein, M. M., Rodil, E., and Vera, J. H. (2005). A novel method for the preparation of silver chloride nanoparticles starting from their solid powder using microemulsions. *Journal of Colloid and Interface Science*, *288*(2), 457-467.

Hussain, J. I., Kumar, S., Hashmi, A. A., and Khan, Z. (2011). Silver nanoparticles: preparation, characterization, and kinetics. *Advanced Materials Letters*, *2*(3), 188-194.

Hussain, S. T., and Khan, M. B. (2013). *U.S. Patent No. 8,487,147*. Washington, DC: U.S. Patent and Trademark Office.

Husseiny, M. I., El-Aziz, M. A., Badr, Y., and Mahmoud, M. A. (2007). Biosynthesis of gold nanoparticles using P*seudomonas aeruginosa*. *Spectrochimica Acta Part A: Molecular and Biomolecular Spectroscopy*, *67*(3), 1003-1006.

Hutchings, G. J., Brust, M., and Schmidbaur, H. (2008). Gold—an introductory perspective. *Chemical Society Reviews*, *37*(9), 1759-1765.

Hutchison, J. E. (2008). Greener nanoscience: a proactive approach to advancing applications and reducing implications of nanotechnology. *Acs Nano*, *2*(3), 395-402.

Hvolbaek, B., Janssens, T. V., Clausen, B. S., Falsig, H., Christensen, C. H., and Nørskov, J. K. (2007). Catalytic activity of Au nanoparticles. *Nano Today*, *2*(4), 14-18.

Idegami, K., Chikae, M., Kerman, K., Nagatani, N., Yuhi, T., Endo, T., and Tamiya, E. (2008). Gold nanoparticle-based redox signal enhancement for sensitive detection of human chorionic gonadotropin hormone. *Electroanalysis*, *20*(1), 14-21.

Ingale, A. G., and Chaudhari, A. N. (2013). Biogenic synthesis of nanoparticles and potential applications: an eco-friendly approach. *Journal of Nanomedicine and Nanotechology*, *4*(165), 1-7.

Iravani, S., Korbekandi, H., Mirmohammadi, S. V., and Zolfaghari, B. (2014). Synthesis of silver nanoparticles: chemical, physical and biological methods. *Research in Pharmaceutical Sciences*, *9*(6), 385.

Israelsen, N. D., Hanson, C., and Vargis, E. (2015). Nanoparticle properties and synthesis effects on surface-enhanced Raman scattering enhancement factor: an introduction. *The Scientific World Journal*, *2015*. http://dx.doi.org/10.1155/2015/124582.

Jain, P. K., Lee, K. S., El-Sayed, I. H., and El-Sayed, M. A. (2006). Calculated absorption and scattering properties of gold nanoparticles of different size, shape, and composition: applications in biological imaging and biomedicine. *The Journal of Physical Chemistry B*, *110*(14), 7238-7248.

Jain, N., Bhargava, A., Rathi, M., Dilip, R. V., and Panwar, J. (2015). Removal of protein capping enhances the antibacterial efficiency of biosynthesized silver nanoparticles. *PloS one*, *10*(7), e0134337.

Jang, N. H., Suh, J. S., and Moskovits, M. (1997). Effect of surface geometry on the photochemical reaction of 1,10-phenanthroline adsorbed on silver colloid surfaces. *The Journal of Physical Chemistry B*, *101*(41), 8279-8285.

Jang, S. Y., Song, Y. M., Kim, H. S., Cho, Y. J., Seo, Y. S., Jung, G. B., and Kim, B. (2010). Three synthetic routes to single-crystalline PbS nanowires with controlled growth direction and their electrical transport properties. *ACS Nano*, *4*(4), 2391-2401.

Jena, B. K., and Raj, C. R. (2007). Shape-controlled synthesis of gold nanoprism and nanoperiwinkles with pronounced electrocatalytic activity. *The Journal of Physical Chemistry C*, *111*(42), 15146-15153.

Jena, J., Pradhan, N., Nayak, R. R., Dash, B. P., Sukla, L. B., Panda, P. K., and Mishra, B. K. (2014). *Microalga scenedesmus* sp.: a potential low-cost green machine for silver nanoparticle synthesis. *Journal of Microbiology and Biotechnology*, *24*(4), 522-533.

Jeong, S. H., Choi, H., Kim, J. Y., and Lee, T. W. (2015). Silver-based nanoparticles for surface plasmon resonance in organic optoelectronics. *Particle and Particle Systems Characterization*, *32*(2), 164-175.

Johnston, C. W., Wyatt, M. A., Li, X., Ibrahim, A., Shuster, J., Southam, G., and Magarvey, N. A. (2013). Gold biomineralization by a metallophore from a gold-associated microbe. *Nature Chemical Biology*, *9*(4), 241-243.

Juibari, M. M., Yeganeh, L. P., Abbasalizadeh, S., Azarbaijani, R., Mousavi, S. H., Tabatabaei, M., and Salekdeh, G. H. (2015). Investigation of a hot-spring extremophilic *Ureibacillus thermosphaericus* strain Thermo-BF for extracellular biosynthesis of functionalized gold nanoparticles. *BioNanoScience*, *5*(4), 233-241.

Kang, F., Alvarez, P. J., and Zhu, D. (2013). Microbial extracellular polymeric substances reduce Ag^{+} to silver nanoparticles and antagonize bactericidal activity. *Environmental Science and Technology*, *48*(1), 316-322.

Karim, M., Aktaruzzaman, M. D., Ashrafuzzaman, M., and Zaman, B. (2014). A conventional synthesis approach to prepare lead sulfide (PbS) nanoparticles via solvothermal method. *Chalcogenide Letters*, *11*(10), 531-539.

Karami, H., Ghasemi, M., and Matini, S. (2013). Synthesis, characterization and application of lead sulfide nanostructures as ammonia gas sensing agent. *International Journal of Electrochemical Science*, *8*(10), 11661-11679.

Kaur, P., Jain, P., Kumar, A., and Thakur, R. (2014). Biogenesis of PbS nanocrystals by using rhizosphere fungus i.e., *Aspergillus* sp. isolated from the rhizosphere of chickpea. *BioNanoScience*, *4*(2), 189-194.

Kerr, M. A., and Yan, F. (2016). Bromide-assisted anisotropic growth of gold nanoparticles as substrates for surface-enhanced Raman scattering. *Journal of Spectroscopy*, *2016*.

Kessler, R. (2011). Engineered nanoparticles in consumer products: understanding a new ingredient. *Environmental Health Perspectives*, *119*(3), A120-A125.

Khan, A. S. (Ed.). (2012). *Nanotechnology: ethical and social implications*. (pp. 345) New York: CRC Press.

Khan, I. A., Sajid, N., Badshah, A., Wattoo, M. H., Anjum, D. H., and Nadeem, M. A. (2015). CO oxidation catalyzed by Ag nanoparticles supported on SnO/CeO2. *Journal of the Brazilian Chemical Society*, *26*(4), 695-704.

Khan, Z., Al-Thabaiti, S. A., and Bashir, O. (2016). Natural sugar surfactant capped gold nano-disks: Aggregation, green synthesis and morphology. *Dyes and Pigments*, *124*, 210-221.

Kharissova, O. V., Dias, H. R., Kharisov, B. I., Pérez, B. O., and Pérez, V. M. J. (2013). The greener synthesis of nanoparticles. *Trends in Biotechnology*, *31*(4), 240-248.

Kim, S. H, Fisher, B., Eisler, H. J., and Bawendi, M. (2003). Type-II quantum dots: CdTe/CdSe (core/shell) and CdSe/ZnTe (core/shell) heterostructures. *Journal of the American Chemical Society*, *125*(38), 11466-11467.

Kim, S. H., Choi, B. S., Kang, K., Choi, Y. S., and Yang, S. I. (2007). Low temperature synthesis and growth mechanism of Ag nanowires. *Journal of Alloys and Compounds*, *433*(1), 261-264.

Kim, H. S., Kim, B. K., Yang, Y., Peng, X., Lee, S. G., Yu, D., and Doh, Y. J. (2016). Gate-tunable superconducting quantum interference devices of PbS nanowires. *Applied Physics Express*, *9*(2), 023102.

Klaus, T., Joerger, R., Olsson, E., and Granqvist, C. G. (1999). Silver-based crystalline nanoparticles, microbially fabricated. *Proceedings of the National Academy of Sciences U.S.A*, *96*(24), 13611-13614.

Konishi, Y., Ohno, K., Saitoh, N., Nomura, T., and Nagamine, S. (2004). Microbial synthesis of gold nanoparticles by metal reducing bacterium. *Transactions of the Materials Research Society of Japan*, *29*, 2341-2343.

Kowshik, M., Vogel, W., Urban, J., Kulkarni, S. K., and Paknikar, K. M. (2002). Microbial synthesis of semiconductor PbS nanocrystallites. *Advanced Materials*, *14*(11), 815.

Krishnan, S., Narayan, S., and Chadha, A. (2016). Whole resting cells vs. cell free extracts of *Candida parapsilosis* ATCC 7330 for the synthesis of gold nanoparticles. *AMB Express*, *6*(1), 92.

Kuang, H., Xing, C., Hao, C., Liu, L., Wang, L., and Xu, C. (2013). Rapid and highly sensitive detection of lead ions in drinking water based on a strip immunosensor. *Sensors*, *13*(4), 4214-4224.

Kumar, V. A., Nakajima, Y., Uchida, T., Hanajiri, T., and Maekawa, T. (2016). Synthesis of nanoparticles composed of silver and silver chloride for a plasmonic photocatalyst using an extract from needles of *Pinus densiflora*. *Materials Letters*, *176*, 169-172.

Kumar-Krishnan, S., Hernandez-Rangel, A., Pal, U., Ceballos-Sanchez, O., Flores-Ruiz, F. J., Prokhorov, E., Meyyappan, M. (2016). Surface functionalized halloysite nanotubes decorated with silver nanoparticles for enzyme immobilization and biosensing. *Journal of Materials Chemistry B*, *4*(15), 2553-2560.

LaMer, V. K., and Dinegar, R. H. (1950). Theory, production and mechanism of formation of monodispersed hydrosols. *Journal of the American Chemical Society*, *72*(11), 4847-4854.

LaMer, V. K. (1952). Nucleation in phase transitions. *Industrial and Engineering Chemistry*, *44*(6), 1270-1277.

Lara, H. H., Ixtepan-Turrent, L., Treviño, E. N. G., and Singh, D. K. (2011). Use of silver nanoparticles increased inhibition of cell-associated HIV-1 infection by neutralizing antibodies developed against HIV-1 envelope proteins. *Journal of Nanobiotechnology*, *9*(1), 1.

Lea, M. C. (1889). Allotropic forms of silver. *American Journal of Science*, (222), 476-491.

Lee, E. J., Ribeiro, C., Longo, E., and Leite, E. R. (2005). Oriented attachment: An effective mechanism in the formation of anisotropic nanocrystals. *The Journal of Physical Chemistry B*, *109*(44), 20842-20846.

Lee, S. Y., Kim, H. U., Park, J. H., Park, J. M., and Kim, T. Y. (2009). Metabolic engineering of microorganisms: general strategies and drug production. *Drug Discovery Today*, *14*(1), 78-88.

Lee, J., Hua, B., Park, S., Ha, M., Lee, Y., Fan, Z., and Ko, H. (2014). Tailoring surface plasmons of high-density gold nanostar assemblies on metal films for surface-enhanced Raman spectroscopy. *Nanoscale*, *6*(1), 616-623.

Lei, W., Faraone, L., Tan, H. H., and Lu, W. (2014). Low-Dimensional nanostructures for optoelectronic applications. *Journal of Nanomaterials*, *2014*.

Li, Y., and Shi, G. (2005). Electrochemical growth of two-dimensional gold nanostructures on a thin polypyrrole film modified ITO electrode. *The Journal of Physical Chemistry B*, *109*(50), 23787-23793.

Li, C., Shi, G., Xu, H., Guang, S., Yin, R., and Song, Y. (2007). Nonlinear optical properties of the PbS nanorods synthesized via surfactant-assisted hydrolysis. *Materials Letters*, *61*(8), 1809-1811.

Li, X., Xu, H., Chen, Z. S., and Chen, G. (2011). Biosynthesis of nanoparticles by microorganisms and their applications. *Journal of Nanomaterials*, *2011*, 8.

Li, S. W., Zhang, X., and Sheng, G. P. (2016). Silver nanoparticles formation by extracellular polymeric substances (EPS) from electroactive bacteria. *Environmental Science and Pollution Research*, *23*(9), 8627-8633.

Lin, S. Y., Liu, S. W., Lin, C. M., and Chen, C. H. (2002). Recognition of potassium ion in water by 15-crown-5 functionalized gold nanoparticles. *Analytical Chemistry*, *74*(2), 330-335.

Lin, S.H., Lok, C.N., and Che, C.M. (2014). Biosynthesis of silver nanoparticles from silver (i) reduction by the periplasmic nitrate reductase c-type cytochrome subunit NapC in a silver-resistant *E. coli*. *Chemical Science*, *5*(8), 3144-3150.

Link, S., and El-Sayed, M. A. (2000). Shape and size dependence of radiative, non-radiative and photothermal properties of gold nanocrystals. *International Reviews in Physical Chemistry*, *19*(3), 409-453.

Liu, T. Y., Li, M., Ouyang, J., Zaman, M. B., Wang, R., Wu, X., and Yu, K. (2009). Non-injection and low-temperature approach to colloidal photoluminescent PbS nanocrystals with narrow bandwidth. *The Journal of Physical Chemistry C*, *113*(6), 2301-2308.

Liyanage, D. D., Thamali, R. J., Kumbalatara, A. A. K., Weliwita, J. A., and Witharana, S. (2016). An analysis of nanoparticle settling times in liquids. *Journal of Nanomaterials*, *2016*, 44.

Liz-Marzán, L. M. (2004). Nanometals: formation and color. *Materials Today*, *7*(2), 26-31.

Lloyd, J. R. (2003). Microbial reduction of metals and radionuclides. *FEMS Microbiology Reviews*, *27*(2-3), 411-425.

Lorestani, F., Shahnavaz, Z., Mn, P., Alias, Y., and Manan, N. S. (2015). One-step hydrothermal green synthesis of silver nanoparticle-carbon nanotube reduced-graphene oxide composite and its application as hydrogen peroxide sensor. *Sensors and Actuators B: Chemical*, *208*, 389-398.

Lu, X., Rycenga, M., Skrabalak, S. E., Wiley, B., and Xia, Y. (2009). Chemical synthesis of novel plasmonic nanoparticles. *Annual Review of Physical Chemistry*, *60*, 167-192.

Lu, Y., Feng, S., Liu, X., and Chen, L. (2013). Surface-enhanced Raman scattering study of silver nanoparticles prepared by using MC as a template. *Journal of Nanomaterials*, *2013*, 170.

Maciollek, A., and Ritter, H. (2014). One pot synthesis of silver nanoparticles using a cyclodextrin containing polymer as reductant and stabilizer. *Beilstein Journal of Nanotechnology*, *5*(1), 380-385.

Makarov, V. V., Love, A. J., Sinitsyna, O. V., Makarova, S. S., Yaminsky, I. V., Taliansky, M. E., and Kalinina, N. O. (2014). “Green” nanotechnologies: synthesis of metal nanoparticles using plants. *Acta Naturae*, *6*(1), 20.

Marshall, M. J., Beliaev, A. S., Dohnalkova, A. C., Kennedy, D. W., Shi, L., Wang, Z., and Reed, S. B. (2006). c-Type cytochrome-dependent formation of U (IV) nanoparticles by *Shewanella oneidensis*. *PLoS Biology*, *4*(8), e268.

Martinez-Manez, R., and Sancenón, F. (2003). Fluorogenic and chromogenic chemosensors and reagents for anions. *Chemical Reviews*, *103*(11), 4419-4476.

Mishra, S., Singh, B. R., Singh, A., Keswani, C., Naqvi, A. H., and Singh, H. B. (2014). Biofabricated silver nanoparticles act as a strong fungicide against *Bipolaris sorokiniana* causing spot blotch disease in wheat. *Public Library of Science One*, *9*(5), e97881.

Mody, V. V., Siwale, R., Singh, A., and Mody, H. R. (2010). Introduction to metallic nanoparticles. *Journal of Pharmacy and Bioallied Sciences*, *2*(4), 282.

Mondal, S., Basu, S., Begum, N. A., and Mandal, D. (2014). A brief introduction to the development of biogenic synthesis of metal nanoparticles. *Journal of Nano Research*, *27*(1), 41-52.

Moon, J. W., Rawn, C. J., Rondinone, A. J., Love, L. J., Roh, Y., Everett, S. M., and Phelps, T. J. (2010). Large-scale production of magnetic nanoparticles using bacterial fermentation. *Journal of Industrial Microbiology and Biotechnology*, *37*(10), 1023-1031.

Moon, J., Kim, T. K., VanSaders, B., Choi, C., Liu, Z., Jin, S., and Chen, R. (2015). Black oxide nanoparticles as durable solar absorbing material for high-temperature concentrating solar power system. *Solar Energy Materials and Solar Cells*, *134*, 417-424.

Morillo, J. A., Aguilera, M., Ramos-Cormenzana, A., and Monteoliva-Sánchez, M. (2006). Production of a metal-binding exopolysaccharide by *Paenibacillus jamilae* using two-phase olive-mill waste as fermentation substrate. *Current Microbiology*, *53*(3), 189-193.

Mourato, A., Gadanho, M., Lino, A. R., and Tenreiro, R. (2011). Biosynthesis of crystalline silver and gold nanoparticles by extremophilic yeasts. *Bioinorganic Chemistry and Applications*, *2011*, 54607.

Mufamadi, S. (2015). Nanotechnology economy: Can it be an alternative solution to close the poverty gap? Retrieved from http://www.npep.co.za/newsletters/13-newnano/100-nanotechnology-economy-can-it-be-an-alternative-solution-to-close-the-poverty-gap

Mufamadi, S. (2016). South Africa needs to start to venture into nanotechnology commercialisation by employing sustainable models. Retrieved from http://sciencestars.co.za/south-africa-needs-to-start-to-venture-into-nanotechnology-commercialisation-by-employing-sustainable-models/

Mulholland, K. L. and Dyer, J. A. (1998) Organic Solvents, in *Pollution Prevention: Methodology, Technologies and Practices* (pp. 147–156). New Jersey: John Wiley and Sons.

Murugan, M., Anthony, K. J. P., Jeyaraj, M., Rathinam, N. K., and Gurunathan, S. (2014). Biofabrication of gold nanoparticles and its biocompatibility in human breast adenocarcinoma cells (MCF-7). *Journal of Industrial and Engineering Chemistry*, *20*(4), 1713-1719.

Musee, N., Brent, A. C., Jacobs, A., and Ashton, P. J. (2010). A South African research agenda to investigate the potential environmental, health and safety risks of nanotechnology. *South African Journal of Science*, *106*(3-4), 01-06.

Myroshnychenko, V., Rodríguez-Fernández, J., Pastoriza-Santos, I., Funston, A. M., Novo, C., Mulvaney, P., and de Abajo, F. J. G. (2008). Modelling the optical response of gold nanoparticles. *Chemical Society Reviews*, *37*(9), 1792-1805.

Nadagouda, M. N., and Varma, R. S. (2006). Green and controlled synthesis of gold and platinum nanomaterials using vitamin B2: density-assisted self-assembly of nanospheres, wires and rods. *Green Chemistry*, *8*(6), 516-518.

Nair, B., and Pradeep, T. (2002). Coalescence of nanoclusters and formation of submicron crystallites assisted by *Lactobacillus* strains. *Crystal Growth and Design*, *2*(4), 293-298.

Nangia, Y., Wangoo, N., Sharma, S., Wu, J. S., Dravid, V., Shekhawat, G. S., and Suri, C. R. (2009). Facile biosynthesis of phosphate capped gold nanoparticles by a bacterial isolate *Stenotrophomonas maltophilia*. *Applied Physics Letters*, *94*(23), 233901.

Narayanan, K. B., and Sakthivel, N. (2010). Biological synthesis of metal nanoparticles by microbes. *Advances in Colloid and Interface Science*, *156*(1), 1-13.

Nath, D., and Banerjee, P. (2013). Green nanotechnology–A new hope for medical biology. *Environmental Toxicology and Pharmacology*, *36*(3), 997-1014.

Nehl, C. L., and Hafner, J. H. (2008). Shape-dependent plasmon resonances of gold nanoparticles. *Journal of Materials Chemistry*, *18*(21), 2415-2419.

Nelayah, J., Kociak, M., Stéphan, O., de Abajo, F. J. G., Tencé, M., Henrard, L., and Colliex, C. (2007). Mapping surface plasmons on a single metallic nanoparticle. *Nature Physics*, *3*(5), 348-353.

Nepple, B. B., Flynn, I., and Bachofen, R. (1999). Morphological changes in phototrophic bacteria induced by metalloid oxyanions. *Microbiological Research*, *154*(2), 191-198.

Nowack, B., Krug, H. F., and Height, M. (2011). 120 years of nanosilver history: implications for policy makers. *Environmental Science and Technology*, *45*(4), 1177-1183.

Ogawa, S., Hu, K., Fan, F. R. F., and Bard, A. J. (1997). Photoelectrochemistry of films of quantum size lead sulfide particles incorporated in self-assembled monolayers on gold. *The Journal of Physical Chemistry B*, *101*(29), 5707-5711.

Oliveira, M. M., Ugarte, D., Zanchet, D., and Zarbin, A. J. (2005). Influence of synthetic parameters on the size, structure, and stability of dodecanethiol-stabilized silver nanoparticles. *Journal of Colloid and Interface Science*, *292*(2), 429-435.

Ostwald, W. (1900). Über die vermeintliche Isomerie des roten und gelben Quecksilberoxyds und die Oberflächenspannung fester Körper. *Zeitschrift für Physikalische Chemie*, *34*, 495-503.

Pal, A., and Paul, A. K. (2008). Microbial extracellular polymeric substances: central elements in heavy metal bioremediation. *Indian Journal of Microbiology*, *48*(1), 49.

Pantidos, N., and Horsfall, L. E. (2014). Biological synthesis of metallic nanoparticles by bacteria, fungi and plants. *Journal of Nanomedicine and Nanotechnology*, *2014*.

Parikh, R. Y., Singh, S., Prasad, B. L. V., Patole, M. S., Sastry, M., and Shouche, Y. S. (2008). Extracellular synthesis of crystalline silver nanoparticles and molecular evidence of silver resistance from *Morganella* sp.: towards understanding biochemical synthesis mechanism. *ChemBioChem*, *9*(9), 1415-1422.

Parikh, R. Y., Ramanathan, R., Coloe, P. J., Bhargava, S. K., Patole, M. S., Shouche, Y. S., and Bansal, V. (2011). Genus-wide physicochemical evidence of extracellular crystalline silver nanoparticles biosynthesis by *Morganella* spp. *PLoS One*, *6*(6), e21401.

Park, T. J., Lee, S. Y., Heo, N. S., and Seo, T. S. (2010). *In vivo* synthesis of diverse metal nanoparticles by recombinant *Escherichia coli*. *Angewandte Chemie International Edition*, *49*(39), 7019-7024.

Park, S., Park, H. H., Kim, S. Y., Kim, S. J., Woo, K., and Ko, G. (2014). Antiviral properties of silver nanoparticles on a magnetic hybrid colloid. *Applied and Environmental Microbiology*, *80*(8), 2343-2350.)

Park, T. J., Lee, K. G., and Lee, S. Y. (2016). Advances in microbial biosynthesis of metal nanoparticles. *Applied Microbiology and Biotechnology*, *100*(2), 521-534.

Patel, J. D., Mighri, F., and Ajji, A. (2012). Room temperature synthesis of aminocaproic acid-capped lead sulphide nanoparticles. *Materials Sciences and Applications*, *3*, 125-130.

Paul, B., Bhuyan, B., Purkayastha, D. D., Dey, M., and Dhar, S. S. (2015). Green synthesis of gold nanoparticles using *Pogestemon benghalensis* (B) O. Ktz. leaf extract and studies of their photocatalytic activity in degradation of methylene blue. *Materials Letters*, *148*, 37-40.

Paulkumar, K., Rajeshkumar, S., Gnanajobitha, G., Vanaja, M., Malarkodi, C., and Annadurai, G. (2013). Biosynthesis of silver chloride nanoparticles using *Bacillus subtilis* MTCC 3053 and assessment of its antifungal activity. *ISRN Nanomaterials*, *2013*.

Pileni, M. P. (1998) Size and morphology control of nanoparticle growth in organized surfactant assemblies, in J. H. Fendler (Ed), *Nanoparticles and Nanostructured Films: Preparation, Characterization and Applications* (pp. 71-98). Weinheim, Germany. Wiley-VCH.

Polte, J., Ahner, T. T., Delissen, F., Sokolov, S., Emmerling, F., Thünemann, A. F., and Kraehnert, R. (2010). Mechanism of gold nanoparticle formation in the classical citrate synthesis method derived from coupled in situ XANES and SAXS evaluation. *Journal of the American Chemical Society*, *132*(4), 1296-1301.

Prado Acosta, M., Valdman, E., Leite, S. G., Battaglini, F., and Ruzal, S. M. (2005). Biosorption of copper by *Paenibacillus polymyxa* cells and their exopolysaccharide. *World Journal of Microbiology and Biotechnology*, *21*(6), 1157-1163.

Putz, A. M., Horváth, Z. E., Gonter, K., and Almásy, L. (2015). One-pot synthesis and characterization of nano-size silver chloride. *Digest Journal of Nanomaterials and Biostructures*, *10*(1), 89-94.

Qu, X., Alvarez, P. J., and Li, Q. (2013). Applications of nanotechnology in water and wastewater treatment. *Water Research*, *47*(12), 3931-3946.

Qureshi, N., Schripsema, J., Lienhardt, J., and Blaschek, H. P. (2000). Continuous solvent production by *Clostridium beijerinckii* BA101 immobilized by adsorption onto brick. *World Journal of Microbiology and Biotechnology*, *16*(4), 377-382.

Raj, R., Dalei, K., Chakraborty, J., and Das, S. (2016). Extracellular polymeric substances of a marine bacterium mediated synthesis of CdS nanoparticles for removal of cadmium from aqueous solution. *Journal of Colloid and Interface Science*, *462*, 166-175.

Ramanathan, R., Field, M. R., O'Mullane, A. P., Smooker, P. M., Bhargava, S. K., and Bansal, V. (2013). Aqueous phase synthesis of copper nanoparticles: a link between heavy metal resistance and nanoparticle synthesis ability in bacterial systems. *Nanoscale*, *5*(6), 2300-2306.

Rani, K. (2014). A brief review on convergence of diversifying fields of nanotechnology and bio-informatics as an advanced revolutionized device for betterment of humankind. *International Journal of Pharma Research and Health Sciences*, *2*(3), 197-202.

Rao, P. N. (2010), Nanocatalysis: applications in the chemical industry. Retrieved from http://www.nanowerk.com/spotlight/spotid=18846.php.

Raveendran, P., Fu, J., and Wallen, S. L. (2003). Completely "green" synthesis and stabilization of metal nanoparticles. *Journal of the American Chemical Society*, *125*(46), 13940-13941.

Reidy, B., Haase, A., Luch, A., Dawson, K. A., and Lynch, I. (2013). Mechanisms of silver nanoparticle release, transformation and toxicity: a critical review of current knowledge and recommendations for future studies and applications. *Materials*, *6*(6), 2295-2350.

Riba, I., DelValls, T. A., Forja, J. M., and Gómez-Parra, A. (2002). Influence of the Aznalcóllar mining spill on the vertical distribution of heavy metals in sediments from the Guadalquivir estuary (SW Spain). *Marine Pollution Bulletin*, *44*(1), 39-47.

Roco, M. C., and Bainbridge, W. S. (2005). Societal implications of nanoscience and nanotechnology: Maximizing human benefit. *Journal of Nanoparticle Research*, *7*(1), 1-13.

Rohwerder, T., Gehrke, T., Kinzler, K., and Sand, W. (2003). Bioleaching review part A. *Applied Microbiology and Biotechnology*, *63*(3), 239-248.

Rycenga, M., Cobley, C. M., Zeng, J., Li, W., Moran, C. H., Zhang, Q., and Xia, Y. (2011). Controlling the synthesis and assembly of silver nanostructures for plasmonic applications. *Chemical Reviews*, *111*(6), 3669-3712.

Sajanlal, P. R., Sreeprasad, T. S., Samal, A. K., and Pradeep, T. (2011). Anisotropic nanomaterials: structure, growth, assembly, and functions. *Nanotechnology Reviews*, *2*(5883), 4.

Salamanca-Buentello, F., Persad, D. L., Martin, D. K., Daar, A. S., and Singer, P. A. (2005). Nanotechnology and the developing world. *Public Library of Science Medicine*, *2*(5), e97.

Sanghi, R., and Verma, P. (2010). pH dependent fungal proteins in the 'green' synthesis of gold nanoparticles. *Advanced Materials Letters*, *1*(3), 193-9.

Savage, N., and Diallo, M. S. (2005). Nanomaterials and water purification: opportunities and challenges. *Journal of Nanoparticle Research*, *7*(4-5), 331-342.

Schneider, C. A., Rasband, W. S., and Eliceiri, K. W. (2012). NIH Image to ImageJ: 25 years of image analysis. *Nature Methods*, *9*(7), 671-675.

Schofield, C. L., Haines, A. H., Field, R. A., and Russell, D. A. (2006). Silver and gold glyconanoparticles for colorimetric bioassays. *Langmuir*, *22*(15), 6707-6711.

Schröfel, A., Kratošová, G., Šafařík, I., Šafaříková, M., Raška, I., and Shor, L. M. (2014). Applications of biosynthesized metallic nanoparticles–A review. *Acta Biomaterialia*, *10*(10), 4023-4042.

Schulz, F., Homolka, T., Bastús, N. G., Puntes, V., Weller, H., and Vossmeyer, T. (2014). Little adjustments significantly improve the turkevich synthesis of gold nanoparticles. *Langmuir*, *30*(35), 10779-10784.

Seshadri, S., Saranya, K., and Kowshik, M. (2011). Green synthesis of lead sulfide nanoparticles by the lead resistant marine yeast, *Rhodosporidium diobovatum*. *Biotechnology Progress*, *27*(5), 1464-1469.

Shahverdi, A. R., Fakhimi, A., Shahverdi, H. R., and Minaian, S. (2007). Synthesis and effect of silver nanoparticles on the antibacterial activity of different antibiotics against *Staphylococcus aureus* and *Escherichia coli*. *Nanomedicine: Nanotechnology, Biology and Medicine*, *3*(2), 168-171.

Shankar, S. S., Rai, A., Ankamwar, B., Singh, A., Ahmad, A., and Sastry, M. (2004). Biological synthesis of triangular gold nanoprisms. *Nature Materials*, *3*(7), 482-488.

Sharma, H., Mishra, P. K., Talegaonkar, S., and Vaidya, B. (2015). Metal nanoparticles: a theranostic nanotool against cancer. *Drug Discovery Today*, *20*(9), 1143-1151.

Sheldon, R. A. (2016). Green chemistry and resource efficiency: towards a green economy. *Green Chemistry*, *18*, 3180-3183.

Shivaji, S., Madhu, S., and Singh, S. (2011). Extracellular synthesis of antibacterial silver nanoparticles using psychrophilic bacteria. *Process Biochemistry*, *46*(9), 1800-1807.

Shukla, S., Leem, H., Lee, J. S., and Kim, M. (2014). Immunochromatographic strip assay for the rapid and sensitive detection of *Salmonella Typhimurium* in artificially contaminated tomato samples. *Canadian Journal of Microbiology*, *60*(6), 399-406.

Shyu, R. H., Shyu, H. F., Liu, H. W., and Tang, S. S. (2002). Colloidal gold-based immunochromatographic assay for detection of ricin. *Toxicon*, *40*(3), 255-258.

Siegel, J., Staszek, M., Polívková, M., Řezníčková, A., Rimpelová, S., and Švorčík, V. (2016). Green synthesized noble metals for biological applications. *Materials Today: Proceedings*, *3*(2), 608-616.

Singh, M., Manikandan, S., and Kumaraguru, A. K. (2011). Nanoparticles: a new technology with wide applications. *Journal of Nanomedicine and Nanotechology*, *1*(1), 1-11.

Singh, P., Kim, Y. J., Zhang, D., and Yang, D. C. (2016). Biological synthesis of nanoparticles from plants and microorganisms. *Trends in Biotechnology*, *34*(7), 588–599.

Song, J., Roh, J., Lee, I., and Jang, J. (2013). Low temperature aqueous phase synthesis of silver/silver chloride plasmonic nanoparticles as visible light photocatalysts. *Dalton Transactions*, *42*(38), 13897-13904.

Sreeprasad, T. S., and Pradeep, T. (2013). Noble metal nanoparticles. In Vajtai, R. (Ed.). (2013). *Springer Handbook of Nanomaterials* (pp. 303-388). Berlin, Heidelberg: Springer.

Srivastava, S., Frankamp, B. L., and Rotello, V. M. (2005). Controlled plasmon resonance of gold nanoparticles self-assembled with PAMAM dendrimers. *Chemistry of Materials*, *17*(3), 487-490.

Srivastava, P., and Kowshik, M. (2017). Fluorescent lead (IV) sulfide nanoparticles synthesized by *Idiomarina* sp. PR58-8 for bio-imaging applications. *Applied and Environmental Microbiology*, AEM-03091.

Stark, W. J., Stoessel, P. R., Wohlleben, W., and Hafner, A. (2015). Industrial applications of nanoparticles. *Chemical Society Reviews*, *44*(16), 5793-5805.

Suib, S. L. (Ed.). (2013). *New and Future Developments in Catalysis: Catalysis by Nanoparticles* (pp. 25). Newnes: Oxford:.

Suresh, A. K., Pelletier, D. A., Wang, W., Moon, J. W., Gu, B., Mortensen, N. P., and Doktycz, M. J. (2010). Silver nanocrystallites: biofabrication using *Shewanella oneidensis*, and an evaluation of their comparative toxicity on Gram-negative and Gram-positive bacteria. *Environmental Science and Technology*, *44*(13), 5210-5215.

Sutton, J., Jinhage, A., Leape, J., Newfarmer, R., and Page, J. (2016). Harnessing FDI for job creation and industrialisation in Africa. IGC Growth Brief Series 006. London: International Growth Centre.

Sweeney, R. Y., Mao, C., Gao, X., Burt, J. L., Belcher, A. M., Georgiou, G., and Iverson, B. L. (2004). Bacterial biosynthesis of cadmium sulfide nanocrystals. *Chemistry and Biology*, *11*(11), 1553-1559.

Tavakoli, A., Sohrabi, M., and Kargari, A. (2007). A review of methods for synthesis of nanostructured metals with emphasis on iron compounds. *Chemical Papers*, *61*(3), 151-170.

Taylor, C., Matzke, M., Kroll, A., Read, D. S., Svendsen, C., and Crossley, A. (2016). Toxic interactions of different silver forms with freshwater green algae and cyanobacteria and their effects on mechanistic endpoints and the production of extracellular polymeric substances. *Environmental Science: Nano*, *3*(2), 396-408.

Telkar, M. M., Rode, C. V., Chaudhari, R. V., Joshi, S. S., and Nalawade, A. M. (2004). Shape-controlled preparation and catalytic activity of metal nanoparticles for hydrogenation of 2-butyne-1, 4-diol and styrene oxide. *Applied Catalysis A: General*, *273*(1), 11-19.

Thakkar, K. N., Mhatre, S. S., and Parikh, R. Y. (2010). Biological synthesis of metallic nanoparticles. *Nanomedicine: Nanotechnology, Biology and Medicine*, *6*(2), 257-262.

Thanh, N. T., Maclean, N., and Mahiddine, S. (2014). Mechanisms of nucleation and growth of nanoparticles in solution. *Chemical reviews*, *114*(15), 7610-7630.

Thomas, V., Yallapu, M. M., Sreedhar, B., and Bajpai, S. K. (2007). A versatile strategy to fabricate hydrogel–silver nanocomposites and investigation of their antimicrobial activity. *Journal of Colloid and Interface Science*, *315*(1), 389-395.

Tiwari, J. P., and Rao, C. R. (2008). Template synthesized high conducting silver chloride nanoplates. *Solid State Ionics*, *179*(9), 299-304.

Tiwari, J. N., Tiwari, R. N., and Kim, K. S. (2012). Zero-dimensional, one-dimensional, two-dimensional and three-dimensional nanostructured materials for advanced electrochemical energy devices. *Progress in Materials Science*, *57*(4), 724-803.

Tojo, C., Barroso, F., and de Dios, M. (2006). Critical nucleus size effects on nanoparticle formation in microemulsions: A comparison study between experimental and simulation results. *Journal of Colloid and Interface Science*, *296*(2), 591-598.

Travis, C. C., and Hester, S. T. (1991). Global chemical pollution. *Environmental Science and Technology*, *25*(5), 814-819.

Truong, L., Moody, I. S., Stankus, D. P., Nason, J. A., Lonergan, M. C., and Tanguay, R. L. (2011). Differential stability of lead sulfide nanoparticles influences biological responses in embryonic zebrafish. *Archives of Toxicology*, *85*(7), 787-798.

Turkevich, J., Stevenson, P. C., and Hillier, J. (1951). A study of the nucleation and growth processes in the synthesis of colloidal gold. *Discussions of the Faraday Society*, *11*, 55-75.

Umer, A., Naveed, S., Ramzan, N., and Rafique, M. S. (2012). Selection of a suitable method for the synthesis of copper nanoparticles. *Nano*, *7*(05), 1230005.

Vaidyanathan, R., Gopalram, S., Kalishwaralal, K., Deepak, V., Pandian, S. R. K., and Gurunathan, S. (2010). Enhanced silver nanoparticle synthesis by optimization of nitrate reductase activity. *Colloids and Surfaces B: Biointerfaces*, *75*(1), 335-341.

Valverde, A., Peix, A., Rivas, R., Velázquez, E., Salazar, S., Santa-Regina, I., and Igual, J. M. (2008). *Paenibacillus castaneae* sp. nov., isolated from the phyllosphere of *Castanea sativa* Miller. *International Journal of Systematic and Evolutionary Microbiology*, *58*(11), 2560-2564.

Vance, M. E., Kuiken, T., Vejerano, E. P., McGinnis, S. P., Hochella Jr, M. F., Rejeski, D., and Hull, M. S. (2015). Nanotechnology in the real world: Redeveloping the nanomaterial consumer products inventory. *Beilstein Journal of Nanotechnology*, *6*(1), 1769-1780.

Varia, J. C., Martinez, S. S., Velasquez-Orta, S., and Bull, S. (2014). Microbiological influence of metal ion electrodeposition: Studies using graphite electrodes, $[AuCl^4]^-$ and *Shewanella putrefaciens*. *Electrochimica Acta*, *115*, 344-351.

Varia, J. C., Zegeye, A., Velasquez-Orta, S., and Bull, S. (2016). Process analysis of $AuCl^{4-}$ sorption leading to gold nanoparticle synthesis by *Shewanella putrefaciens*. *Chemical Engineering Journal*, *288*, 482-488.

Venkatesh, K. S., Palani, N. S., Krishnamoorthi, S. R., Thirumal, V., and Ilangovan, R. (2013). Fungus mediated biosynthesis and characterization of zinc oxide nanorods. In S. Bhardwaj, M. S. Shekhawat, and B. Suthar (Eds.), *AIP Conference Proceedings* (Vol. 1536, No. 1, pp. 93-94). AIP.

Verma, V. C., Anand, S., Ulrichs, C., and Singh, S. K. (2013). Biogenic gold nanotriangles from *Saccharomonospora* sp., an endophytic actinomycetes of *Azadirachta indica* A. Juss. *International Nano Letters*, *3*(1), 1-7.

Wahed, M. S. A., Mohamed, E. A., El-Sayed, M. I., M'nif, A., and Sillanpää, M. (2015). Crystallization sequence during evaporation of a high concentrated brine involving the system Na–K–Mg–Cl–SO 4-H 2 O. *Desalination*, *355*, 11-21.

Wang, S., and Yang, S. (2000). Preparation and characterization of oriented PbS crystalline nanorods in polymer films. *Langmuir*, *16*(2), 389-397.

Wang, Y., and Xia, Y. (2004). Bottom-up and top-down approaches to the synthesis of monodispersed spherical colloids of low melting-point metals. *Nano Letters*, *4*(10), 2047-2050.

Wang, Y., Dai, Q., Yang, X., Zou, B., Li, D., Liu, B., and Zou, G. (2011). A facile approach to PbS nanoflowers and their shape-tunable single crystal hollow nanostructures: Morphology evolution. *CrystEngComm*, *13*(1), 199-203.

Wattoo, M. H. S., Quddos, A., Wadood, A., Khan, M. B., Wattoo, F. H., Tirmizi, S. A., and Mahmood, K. (2012). Synthesis, characterization and impregnation of lead sulphide semiconductor nanoparticles on polymer matrix. *Journal of Saudi Chemical Society*, *16*(3), 257-261.

Wei, L., Lu, J., Xu, H., Patel, A., Chen, Z. S., and Chen, G. (2015). Silver nanoparticles: synthesis, properties, and therapeutic applications. *Drug Discovery Today*, *20*(5), 595-601.

White, C., Tancos, M., and Lytle, D. A. (2011). Microbial community profile of a lead service line removed from a drinking water distribution system. *Applied and Environmental Microbiology*, *77*(15), 5557-5561.

Wiley, B., Sun, Y., Mayers, B., and Xia, Y. (2005). Shape-controlled synthesis of metal nanostructures: the case of silver. *Chemistry–A European Journal*, *11*(2), 454-463.

Wiley, B. J., Im, S. H., Li, Z. Y., McLellan, J., Siekkinen, and Xia, Y. (2006). Manoeuvring the surface plasmon resonance of silver nanostructures through shape-controlled synthesis. *The Journal of Physical Chemistry B*, *110*(32), 15666-15675.

Williams, C. J., Aderhold, D., and Edyvean, R. G. J. (1998). Comparison between biosorbents for the removal of metal ions from aqueous solutions. *Water Research*, *32*(1), 216-224.

Wu, Q. S., and Ding, Y. P. (2006). Synthesis and optical properties of the semiconductor lead sulfide nanobelts. *Bulletin of the Korean Chemical Society*, *27*(3), 377-380.

Wu, Z., Yang, S., and Wu, W. (2016). Shape control of inorganic nanoparticles from solution. *Nanoscale*, *8*(3), 1237-1259.

Xiang, D., Yang, Z., Duan, W., Li, X., Yin, J., Shigdar, S., and Xiang, B. (2013). Inhibition of A/Human/Hubei/3/2005 (H3N2) influenza virus infection by silver nanoparticles *in vitro* and *in vivo*. *International Journal of Nanomedicine*, *8*(1), 4103-4114.)

Yadav, R., Yadav, N., and Kharya, M. D. (2014). A review: Quality control of residual solvents in pharmaceuticals. *World Journal of Pharmacy and Pharmaceutical Science*, *3*, 526-538.

Yan, L., Zhang, S., Chen, P., Liu, H., Yin, H., and Li, H. (2012). Magnetotactic bacteria, magnetosomes and their application. *Microbiological Research*, *167*(9), 507-519.

Yeh, Y. C., Creran, B., and Rotello, V. M. (2012). Gold nanoparticles: preparation, properties, and applications in bionanotechnology. *Nanoscale*, *4*(6), 1871-1880.

Youtie, J., Shapira, P., and Porter, A. L. (2008). Nanotechnology publications and citations by leading countries and blocs. *Journal of Nanoparticle Research*, *10*(6), 981-986.

Zhang, Y., Yu, K., Jiang, D., Zhu, Z., Geng, H., and Luo, L. (2005a). Zinc oxide nanorod and nanowire for humidity sensor. *Applied Surface Science*, *242*(1), 212-217.

Zhang, H., Li, Q., Lu, Y., Sun, D., Lin, X., Deng, X., He, N., and Zheng, S. (2005b) Biosorption and bioreduction of diamine silver complex by *Corynebacterium*. *Journal of Chemical Technology and Biotechnology, 80*, 285–290.

Zhang, Q., Xie, J., Yu, Y., and Lee, J. Y. (2010). Monodispersity control in the synthesis of monometallic and bimetallic quasi-spherical gold and silver nanoparticles. *Nanoscale*, *2*(10), 1962-1975.

Zhang, X., Yan, S., Tyagi, R. D., and Surampalli, R. Y. (2011). Synthesis of nanoparticles by microorganisms and their application in enhancing microbiological reaction rates. *Chemosphere*, *82*(4), 489-494.

Zhang, X. F., Shen, W., and Gurunathan, S. (2016). Biologically Synthesized Gold Nanoparticles Ameliorate Cold and Heat Stress-Induced Oxidative Stress in *Escherichia coli*. *Molecules*, *21*(6), 731.

Zhao, P., Li, N., and Astruc, D. (2013). State of the art in gold nanoparticle synthesis. *Coordination Chemistry Reviews*, *257*(3), 638-665.

Zhou, H., Fan, T., Han, T., Li, X., Ding, J., Zhang, D., and Ogawa, H. (2009). Bacteria-based controlled assembly of metal chalcogenide hollow nanostructures with enhanced light-harvesting and photocatalytic properties. *Nanotechnology*, *20*(8), 085603.

Zhou, H., Yu, F., Guo, C. F., Wang, Z., Lan, Y., Wang, G., and Ren, Z. (2015). Well-oriented epitaxial gold nanotriangles and bowties on MoS 2 for surface-enhanced Raman scattering. *Nanoscale*, *7*(20), 9153-9157.

Zhu, N., Zhang, A., Wang, Q., He, P., and Fang, Y. (2004). Lead sulfide nanoparticle as oligonucleotides labels for electrochemical stripping detection of DNA hybridization. *Electroanalysis*, *16*(7), 577-582.